On the Nature of Starbursts

A DISSERTATION
SUBMITTED TO THE FACULTY OF THE GRADUATE SCHOOL
OF THE UNIVERSITY OF MINNESOTA
BY

Kristen Brookes W. McQuinn

IN PARTIAL FULFILLMENT OF THE REQUIREMENTS
FOR THE DEGREE OF
Doctor Of Philosophy

May, 2010

Acknowledgements

First and foremost, I am grateful to my advisor, Evan Skillman, whose ability to consistently see the forest through the trees has guided both my research and my way of thinking; you have helped turned an engineer into an astrophysicist. I sincerely thank you for seeing the possibilities of success for a part-time, female, graduate student with young children. I have never doubted in my ability or my determination to complete my studies, but internal commitment also needs opportunity. Thank you for helping to create that opportunity for me at the University of Minnesota and supporting me through my years of research.

I thank the other graduate students and post docs who have helped me along the way. Without the knowledge share and camaraderie of my peers, the work would be harder and frustrating. In particular, I would like to thank Carlos Martinis, with whom I studied countless hours in our course work and in preparation for the written exam at Boston University, Dale Jackson and Elisha Polomski who helped me gain my footing when I arrived at the University of Minnesota, and my office mates of late, Steven Warren and Danielle Berg, who, respectively, have been my sounding board for the day-to-day details of research and a positive, encouraging energy in the office.

For helping me continue to see and believe in my own potential, I am grateful to the women in my life. Lacking a role model in my field, you stepped in to show me how to navigate career goals while being the primary care-giver for my children. In particular, I want to thank Erika Cluegh and Kitty Friedman for their long talks, support, and inspiration. You not only believed that this was possible for me, but you also saw I had an important contribution to make. Thank you for helping me see my path as being full of opportunity, instead of full of limitations.

I am grateful to my children, Cole and Carling, whose love, kindness, and silliness

make my life richer. Unknowingly, you help balance my ambitions with the softer side of life. I hope your lives have been shaped for the better by my professional goals and achievements. I hope I have successfully modeled what it looks like to raise a family while being true to what is important to you. I hope that you have internalized how important it is to pursue your own dreams because dreams matter.

I am grateful to my husband, Matt, whose constancy, love, support, and perspective have helped make this achievement possible for me.

Dedication

The PhD journey is unique to each who undertake such an endeavor. For me, the journey spans across a decade and two states, through my wedding, the birth of my two children, and their years to reach elementary school. The one constant outside of myself through this journey has been my husband, Matt. Matt has encouraged and supported my dream to become a scientist from the very beginning. He has been my advocate through the ad hoc way I applied to graduate programs from Buenos Aires to the single-minded approach I took to finish my dissertation research. He has been through the intense, eye-on-the-prize focus of the first two years of grad school when nothing mattered but the assignments and sleep. I have leaned on him through the many years of research while I tried to be a full-time mom and part-time graduate student each and every day. Never have I felt I was doing this alone. We made a commitment to fit work into my life while we made my top time commitment our children. While I have been the one to manage the day-to-day happenings in our young children's lives, Matt has been there to talk me down from the ledge when I felt overwhelmed and see the solutions when I was bogged down by the details and sleep-deprivation. He has stepped in to help me carry the dual load whenever I have asked, and sometimes when I have not. Together, we have made it possible for me to pursue a career in science. I am grateful I have spent so many years of my life with him and grateful for the years to come.

I dedicate this work to you, Matt.

Abstract

Starbursts are a fascinating phenomenon that can significantly impact the host galaxy and the surrounding intergalactic medium. Understanding the nature of a starburst requires a detailed analysis of the resolved stellar populations and the recent star formation history (SFH) of the galaxy. Using a CMD fitting technique and stellar evolution models, we derive the SFHs of twenty nearby dwarf starburst galaxies from Hubble Space Telescope V and I band images. The star formation rates (SFRs) from this diverse sample of dwarf galaxies span three orders of magnitude but all show elevated levels of star formation (SF) in their recent past when viewed in the context of the host galaxy's past SFH. Fifteen of the twenty galaxies show currently bursting SF and five galaxies show "fossil" bursts. From our reconstructed SFHs, it is evident that the elevated SFRs of a burst are sustained for hundreds of Myr. The SF migrates around the host galaxies in many cases as derived from the temporally and spatially resolved stellar populations and is a cumulation of SF not only in star clusters but also in field regions of low surface brightness in the galaxies. Contrary to the shorter time of 3-10 Myr often cited, the starburst durations we measure range from $450 - 600$ Myr in fifteen of the dwarf galaxies and up to 1.3 Gyr in four galaxies; comparable to or longer than the dynamical timescales for each system. The same feedback loop from massive stars that may quench flickering SF does not disrupt the overall burst event in this sample of galaxies. In the fifteen galaxies that show ongoing bursts, the final durations may be longer than we report here. One galaxy shows a burst that has been ongoing for only 20 Myr; we are likely seeing the beginning of a burst event in this system. Using the duration of the starbursts, we calculate that the bursts deposited $10^{53.9} - 10^{57.2}$ erg of energy into the interstellar medium through stellar winds and supernovae and produced 3.2%−26% of the host galaxy's mass. We also explore two other metrics for identifying starbursts:

the gas consumption timescale and the strength of Hα emission produced by the burst. Interestingly, four galaxies classified as starbursts in our most recent time bin of 4-10 Myr show non-starburst levels of Hα emission from the last $\sim$5 Myr indicating that, while the bursts are long-lasting events, the SFR can change on timescales of only a few Myr.

Contents

List of Tables

List of Figures

Chapter 1

Introduction

"Stars shine so silver in the night sky, silver like metal glinting in the moonlight."
Carling McQuinn, Age 7

"Stars are beautiful glowing balls of fire moving across the night sky. I hope I see some tonight."
Cole McQuinn, Age 8

Starbursts are a complex star formation process that can have a powerful impact on the evolution state of the host galaxy. This doctoral thesis focuses on understanding the nature of starbursts in a sample of nearby dwarf galaxies. In this introductory chapter, I present a summary of my research and results; the remainder of this thesis presents these concepts and results in more detail.

1.1 What is a Starburst?

We begin with a description of a galaxy and the star formation process. The visible part of galaxies are primarily made up of gas, dust, stars, and stellar remnants. These four components are intimately connected. The gas and dust coalesce to form stars, while the stars partly replenish the gas and dust through stellar winds and supernovae explosions leaving behind stellar remnants in the form of white dwarfs, neutron stars, and black holes. Over time, this cyclical process changes what a galaxy looks like, from

a system dominated by pristine hydrogen and helium gas in the early universe, to a galaxy with little gas content but rich both in older stars and heavy elements formed by stellar nuclearsynthesis.

When stars are being formed at a higher rate than average, we call this galaxy a "starburst galaxy". Starbursts are unsustainable on a cosmic timescale as the gas supply fueling the high rate of star formation in a burst is finite and exhaustible (Roberts 1963). Even though starbursts are short-lived (Searle et al. 1973), the increased exchange between the gas, dust, star, and stellar remnant cycle can have a significant impact on the host galaxy (Dekel & Silk 1986). I present an example of what a starburst galaxy looks like in Figure 1.1, an image taken by instruments on board the Hubble Space Telescope.

The ingredients required to make a starburst are a galaxy system with a significant reservoir of gas and a triggering event to push the gas into forming stars at an accelerated rate. In the nearby universe, where galaxies are close enough to observe and study in detail, there is a population of smaller galaxies, called dwarf galaxies, that contain significant reservoirs of gas and are often isolated from larger groups or clusters of galaxies. These systems have formed stars since the early universe, but typically at a slower rate than other galaxies. The star formation has proceeded at lower rate because dwarf galaxies lack an internal mechanism, like spiral arms in a spiral galaxy, to continually push the gas into making stars, so star formation just putters along wherever and whenever local conditions are favorable. Ripe for a burst of star formation, these nearby dwarf galaxies can be coaxed into rapidly forming stars if, for example, another galaxy passes by and gives it a gravitational push or pull, much like the moon pushes and pulls on the earth's oceans. These extragalactic tidal forces are thought to be the most common trigger of starbursts in dwarf galaxies (Kennicutt et al. 1987). Once a starburst has begun, it presents an interesting laboratory in which to study extreme star formation and its effects.

1.2 The History and the Observables

Because of the intense star formation that defines a starburst, galaxies undergoing a burst shine brightly and thus, have been readily observed for decades. The young stars formed in a burst are blue in color and stand out against older, and sometimes

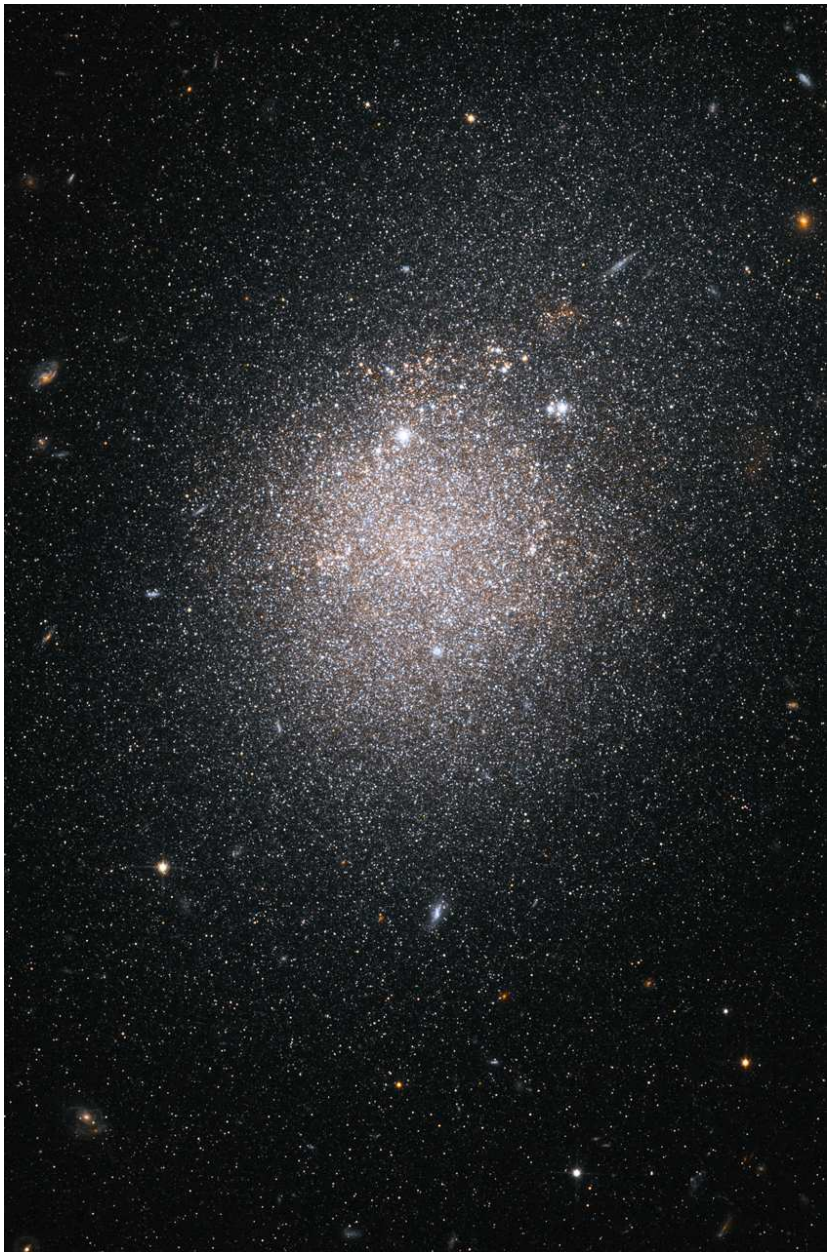

Figure 1.1 A Hubble Space Telescope Image of NGC 4163. Most points of light visible in the image are stars in the starburst dwarf galaxy NGC 4163. A few background galaxies can be seen as well, identifiable by their non-circular shape and larger size. The blue-ish hue generally highlights the younger, more massive stars in the galaxy while the yellow-red hue colors the older stars.

fainter, red stars. Indeed, the first studies on starbursts were performed forty years ago when a collection of galaxies very blue in color were found in images of the night sky (Searle & Sargent 1972; Searle et al. 1973). More recently, with the advent of sophisticated space telescopes, there have been many studies performed on the starburst phenomenon, each unraveling part of this unique star formation process (e.g., Calzetti et al. 1997; Ferguson & Babul 1998; Greggio et al. 1998; Mas-Hesse & Kunth 1999; Thornley et al. 2000; Tremonti et al. 2001; Harris et al. 2004; Lee 2006).

Where previous generations of telescopes were able to measure only the position and brightness of a galaxy, current telescopes are able to measure the position and brightness of individual stars in nearby galaxies. One of the space telescopes of NASA, the Hubble Space Telescope, is a premier example of this technological advance and has not only the optics to separate out individual stars in nearby galaxies, but also the sensitivity to measure the brightness of each star from the most luminous to some fainter limit. The data gathered and archived by Hubble over the past twenty years of observations are accessible to anyone within the scientific community or otherwise[1] .

Numerous starburst galaxies in the nearby universe have been observed by Hubble for various scientific purposes. This thesis capitalizes on the Hubble archive using observations previously obtained. We gathered some of the best archived Hubble observations on this class of galaxies close enough the resolve the individual stars (or "stellar populations") creating a sample of twenty starburst dwarf galaxies (see Table 3.1 for a list of galaxies). The sample of galaxies are found almost exclusively within a 5 Mpc distance of our own galaxy, the Milky Way; the one exception is the well-studied galaxy, SBS 1415+437, located at a distance of 13.6 Mpc. The majority of these systems have been previously identified as starburst galaxies by other authors (see Table 3.1 for specific citations) while a handful were identified in this study based on the properties of their stellar populations.

1.3 The Scientific Goals

We investigated a number of specific aspects of the starburst phenomenon. The first goal, measuring how long a starburst lasts, is the main result of this thesis. The other

[1] http://archive.stsci.edu/index.html

goals include determining the path star formation takes within a galaxy, understanding the spatial extent of the bursting star formation within a galaxy, determining how the energy produced by a starburst is distributed across different energy wavelengths (i.e., the ultraviolet, infrared, and X-ray wavelengths) including measuring the timescale of emission at these different wavelengths. These latter goals comprise the ongoing and planned work on starburst galaxies. Each goal is discussed in turn.

1.3.1 The Duration of a Starburst

Many astronomical events last much longer than the history of humankind, so measuring how long one of these events last means the past must be re-created from clues found in the present day. The is true for starburst as the timescale of star formation is measured in millions of years. Thus, measuring the duration of a starburst event requires reconstructing the history of star formation in a galaxy (i.e., determining the past birthrate of stars), using present-day observations.

This historical reconstruction of star formation is possible using Hubble observations of stellar populations combined with our current understanding on how stars evolve (Bertelli et al. 1994; Dolphin 2002; Marigo & Girardi 2007). The brightness and color of each star in an image are measured and, using knowledge of stellar evolution, the age of individual stars can be deduced or constrained from these measurements. Conceptually, this is akin to taking a photograph of all the people in a town and trying to reconstruct the birthrate of the human population in that town from the photograph using knowledge of how people age. The bursting star formation would be akin to a baby-boom in the town's population and the science goals would be to determine both how long the baby-boom lasted and if all neighborhoods in the town participated in or were affected by the boom in population.

Just like for the starburst galaxies, several steps and assumptions would be applied to achieve these science goals from a mere town photograph. First, an age census would be taken using the photograph. The babies would be identified and counted, as would the small children, adults, the elderly, etc. Using approximate ages for babies, children, etc., we could reconstruct how many townspeople were born per year, historically. In the case of stellar populations, the oldest stars have been around since the formation of a galaxy, thus one can account for nearly fourteen billion years of history. The most

accurate age-dating of people in the photograph would likely be the babies providing robust constraints on the most recent birthrate in the town. Similarly, the Hubble observations we used are best able to constrain the age of youngest stars thus providing excellent footing for measuring recent stellar birthrates (e.g., Greggio et al. 1998; Dohm-Palmer & Skillman 2002).

Second, the birthrate would be adjusted for premature deaths. While this would be difficult to account for in a human population because of the random nature of premature deaths, it is somewhat easier and particularly important for a stellar population. Stars are born in groups, not individually like humans, and have lifespans determined by their "birth weight". Smaller stars, such as our Sun, live for billions of years, while massive stars die within a few to several million years. The number of longer-lived smaller stars born in each group is proportional to the number of shorter-lived massive stars (i.e., for every few big stars formed in a group, there is a predictable larger number of smaller stars formed) (Salpeter 1955). Thus, massive stars, that died long ago and do not show up in the Hubble images (our "premature deaths"), can be accounted for if we know the total number of smaller stars[2] .

Finally, the birthrate in the town can be plotted across time and analyzed for changes. In Figure 1.2, we present an example of such a plot. The horizontal axis measures time in billions of years (Gyr) in the top panel; the bottom panel zooms in on the last 1000 million years (Myr). The vertical axes measure the rate of star formation (SFR) each year in units of the sun (solar mass per year $\equiv M_{\odot}$ per year). From the plot, we can see that the initial assembly of the galaxy was marked by high rates of star formation (top panel from $6-14$ billion years ago). This is analogous to when the town in our example would have been colonized years ago. After this initial period, the rate of star formation was much lower. This lower birthrate continued for an extended period of time until about 500 Myr ago (see bottom panel), at which point, the birthrate of stars increased dramatically. This increased rate of star formation is our starburst and, in this example plot, continues until the present day. The duration of this starburst would be measured as a lower limit of 450 Myr (450 being the middle of the last time bin); it is a lower limit because the elevated birthrate persists today (McQuinn et al.

[2] Other effects such the percentage of stars formed in binary systems are alos taken into account. See 2 and 3 for details.

2010b). This would translate into a baby-boom in the town's population that lasted over multiple generations.

Scientific results must be specifically defined and reproducible. While in this example case, the rate of star formation jumps significantly and the burst is clearly defined in Figure 1.2, the bursts are not always this clearly delineated in time. Thus, a threshold value of star formation was established in order to define what star formation qualified as bursting, and what did not. This threshold is not an absolute value, but varies by galaxy and is based on the historical star formation of the galaxy. Returning to our baby-boom analogy, a smaller town will naturally have a lower birthrate than a larger town; what would be baby-boom birthrate in a small town might not even reach the average birthrate in a large town or city. In addition, other environmental factors may influence the birthrate in a town such as economic conditions, religious doctrines, political climate, etc. Defining a threshold for a baby-boom based on an individual town's historical birthrate average makes more sense and takes into account the particular circumstances and culture of a town.

Similarly for the starburst galaxies, the size of the host galaxy and the internal environment or "culture" influences the stellar birthrate. Thus, star formation in a particular galaxy was considered bursting if stars were formed at greater than twice the average rate in that galaxy. The beginning and end points of the burst are found when the rate of star formation returns to the average. In Figure 1.2, the historical average for this particular galaxy is drawn as a solid red line and twice the average is drawn as a dotted red line (McQuinn et al. 2009). The rates of star formation in this plot are well above these values for 450 Myr.

The shortest starburst duration measured in this sample of twenty dwarf galaxies is 450 Myr. The longest is 1.3 Gyr. In five of the twenty galaxies, the bursts have ended providing a unique sample in which to study "fossil" bursts (McQuinn et al. 2010b). In general, these long-lasting starbursts will have a significant impact on the host galaxy depositing both mass and energy into the galaxy and potentially driving a galactic-scale wind into the surrounding intergalactic medium. These longer durations are also significant in that they outlast the natural rotational timescale of a galaxy. The duration of starbursts had been previously thought to last from $3-10$ million years based on both individual studies and surveys of groups of galaxies. The shorter timescales previously

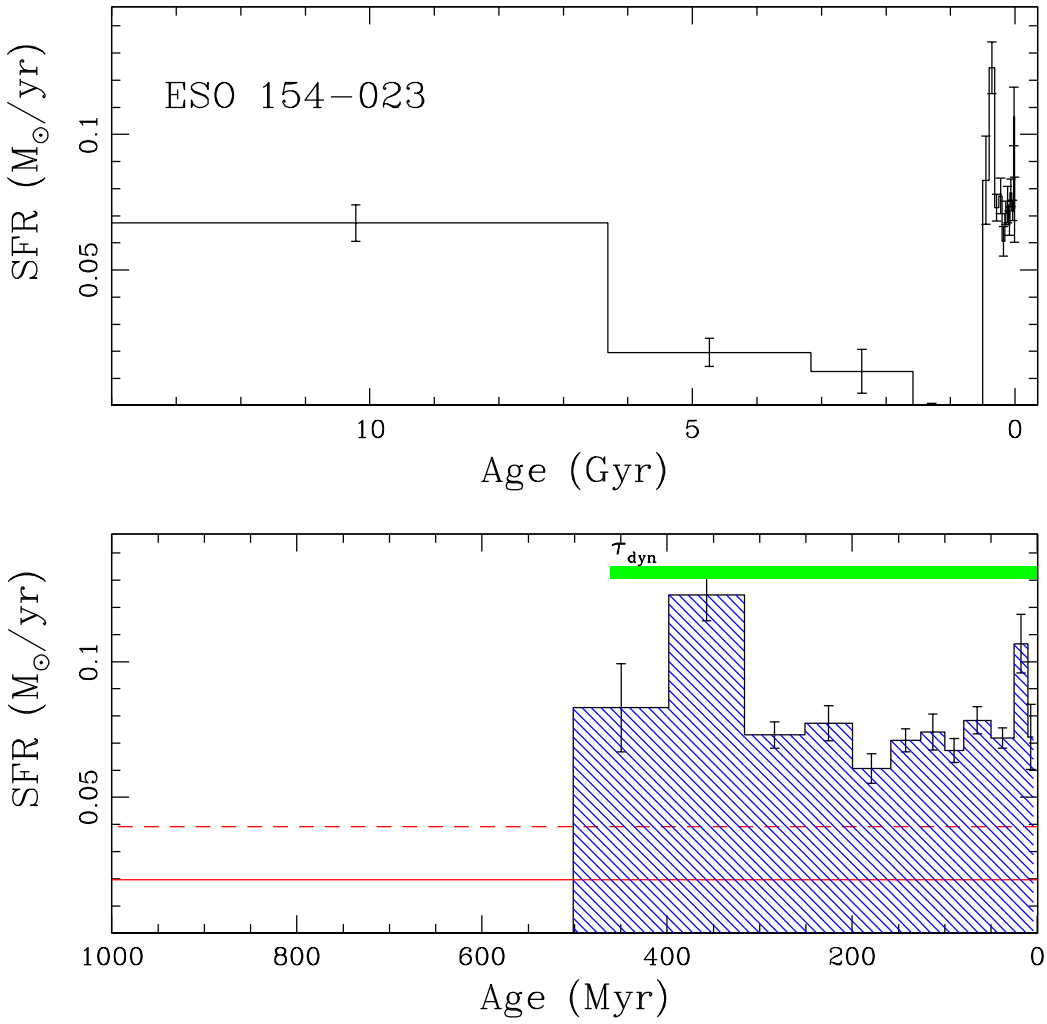

Figure 1.2 The top panel shows the lifetime history of star formation in galaxy ESO 154−023 over the last fourteen billion years. The bottom panel highlights the last one billion years of history. The starburst event is defined in blue in the bottom panel. The duration measured in this case is a lower limit of 450 Myr. The solid red line represents the average rate at which stars where formed in the galaxy over the last six billion years; the dashed red line is twice this average. The recent rate of star formation is much higher than this historical average and is what we call a starburst event. The horizontal green bar represents the amount of time for the galaxy to complete a full rotation about itself.

reported measure smaller scale changes in star formation and not the larger burst event. Returning to our analogy, this would be akin to finding an increase in the birthrate in an individual neighborhood that may or may not be part of a baby-boom event for an entire town.

1.3.2 Determining the Spatial Structure of a Starburst

Wheras this thesis is primarily focused on measuring the duration of starbursts (Chapters 2−4), there are other aspects of a burst that can be studied by leveraging the star formation histories reconstructed for these galaxies. For example, the images from Hubble contain accurate spatial positions of the stellar populations, thus the starbursts can be studied spatially to determine both how much of the galaxy experiences a starburst and the path the star formation takes. In our town analogy, we would be asking if all neighborhoods in the town experience a baby-boom. Did the baby-boom occur only in the highly populated downtown areas? Or did the sparsely populated rural areas outside the town also participate in the baby-boom? Was there any connection between neighboring communities? While it is difficult to imagine people have more children simply because their neighbors do, it is plausible that a pocket of star formation and the resulting supernovae explosions could cause shock waves to propagate to a neighboring cloud of gas and dust pushing the gas into forming new stars, thus creating a new wave of star formation (looking much like people doing the wave in a sports stadium). The focus of my ongoing research is to explore the path star formation takes and whether star formation is "causally connected" as in this example, or whether it is more random or stochastic in nature.

Figures 1.3−1.4 show two examples of the analysis possible in combining the spatial information from Hubble observations with the time information from the star formation histories. The background images in each Figure are smeared Hubble images of a galaxy; the red represents the areas of highest stellar density ("downtown") and dark blue represents areas of lowest stellar density ("surrounding rural areas"). The magenta points represent the positions of individual young stars ("babies"). In Figure 1.3, the galaxy, UGC 9128, is shown four times with stars of different ages plotted each time. In the first panel, the burst dominates in the upper right corner of the galaxy ($300 - 400$ Myr ago), and slowly migrates to the lower right corner in the final two panels (over the

last 200 Myr). Figure 1.4 shows a different galaxy, NGC 1569, whose burst is widespread in the first panel ($100 - 150$ Myr ago) and is centrally located in the final panel (over the last 25 Myr). The bursting star formation moves around each of these two galaxies in a unique way. The larger study will examine all twenty galaxies and look for patterns in the way star formation propagates.

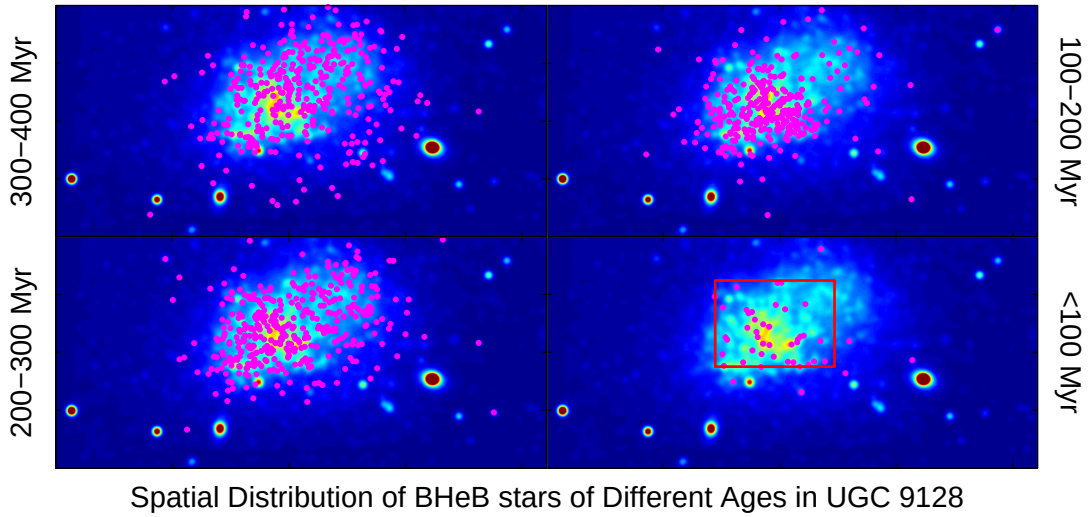

Figure 1.3 A smeared Hubble image of galaxy UGC 9128 is presented four times with stars of different ages plotted in each image in magenta. The star formation in the burst is primarily located in the upper right of the galaxy in the first panel ($300 - 400$ Myr ago) and moves down towards the lower left in the final two panels (over the last 200 Myr).

1.3.3 Multi-Wavelength Star Formation Rates and Emission Timescales

This work has used the position, brightness, and color of individual stars in Hubble optical images to investigate the starburst star formation process. Yet, stars radiate energy at all wavelengths including the ultraviolet, infrared, and X-ray regimes. The next stage of research will focus on studying the ultraviolet light from the stars using data currently being obtained by another NASA space telescope, the Galaxy Evolution Explorer or GALEX.

Most of the ultraviolet light originates from the largest and youngest stars in the galaxies and traces the new, bursting star formation; the underlying older stars do not

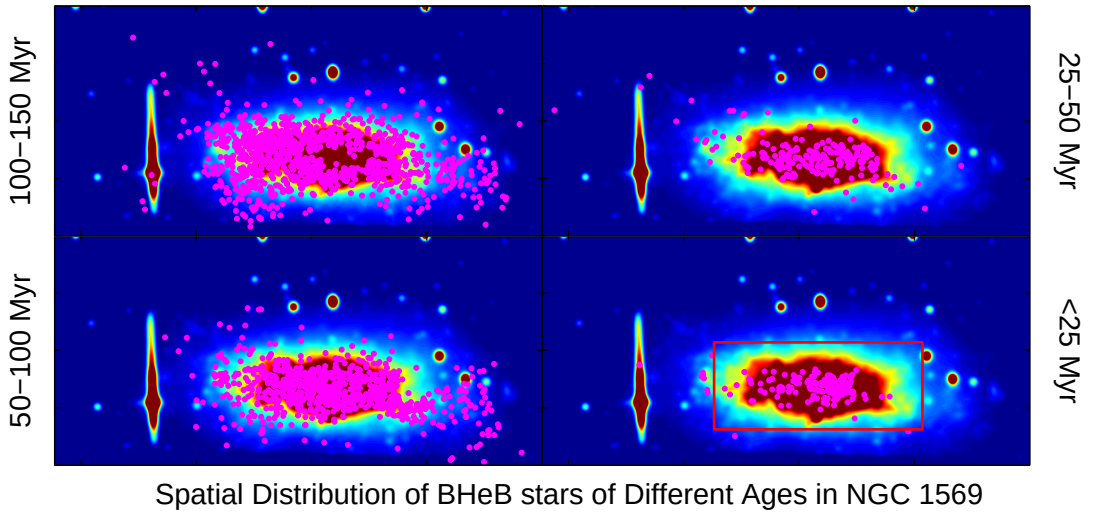

Figure 1.4 Similar to Figure 1.3, a smeared Hubble image of galaxy NGC 1569 is presented with stars of different ages plotted in magenta. The star formation pattern is different in this galaxy with the burst being widespread in the first panel ($100 - 150$ Myr ago) and centrally located in the final panel (last 25 Myr).

radiate much ultraviolet light. An example of what a galaxy looks like in ultraviolet light is presented in Figure 1.5 (P.I. Bigiel); the young stellar population is clearly visible while the underlying, older stellar population is mostly absent from the image. Combining the star formation histories with ultraviolet images like this one, my post-doctorate research will measure how long the ultraviolet emission from these young stars lasts. Additionally, the rate at which stars are formed can be calculated directly from the amount of ultraviolet light emitted (Kennicutt 1998), thus providing a comparison to the rate of star formation derived from the Hubble optical images. For galaxies in the distant universe, the brightness of a galaxy is one of the few measurable quantities. Connecting the ultraviolet light with a rate of star formation calculated from star formation history techniques will provide an independent calibration that can be applied to observations of distant systems.

These two parameters, the timescale of emitted light and a calibration of the star formation rate, will also be determined for infrared light using archived infrared observations already obtained from a third NASA space telescope, Spitzer. Additionally,

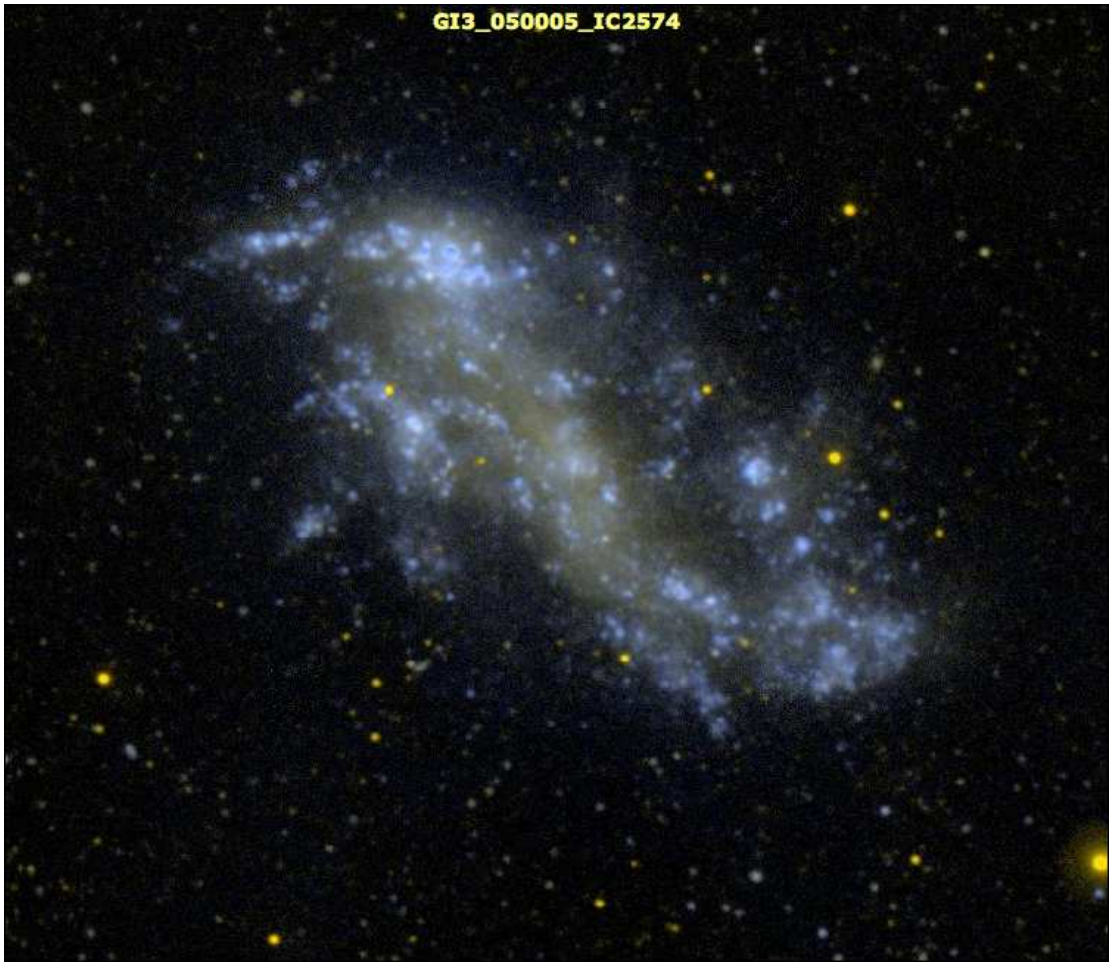

Figure 1.5 A GALEX space telescope UV image of IC 2574 (P.I. Bigiel). This spectacular image shows what a galaxy looks like in UV light; the blue traces areas of where massive stars have recently been formed. Our new project will obtain observations like this on a sample of starburst dwarf galaxies.

observations proposed to a fourth NASA space telescope, Chandra, would image a subset of these galaxies in X-ray light. If accepted, similar analysis will be applied to the X-ray light.

Knowing the star formation history and length of a burst for a galaxy, the amount of energy created by a burst can be estimated (McQuinn et al. 2010b). This energy is distributed across all wavelength and light. Using the energy estimated from the reconstructed star formation histories, ultraviolet images from GALEX, infrared images from Spitzer, and possibly X-ray images from Chandra, future work will study how a burst's energy is distributed across wavelengths. Images spanning such a wide range in wavelengths will facilitate a detailed study in the energy budget of star formation and reveal much about the nature of starbursts in the nearby universe.

1.4 Structure of this Thesis

The remaining chapters discuss in detail my published, submitted, and ongoing work on the nature of starburst galaxies and are organized as follows. The original work on studying the starburst phenomenon in three prototypical dwarf galaxies is presented in Chapter 2, previously published in McQuinn et al. (2009). The technique of reconstructing the SFH developed in this prototype study was applied to a larger galaxy sample which is discussed in Chapter 3, submitted for publication in McQuinn et al. (2010a). Analysis measuring the duration of the starbursts in this larger sample is presented in Chapter 4, also submitted for publication in McQuinn et al. (2010b). Ongoing research into the spatial structure of starbursts with preliminary results is presented in Chapter 5 (McQuinn et al. in prep). Finally, planned, post-doctorate work investigating the nature of starbursts using ultraviolet and infrared observations is discussed in Chapter 6.

Chapter 2

Duration of Starbursts in Prototype Galaxies (McQuinn et al. 2009)

A slightly modified version of this chapter appears in the published article referenced by Kristen B. W.McQuinn, Evan D. Skillman, John M.Cannon, Julianne J. Dalcanton, Andrew Dolphin, David Stark, Daniel Weisz, 2009, ApJ, 695, 561. Reproduced here with permission.

ABSTRACT

The duration of a starburst is a fundamental parameter affecting the evolution of galaxies yet, to date, observational constraints on the durations of starbursts are not well established. Here we study the recent star formation histories (SFHs) of three nearby dwarf galaxies to rigorously quantify the duration of their starburst events using a uniform and consistent approach. We find that the bursts range from $\sim 200-\sim 400$ Myr in duration resolving the tension between the shorter timescales often derived observationally with the longer timescales derived from dynamical arguments. If these three starbursts are typical of starbursts in dwarf galaxies, then the short timescales ($3-10$ Myr) associated with starbursts in previous studies are best understood as "flickering" events which are simply small components of the larger starburst. In this sample of

three nearby dwarfs, the bursts are not localized events. All three systems show bursting levels of star formation in regions of both high and low stellar density. The enhanced star formation moves around the galaxy during the bursts and covers a large fraction of the area of the galaxy. These massive, long duration bursts can significantly affect the structure, dynamics, and chemical evolution of the host galaxy and can be the progenitors of "superwinds" that drive much of the recently chemically enriched material from the galaxy into the intergalactic medium.

2.1 A Perspective on Starburst Durations

2.1.1 Duration: A Fundamental Property of a Starburst

Starbursts are finite episodes of intense star formation which have been observed in dwarf, spiral, and interacting galaxies both in the local universe and in galaxies at high redshift (z $\gtrsim$ 1) where they are thought to be more common (e.g., Thompson 2005). The concentrated star formation of a burst may have a significant impact on the surrounding environments through both energy and mass transfer altering not only the structure and composition of the host galaxy but also the local intergalactic medium (IGM) outside of the host galaxy (e.g., Strickland & Stevens 2000; Martin et al. 2002). For low mass dwarf systems,[1] the effect of a starburst on the galaxy and its evolution can be dramatic given the large energy output of starburst (i.e., supernovae and mass loss driven winds) compared with the dwarfs' smaller potential wells (Dekel & Silk 1986).

The impact of starbursts on galactic structure may have been more important in the early star-forming universe. Recent studies have estimated that 6% of locally detected galaxies show evidence of starbursts based on their Hα emission line (Lee 2006). The percentage of galaxies exhibiting starburst characteristics increases to 15 % for galaxies detected at $z = 1$ (O'Connell 2005). Although there is a significant selection effect against detecting distant non-bursting galaxies, a greater fraction of star formation occurring in bursts in the early universe is expected due to the increased frequency of galaxy interactions (a known starburst trigger; Kennicutt et al. 1987) and the greater gas fractions found at these earlier epochs. While bursting, the energy output of a

[1] Using the K-band luminosity as a tracer of stellar mass, a dwarf galaxy is defined by $M_K > -21$ (Gil de Paz et al. 2003)

starburst dominates the total luminosity of the host galaxy. As a group, local starbursts ($z \ll 1$) provide $\sim$10% of the radiant energy production and $\sim 20 - 25\%$ of all high mass star formation in the local universe (e.g., Heckman 1998; Brinchmann et al. 2004; Lee 2006).

There are a number of competing theories on the role starbursts play in shaping the host galaxy and the impact of starbursts on the host galaxy's evolutionary track. Many authors (e.g., Loose et al. 1986; Silk et al. 1987; Davies & Phillipps 1988; Mayer et al. 2001a,b, 2006) have postulated that starbursts may be a phase of evolution morphing dwarf irregulars (dIrrs) into dwarf spheriodals (dSphs) or ellipticals (dEs). The role of starbursts in this evolutionary scenario may be to assist in the depletion of gas while accounting for the loss of metals to the IGM and to perhaps play a somewhat lesser role in shaping the global structure and dynamics of the galaxy. Using a larger set of dwarf galaxy observations, van Zee et al. (2004) resolve inconsistencies between the angular momentum distribution of dEs and of dIrrs (van Zee et al. 2001b) which could not be previously accounted for if dIrrs morph into dEs. Along a different line of thought, Salzer et al. (2002) suggested starbursts make up a distinct class of dwarfs and that the progenitors of starburst dwarf galaxies are not typical dwarf galaxies. Starbursts would therefore play a more active role in determining the structure of the host galaxy. Despite the uncertainties around the galaxy classification scheme of starbursts (Kennicutt 1998) and the details of its impact (Heckman 2005), it is commonly accepted that starburst events are a significant phenomenon affecting the host galaxy and its environs.

The strength of a starburst can be characterized by three fundamental parameters: its size relative to the host galaxy, the relative intensity of the star formation, and the duration of the burst. If bursts are short in duration, the intensity and size may determine how much impact the burst has on the galaxy, but, if the durations are long, then the overall affect on a galaxy's evolution and structure may be dramatic whether the burst is relatively large, strong or otherwise. The strength of a starburst affects many other processes within the host galaxy. For example, starbursts can drive galactic winds, a potentially important enrichment and heating process of the IGM and a possible natural explanation for the galaxy mass-metallicity relationship (e.g., Lee et al. 2006, and references therein). Understanding the duration parameter is fundamental in understanding the relationship between starbursts and galactic winds (e.g.,

Recchi et al. 2006). It is plausible that longer durations lead more naturally to 'superwinds' (Cooper et al. 2008) therefore successful modeling of galactic winds and the evolution of dwarf galaxies requires an accurate measurement of the duration of a starburst (e.g., Spaans & Norman 1997; Romano et al. 2006). Similarly, models of outflows from bursting systems (i.e., blow-outs and blow-aways) which show different characteristics for an instantaneous burst and for bursts where the energy input is temporally extended (e.g., Mac Low & Ferrara 1999; Ferrara & Tolstoy 2000) need an accurate determination of burst duration. In addition, the burst duration directly affects other inferred parameters such as the chemical yield and the age of the galaxy (Kobulnicky & Skillman 1997). Likewise, interpreting galaxy luminosity functions is dependent upon the burst duration since it is the duration that directly affects the slope of the faint end of the luminosity function as burst galaxies spend more time at low luminosities than at high luminosities (e.g., Hogg & Phinney 1997).

2.1.2 Long vs. Short Durations

Starbursts are thought to be a short-lived phenomenon from an astronomical perspective. Two early papers in the study of dwarf starburst galaxies (Searle & Sargent 1972; Searle et al. 1973) inferred from the composition and colors of these "isolated extragalactic H II regions" that the galaxies are "undergoing intermittent and unusually intense bursts of star formation" (Searle et al. 1973). These authors reason from observations that the blue colors of starburst galaxies are a result of flashes of star formation over timescales of 10^8 yr superimposed over a lower average rate of star formation from the birth of the galaxy 10^{10} yr ago. The shorter timescale indicates that these periods of intense star formation are discontinuous and must be finite or cyclical in nature. The duration of a single burst could be dictated primarily by fuel limitations or by energy and mass transfer feedback mechanisms from the stellar populations of the burst (i.e., supernovae and stellar winds, Thornley et al. 2000; Ferguson & Babul 1998) or by both.

Although starbursts are well-accepted as a short-lived phenomenon, measurements of dwarf galaxy starburst durations are scarce and contradictory, even at the level of distinguishing between possibly artificial delineations of short ("self-quenching"; $\simeq 5$ Myr) and long ($\simeq 100$ Myr) bursts. Observational studies of the emission from Wolf-Rayet (W-R) stars (Schaerer, Contini, & Kunth 1999; Mas-Hesse & Kunth 1999) find

burst durations of $\sim 2-4$ Myr. In the study of W-R galaxies, the strength of the He II λ4686 line relative to the Hβ line is correlated to the total number of W-R stars. A high ratio is interpreted as a short burst producing many W-R stars simultaneously, while a long burst would distribute the W-R stars in time resulting in a relatively weak λ4686 line (i.e., that longer duration bursts tend to dampen spectral features and lead to lower burst parameter strengths). Although the W-R star measurements typically sample a very small area of the galaxy, these studies assume that the spectroscopic observations sample the entire burst population.

On a larger scale, Thornley et al. (2000) studied 27 starburst galaxies using infrared line emission ratios to confirm the presence of massive stars ($M \simeq 50-100$ $M_{\odot}$) in starburst sites. These authors find a declining radiation field hardness inferred from neon ionic abundance ratios, implying that the most massive stars producing the Ne lines have already evolved off the main sequence. The same study used the declining ratio of the bolometric to Lyman continuum luminosity ratio as a timescale for lower mass stars to evolve off the main sequence thereby constraining the IMF and invoking a short duration of $1-10$ Myr to explain the emission ratios. They further suggest stellar winds and supernovae disrupt the gas distribution and destroy the starburst environment limiting durations to $< 10^7$ yr rather than a longer burst governed by a gas consumption timescale.

The studies of star clusters in nearby bursting galaxies have used a number of different methods to measure the duration of starbursts. Tremonti et al. (2001) found ages of $1-8$ Myr for the central clusters in NGC 5253 by fitting starburst models to ultraviolet (UV) spectra, which are sensitive to the young, high-mass, stellar population. They report that the field was populated by stellar clusters dissolving on timescales of 10 Myr. Cluster dissolution would create a bias against observing older clusters constraining the measurement of a burst duration to star formation within an individual stellar cluster. Harris et al. (2004) also report a duration of 10 Myr in star cluster regions in NGC 5253 and in NGC 3077, based on theoretical population synthesis models. In contrast, durations of at least 100 Myr in NGC 5253 have been found by combining the ages of the diffuse stellar population with the bright stellar clusters determined using optical imaging, and Hα and Hβ spectra (Calzetti et al. 1997). Separately, Östlin et al. (2003) used UV and optical observations of ESO 338-IG04 coupled with spectral evolutionary

synthesis models to place a lower bound on burst durations in star clusters at $\sim 40-50$ Myr.

A similar tension between young ($\sim$10 Myr) ages in localized star clusters and older ($\sim$ 100 Myr) ages in the broader star forming regions has also been seen in NGC 1569. Young star clusters and areas of enhanced star formation in NGC 1569 have been dated with ages $\lesssim$30 Myr (Hunter et al. 2000) using integrated UVI colors, although analysis of the optical color magnitude diagrams of the field stars in NGC 1569 yielded elevated star formation over the last 100 Myr (Greggio et al. 1998). Starburst scenarios that incorporate star formation inside and outside stellar clusters find durations based on the UBI colors of the clusters and diffuse light of $10-100$ Myr corresponding to up to 10 times the theoretical crossing time (Meurer 2000). Synthesis modeling in the Hα equivalent width and B$-$V and U$-$B color plane by Lee (2006) converges on bursts with durations of $50-100$ Myr.

On the theoretical side, Tosi et al. (1989) modeled dwarf irregulars in the Local Group by comparing observational color-magnitude diagrams with theoretical simulations and report a burst duration of 5 Myr for the WLM galaxy. Ferguson et al. (1998) also posit that feedback from the burst (stellar winds and supernovae (SNe)) quench future star formation so that only short-duration bursts are possible in very faint (B $\gtrsim$ 24) dwarf galaxies. These authors use the physical conditions, degree of 'burstiness', the detectability of low luminosity galaxies and the fiducial 10 Myr duration to model faint dwarf galaxies, supported by the reasoning that at longer times the type II SNe produced by the burst would heat the interstellar medium preventing any further star formation. In another simulation, Stinson et al. (2007) describe bursting star formation as driving heated gas into a galaxy's halo which quenches star formation. The same gas cools and is later accreted back onto the galaxy triggering another burst in star formation. These authors report an oscillatory period of star formation of $\sim 300-400$ Myr for lower mass to higher mass halos.

In this paper, we present uniform measurements of the durations of starbursts in three nearby bursting dwarf galaxies: NGC 4163, NGC 4068, and IC 4662. The durations are explicitly determined using detailed recent ($\lesssim$1 Gyr) star formation histories derived from resolved stellar populations seen with the Hubble Space Telescope (HST). We apply the same photometric techniques and treatment of differential extinction to

the three galaxies. Our emphasis on uniformity permits a direct comparison of the star formation histories from each galaxy while minimizing systematic uncertainties. §2.2 describes the galaxy sample, the observations and the data reduction process, §2.3 discusses the analysis to determine the burst durations, §2.4 compares our results with past studies and discuss the implications of longer lasting bursts. The last section (§2.5) gives a brief summary of our results. A follow-up publication will extend the analysis to a larger sample of nearby dwarf starburst galaxies.

2.2 The Data and the Analysis Techniques

2.2.1 The Sample of Galaxies and Their Observations

We have selected three dwarf galaxies, NGC 4163, NGC 4068, and IC 4662, for study. These galaxies were identified by Karachentsev et al. (2006) as starburst[2] galaxies based on the properties of their color magnitude diagrams (CMDs) and the population distribution of their blue and red helium burning (BHeB and RHeB) stars. Identifying a burst using its CMD is based on a global qualitative view of stellar populations of the galaxy rather than on a quantitative analysis. The BHeB stars are intermediate mass stars with helium burning cores (Dohm-Palmer & Skillman 2002). The lifetime of this evolutionary stage is relatively short; the typical age of a BHeB star in this region of the CMD ranges from $\sim 5-600$ Myr. At ages great than ~ 600 Myr, the BHeB branch merges into the red clump. A galaxy with a constant star formation rate (SFR) will have a distribution of BHeBs that gradually increases from bright to faint magnitudes with a tendency towards redder colors at the lower magnitudes. In contrast, the CMDs presented by Karachentsev et al. (2006) show an over-density or clustering of BHeBs at intermediate magnitudes closer to the bluer color of the main sequence stars (MS) indicative of the increased recent star formation found in a burst. The population of

[2] Definitions of a starburst system vary significantly. Some definitions use simple calculations about the gas consumption timescale signifying a finite episode of star formation. Others use a comparison between current bursting star formation rates to the star formation rate associated with normal or quiescent star formation activity in the past (cf., Scalo 1986; Kennicutt 1998). There are starburst definitions that look at the strength of ultraviolet and Hα emission to identify current massive star formation (Lee 2006). Bursts have been inferred from the star formation per unit area in specific regions of a galaxy or in star clusters (e.g., Heckman 2005, and references therein). While no definition can be applied indiscriminantly to galaxies at varying redshifts, each definition is useful in a specific context in identifying systems undergoing these intense and unsustainable periods of star formation.

bright main sequence stars is another indicator of recent star formation.

The observations of all three galaxies were originally observed as part of program HST-GO-9771 (PI: Karachentsev, Karachentsev et al. 2006) and were retrieved from the Space Telescope Science Institute archive. The observations consist of 1200 s F606W and 900 s F814W images of each galaxy obtained using the Advanced Camera for Surveys (ACS) Wide Field Channel (WFC) on the Hubble Space Telescope. The images were cosmic-ray split and were cosmic-ray cleaned and processed by the standard ACS pipeline. The observation details as well as other basic parameters, such as the distance and brightness of the galaxies, are summarized in Table 2.1. The F606W images are shown in Figures 2.1−2.3 for NGC 4163, NGC 4068, and IC 4662 respectively. Areas of high surface brightness typically associated with higher stellar density and active star formation can be identified in each image.

Table 2.1 Observational Parameters for Prototype Galaxies

Galaxy	RA	Decl.	HST ID	λ_{606} (sec)	λ_{814} (sec)	Distance (Mpc)	A_R (mag)	M_B (mag)
NGC 4163	12:12:09.1s	+36:10:09s	GO-9771	1200	900	3.0 ± 0.2	0.052	-13.94 ± 0.19
NGC 4068	12:04:00.8s	+52:35:18s	GO-9771	1200	900	4.3 ± 0.2	0.058	-15.17 ± 0.20
IC 4662	17:47:08.8s	−64:38:30s	GO-9771	1200	900	2.4 ± 0.2	0.188	-15.20 ± 0.17

Note − R.A. and Decl. in J2000 coordinates, Distances from Karachentsev et al. (2006, Uncertainties in the distance are estimated to be 8%), A_R, where $\lambda_R = 650$nm, from Schlegel et al. (1998), M_B from de Vaucouleurs et al. (1991).

2.2.2 Photometry and Artificial Stars

Photometry was performed on the pipeline processed, cosmic ray cleaned images (CRJ files) using the ACS module of the DOLPHOT photometry package (Dolphin 2000). The photometry output of DOLPHOT includes several parameters, defined in Dolphin (2000), which characterize the type of point source measured, the amount of crowding in its surrounding environment, the quality of the measurement, etc. Using these parameters, the photometry output file was filtered to select point sources identified as well-recovered stars with a minimum signal-to-noise ratio of 5 and $|\mathrm{F606}_{sharp}+\mathrm{F814}_{sharp}| \leq 0.39$ where a sharpness value of 0 characterizes a perfectly fit stellar PSF while a sharpness value of ± 0.3 in one wavelength represents a well-fit star.

The snapshot observations of the three galaxies reach a photometric depth comparable to the red clump with an absolute V magnitude of $\sim 0 - 1$ given the distance moduli to the galaxies. This photometric depth is sufficient to rigorously determine the most recent (t $\lesssim$ 1 Gyr) star formation history but lacks the necessary completeness at faint magnitudes to provide more than a rough characterization of the lifetime SFH. A photometric depth of at least $\mathrm{M}_V = 2$ is needed to accurately reconstruct the complete SFH of a galaxy (Dolphin 2002). As an assessment of accuracy of our method, a previous study of the Local Group galaxy Leo A with photometry of similar depth (Tolstoy et al. 1998) found an overall SFH that was later verified by Cole et al. (2007) with deep photometry covering the oldest MS turnoffs. The ancient star formation history can be constrained using the RGB stars found above the observations' limits of

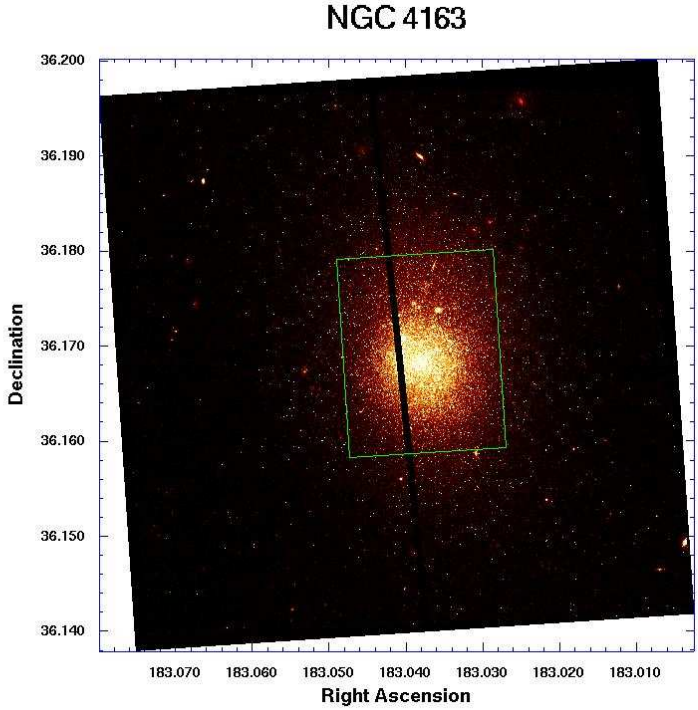

Figure 2.1 ACS F606W image (V filter) of NGC 4163 using 1200 s of exposure. The green box encloses the area of higher stellar density where additional artificial stars were applied. SFH analysis was performed on the entire image and compared with the SFHs derived separately for the region of higher stellar density inside the box and the region of lower stellar density outside the box.

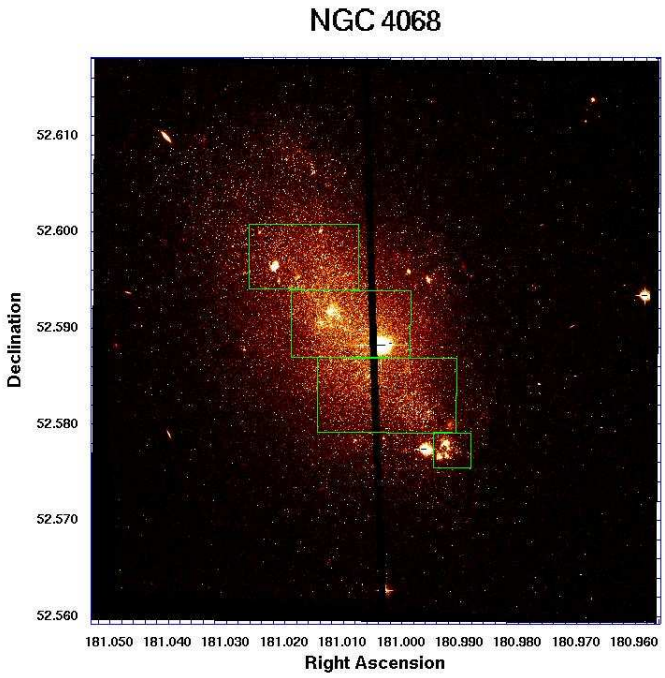

Figure 2.2 ACS F606W image (V filter) of NGC 4068 using 1200 s of exposure. The green boxes encloses the area of higher stellar density where additional artificial stars were applied. SFH analysis was performed on the entire image and compared with the SFHs derived separately for the region of higher stellar density inside the boxes and the region of lower stellar density outside the boxes.

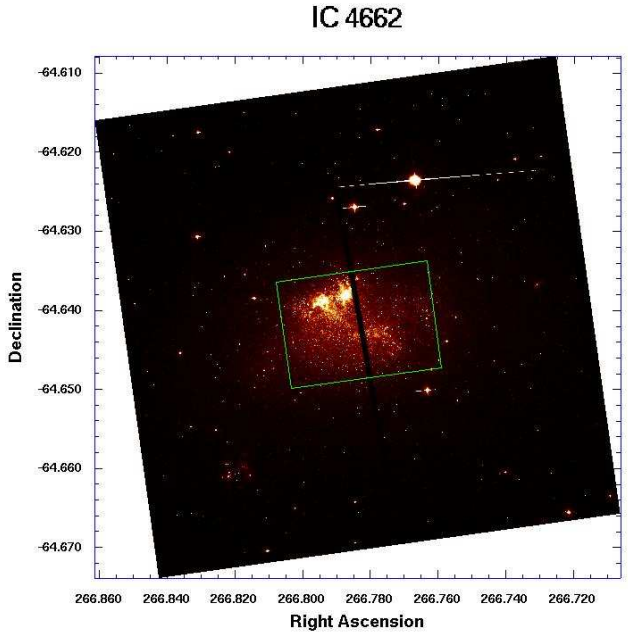

Figure 2.3 ACS F606W image (V filter) of IC 4662 using 1200 s of exposure. The green boxes encloses the area of higher stellar density where additional artificial stars were applied. SFH analysis was performed on the entire image and compared with the SFHs derived separately for the region of higher stellar density inside the boxes and the region of lower stellar density outside the boxes.

these data, but the SFRs have additional uncertainties because of the covariance between time bins (Dolphin 2002). These uncertainties affect the rate within a particular time bin at large look-back times, but the total amount of star formation over the 14 Gyr and the averages are robustly derived numbers determined from our observational data (e.g., Dohm-Palmer et al. 1997).

The CMDs resulting form our photometry for the three galaxies are shown in Figures 2.4−2.6. Typical photometric errors per magnitude bin are shown in each of the CMDs in each figure, and the loci of the MS and BHeB populations are indicated by the superimposed lines. All three CMDs show MS and BHeB branches which are broadened to some extent. This broadening is due to three factors: photometric errors, crowding, and differential extinction. In the areas of highest stellar density, crowding will affect photometric accuracy (e.g., Greggio et al. 1998; Dohm-Palmer & Skillman 2002). The crowding causes an additional photometric uncertainty in the MS and BHeB branches (e.g., $\lesssim$ 0.03 mag at V$\sim$ 24.5) which are underestimated in the average photometric errors presented in the CMDs. We chose to include the point sources in areas of crowding with higher photometric noise rather than eliminate a fraction of the stars in which we are most interested. Both Galactic foreground differential extinction, when present, and differential extinction within the galaxy (see §2.3.1) will broaden the evolutionary sequences. Two of the three - NGC 4163 and NGC 4068 - have little foreground Galactic extinction ($A_R = 0.05$ mag and 0.06 mag, respectively, Schlegel et al. 1998) lying well off the Galactic plane. The third galaxy, IC 4662, lies closer to the Galactic plane with a Galactic latitude $b = -17.8$ We find an A_V value of ~ 0.3 mag, somewhat higher than the Galactic extinction found by Schlegel et al. (1998) of $A_R = 0.19$ mag and $\simeq 0.2-0.4$ mag of differential extinction internal to IC 4662. The additional blending of the evolutionary sequences due to differential extinction in this galaxy is explicitly accounted for in CMD fitting program (see §2.3.1). While these three factors create MS and BHeB branches that are somewhat blurred in the CMDs, one can still distinguish the separation between the two branches and the broadening does not affect the reconstruction of the star formation history.

The CMD of NGC 4163 (Fig. 2.4) contains the fewest number of recovered stars (66,000) and shows the least populated BHeB branch of the three galaxies, but has clearly undergone recent star formation. The more populated BHeB branch of NGC 4068

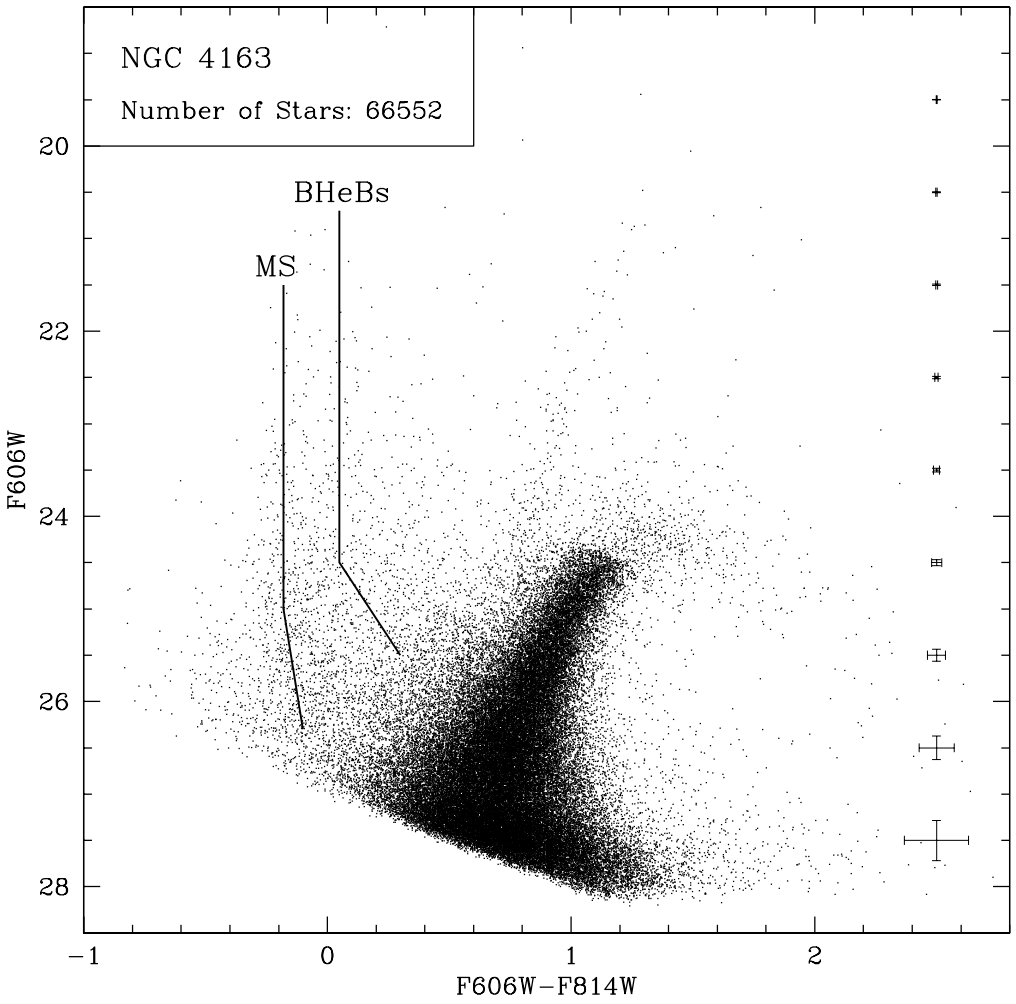

Figure 2.4 The full field V vs. V−I color magnitude diagram for NGC 4163 contains over 66,000 stars. The TRGB, main sequence branch, and BHeB stars are identifiable in the CMD as well as the AGB stars and red supergiants. The distinct BHeB branch at V−I$\sim$ 0 spanning a V magnitude range of 21 and fainter distinguishes this galaxy as a starburst system. There is $\lesssim$ 0.1 mag of foreground extinction not corrected for in the CMD. The data are plotted to a signal-to-noise level of 5 which is approximately the 50% completeness limit.

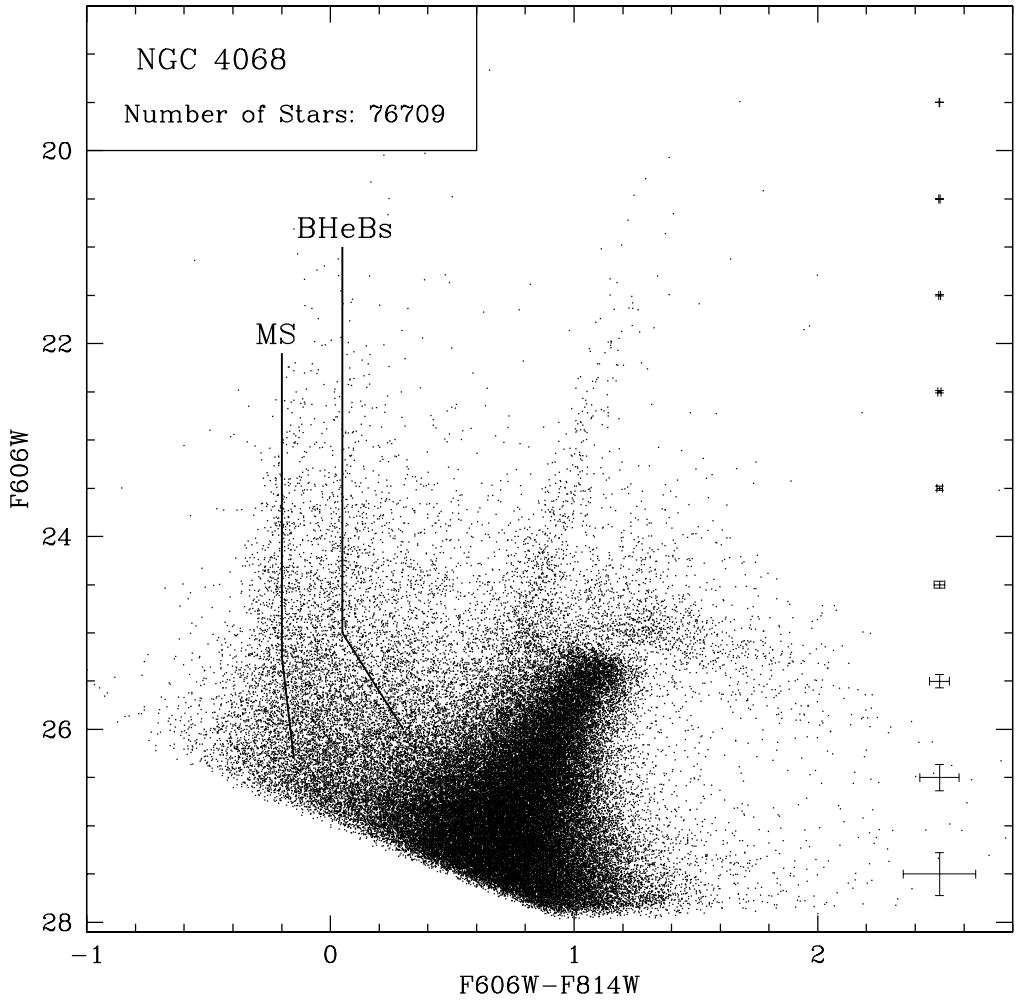

Figure 2.5 The full field V vs. V−I color magnitude diagram for NGC 4068 contains over 76,000 stars. The distinct branch of BHeB stars at V−I$\sim$ 0 spanning a V magnitude range of 21 and fainter is more defined than NGC 4163 suggesting a larger burst in this galaxy. There is $\lesssim$ 0.1 mag of foreground extinction not corrected for in the CMD. The data are plotted to a signal-to-noise level of 5 which is approximately the 50% completeness limit.

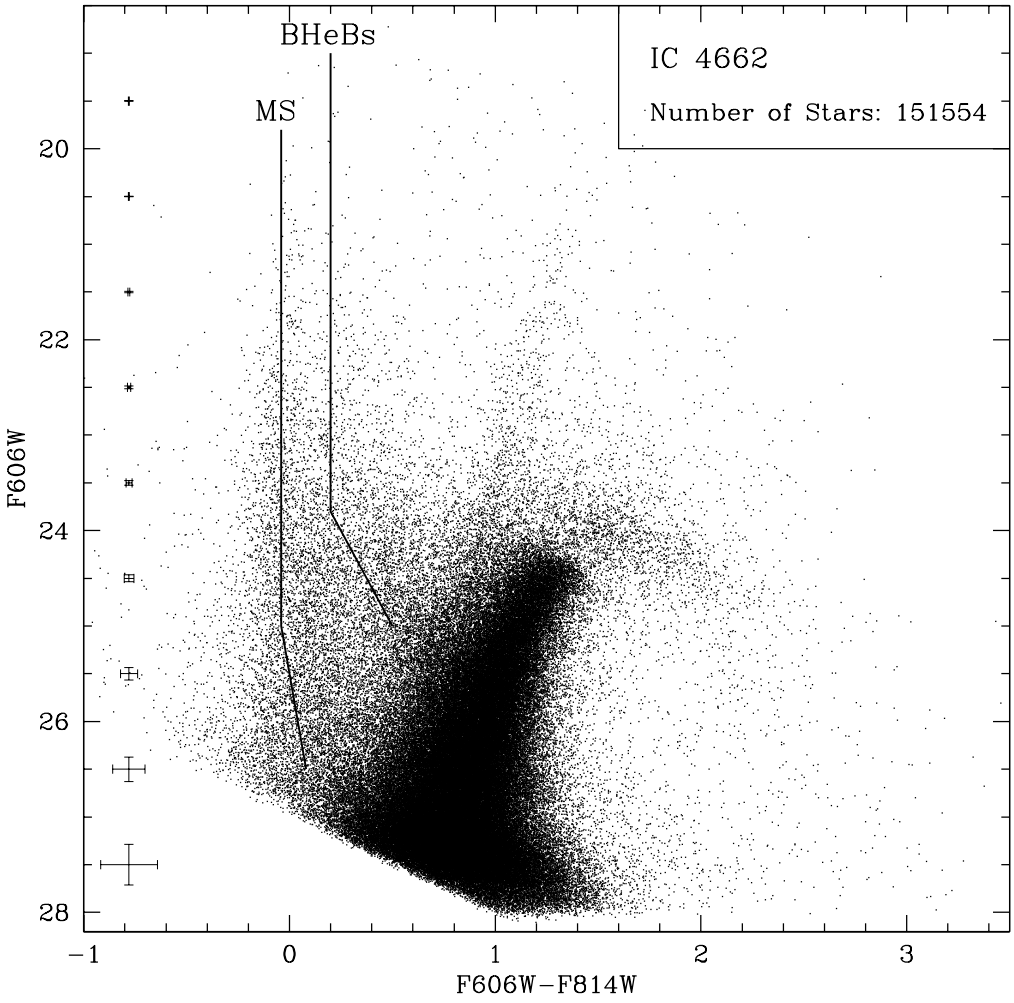

Figure 2.6 The full field V vs. V−I color magnitude diagram for IC 4662 contains over 150,000 stars; the largest number of stars recovered photometrically in our sample. The TRGB, main sequence branch, and BHeB stars are clearly identifiable in the CMD and well populated. The distinct BHeB branch is slightly redward of the other two galaxies at V−I$\sim$ 0.25 spanning a V magnitude range of 19 and fainter, also distinguishing this galaxy as a starburst system. The main sequence and BHeB stars are blended at V magnitudes fainter than 24 due to the higher amount of foreground extinction ($\lesssim$ 0.5 mag) found in the field of view which is not corrected for in the CMD. The data are plotted to a signal-to-noise level of 5 which is approximately the 50% completeness limit.

(Fig. 2.5) indicates a stronger burst. The BHeB branch in IC 4662 (Fig. 2.6) is the most blended with the main sequence due to the higher foreground extinction and differential extinction present in the field of view of this galaxy. There is a small amount of foreground contamination seen in the CMD at bright magnitudes at a $V - I$ color of $\simeq 0.8$. It is the closest of the three galaxies with the deepest observations and contains the largest number of stars (150,000) in our sample.

To quantify the completeness of the data and the photometric uncertainty, we conducted artificial star tests both on the global image of each galaxy and on selected regions of each galaxy (regions highlighted in Figures 2.1-2.3). Taken together, the two regions in each galaxy cover the entire field of view and were selected based on the relatively uniform surface brightness (i.e., stellar density) within each region. Applying false star tests to individual regions was useful in a number of ways. First, it allowed for a detailed SFH to be reconstructed on regions of more uniform characteristics which could then be compared to the global SFH results for a galaxy. Secondly, it allowed for a more precise determination of the location of a burst within a galaxy and facilitated a comparison of the SFRs in different regions. Thirdly, it served as one of the many tests we performed on the photometry probing the fidelity and accuracy of our results. We present completeness plots for the regions of lower and higher stellar density as well as for the global solution for the three galaxies in Figure 2.7. The completeness plateaus at $\simeq 88\%$ in the global and lower density regions due to bad pixels and cosmic rays as the observations were obtained during single HST orbits (CRSPLIT = 2). The completeness for the region of higher stellar density is not easily quantified as the confusion limit is reached in these areas artificially increasing the completeness at bright magnitudes; as an upper limit, the completeness limit must be below the 88% found for the less crowded regions. The CMDs for each galaxy (Figs. 2.4−2.6) are plotted to a signal-to-noise ratio of 5 which corresponds approximately to the 50% completeness limits. The final artificial star lists were filtered using the same parameters applied to the photometric output.

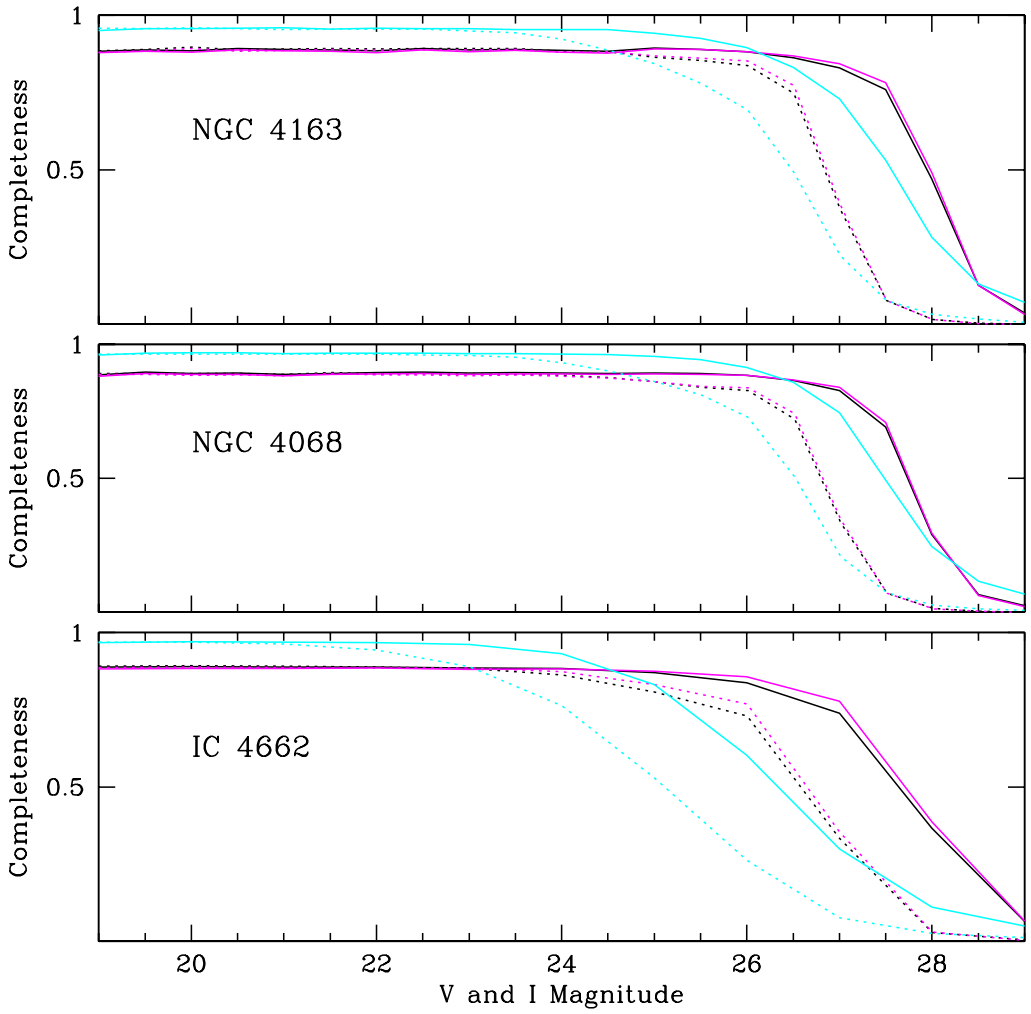

Figure 2.7 Completeness as a function of magnitude for the three galaxies. The V (solid lines) and I (dashed lines) magnitude completeness limits are shown for the global solution (black), the lower density region (magenta), and the higher density region (cyan). The region of higher density reaches the confusion limit at bright magnitudes which artificially elevates the completeness limit.

2.3 The Burst Measurements

2.3.1 Star Formation Histories

The star formation histories of the three galaxies were reconstructed using the color-magnitude diagrams. The photometry, observational errors, and incompleteness (i.e., artificial star recovery fractions) were used along with the stellar evolutionary models of Marigo & Girardi (2007) in the SFH numerical method MATCH (Dolphin 2002). This CMD fitting program constructs a synthetic CMD based on the observed CMD and varies the metallicities and ages of the stellar populations. How well the observed and modeled CMDs match is quantified with a effective χ^2 parameter (Dolphin 2002) and reflects the likelihood of the SFH derived from the model CMD to be the true SFH of the observed galaxy. The χ^2 per degree of freedom for our analysis was 1.3 in all cases except in the high surface brightness regions of IC 4662 where we achieved our best fit of 1.1, indicative of excellent fits. The modeled CMDs are presented as Hess diagrams in Figures 2.8−2.11 alongside the observed CMDs at the same axis scale for comparison. The Figures show that the models characterize all of the features of the CMDs quite well. The best-fit synthetic CMD of the galaxy is based on a SFR as a function of time and metallicity which is the most likely SFH of the galaxy given our inputs and models (i.e., Dolphin et al. 2003; Weisz et al. 2008).

Numerous tests of the numerical method (e.g., Dolphin et al. 2003) have shown that the results robustly determine the SFR as a function of time and metallicity SFR(t,Z). The best modeled CMD fitting the observed data uses the most probable combination of distance to the galaxy and foreground extinction which can be directly compared with literature values. Given the large amount of gas present in a starburst galaxy needed to fuel the star formation, most starburst galaxies exhibit signs of differential extinction in their CMDs which blends the branches of stellar evolution. Therefore, differential extinction is applied within the CMD fitting program to the young stars in each galaxy decreasing linearly from A_v=0.5 for stars younger than 40 Myr to A_v=0.0 for stars older than 100 Myr (Dolphin et al. 2003).

We applied several tests on the data to measure the effects extinction and photometric broadening may have on the SFH solutions in all parts of the CMDs. For example, selecting point sources with a more tightly constrained sharpness parameter

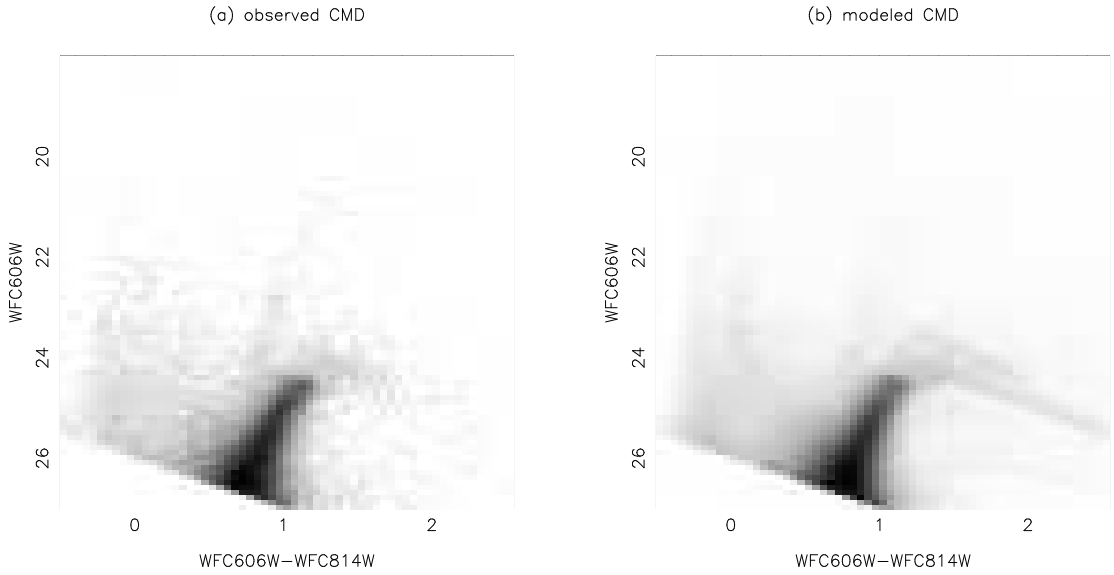

Figure 2.8 The Hess diagram of the NGC 4163 observations and the best-fit synthetic Hess diagram of the galaxy.

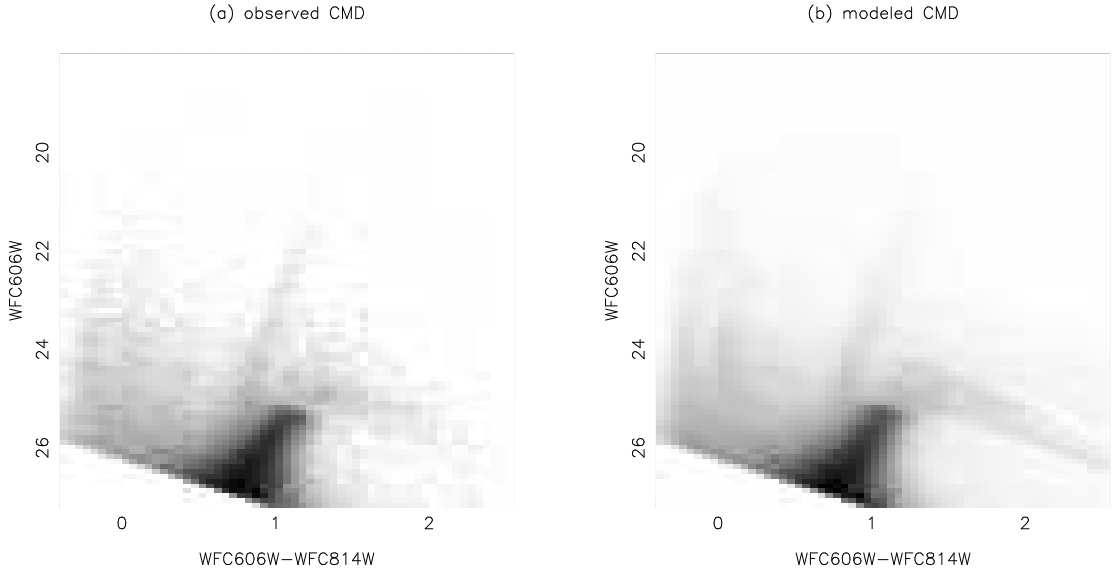

Figure 2.9 The Hess diagram of the NGC 4068 observations and the best-fit synthetic Hess diagram of the galaxy.

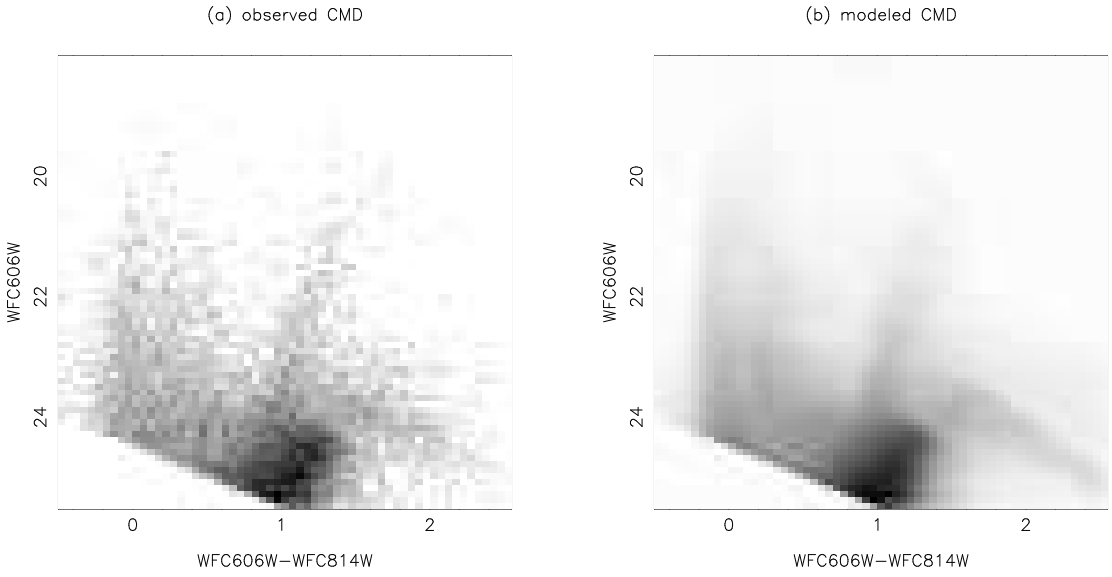

Figure 2.10 The Hess diagram of the IC 4662 observations in the region of highest surface brightness and the best-fit synthetic Hess diagram of this region of the galaxy. Note the spread in the Red Giant Branch evolutionary track due to higher photometric errors from crowding in this part of the galaxy. There is also a significant amount of new star formation as evidenced by the well-populated Main Sequence and Blue Helium Burning branches. One of the signatures of differential extinction can also be seen in the partial blending of these two branches.

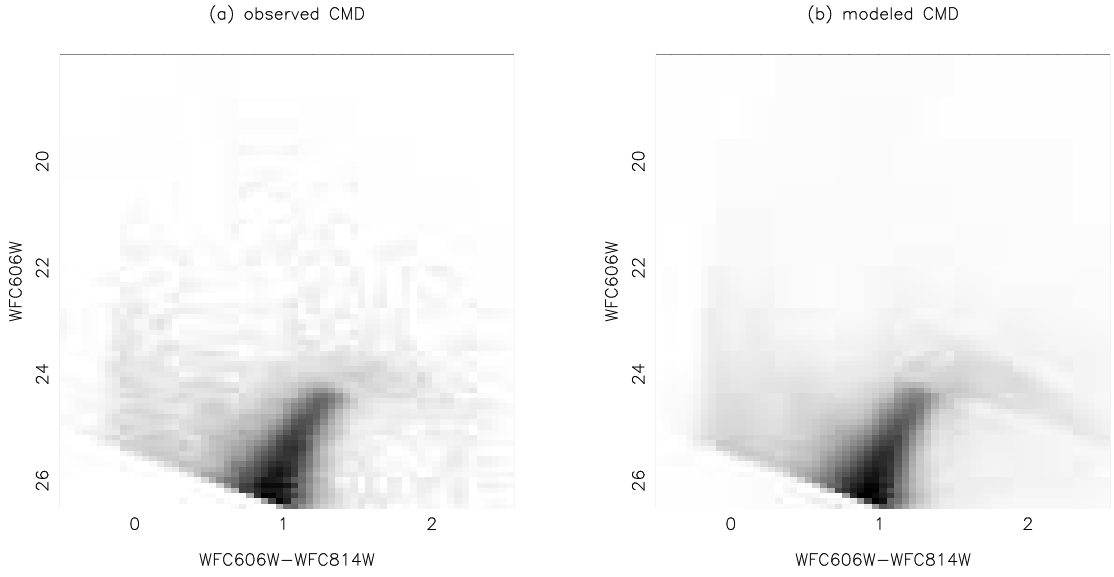

Figure 2.11 The Hess diagram of the IC 4662 observations in the region of lowest surface brightness and the best-fit synthetic Hess diagram of this region of the galaxy. Note the tighter Red Giant Branch evolutionary track than in Figure 2.10 due to lower photometric errors in this less crowded region of IC 4662.

(i.e., $|F606_{sharp}+F814_{sharp}| \leq 0.27$) or point sources outside areas of highest crowding, did not change the SFH profiles or the duration of the burst derived. Likewise, assuming a higher level of extinction in the field of view than is actually thought to be present did not change the SFH profile or the burst duration. While these tests may suppress the absolute values of the SFR, we found that, regardless of the crowding of point sources in regions of higher stellar density and differences in foreground extinction present in our sample, the recent SFHs and the starburst duration measurements were robustly derived and our results remained the same.

The errors from the fitting program quantify the systematic uncertainties in the SFHs due to variations of the real data from the theoretical stellar evolution models. Statistical uncertainties were estimated using Monte Carlo simulations on the star formation history solutions. The final uncertainties presented in the SFRs were calculated by adding in quadrature the statistical uncertainties with the systematic uncertainties in SFRs.

The distance and foreground extinction values fit using the stellar evolutionary isochrones in the program are compared to values found in the literature for all three galaxies in Table 2.2. The distance moduli are in close agreement with the value determined from the TRGB by Karachentsev et al. (2006). The foreground extinction for NGC 4163 and NGC 4068 are very close to the values reported by Schlegel et al. (1998). We find a higher foreground extinction value for IC 4662 which may be a result of the low resolution of the observations by Schlegel et al. (1998).

The regions of varying stellar density studied for differing photometric completeness (§2.2.2) were also analyzed from a star formation history perspective. In two of the three galaxies, NGC 4163 and NGC 4068, the star formation history results for the regions and the global field of view were well fit by the modeled CMDs. The summation of the SFRs from the two regions was nearly identical to the SFRs found for the global data. We use the results from the single, global field of view for these two galaxies throughout the paper to calculate the duration of the starbursts in these two galaxies. The spatial information obtained from the separate regions is retained and analyzed separately in §2.3.3. The star formation history of the third galaxy, IC 4662, was more difficult to fit due to the more complex environment and higher extinction in this galaxy. We found

Table 2.2 Comparison of Distance, Extinction, and Metallicity Values Modeled for the Prototype Galaxies

Galaxy	(m − M)	(m − M)	Total A_V (mag)	Foreground A_R (mag)	[M/H] (dex,mag)	[Fe/H] (dex,mag)
(1)	(2)	(3)	(4)	(5)	(6)	(7)
NGC 4163	27.40±.04	27.36	0.03 ± 0.04	0.05	-0.9,0.2	-1.65,0.14
NGC 4068	28.17±0.04	28.17	0.04 ± 0.04	0.06	-1.0,0.1	NA
IC 4662: HSB[a]	26.80±0.04	26.94	0.3±0.04	0.19	-1.2,0.1	-1.34,0.23
IC 4662: LSB[b]	26.80±0.04	26.94	0.4±0.04	0.19	-1.4,0.3	-1.34,0.23

[a] HSB refers to the high surface brightness region.
[b] LSB refers to the low surface brightness region.

Note − Col. (2) Distance Modulus best fit by the CMD fitting program. The uncertainties are lower bounds as they include only statistical uncertainties. Col. (3) Distance Modulus reported by Karachentsev et al. (2006). Col (4) Foreground and internal extinction best fit by the CMD fitting program. The uncertainties are lower bounds as they include only statistical uncertainties. Col. (5) Galactic extinction at $\lambda_R = 650$ nm reported by Schlegel et al. (1998). Col (6) Metallicity estimated by the CMD fitting program for elements heavier than Hydrogen. Col. (7) Metallicity reported by Sharina et al. (2008). The second value (mag) is the uncertainty of $V - I$ of the RGB at $M_I = -3.5$.

that for IC 4662, splitting the galaxy into two regions of similar stellar density characteristics allowed the CMD fitting program to match the modeled CMD to the observed data more robustly. The higher surface brightness region was best fit by applying 0.4 mag of internal differential extinction while the lower surface brightness region matched best with a slightly lower value of 0.2 mag. The final SFRs were calculated by summing the rates from the two regions and adding their uncertainties in quadrature.

The bursts for NGC 4163, NGC 4068, and IC 4662 identified in the CMDs are confirmed in the reconstruction of each galaxy's star formation history. We present the star formation histories for the lifetime of each galaxy in Figure 2.12 including systematic and statistical uncertainties. The ancient SFRs have been averaged over larger time bins as there is little distinction in the color-magnitude diagram between stars formed with any greater time resolution without deeper observations. The uncertainties in the older time bins are smaller due to this averaging over a longer time period. The recent SFRs are shown with a finer time resolution as these earlier times can be more precisely derived from the data. Figure 2.13 highlights the star formation from the past 1 Gyr only. The higher SFR in the recent time bins reflects the clustering of BHeBs identified in the CMD and delineates these dwarf galaxies as starburst systems. The durations

are clearly resolved by this technique.

NGC 4163. This galaxy is the second closest blue compact dwarf (BCD) galaxy and is part of the Cane Venatici I (CVn I) cloud (Karachentsev et al. 2006). It is the most spherical in morphology of the three dwarf galaxies in our sample. The star formation history in Figure 2.13 shows an elevated SFR in recent time bins but the burst is not ongoing in the present day in this post-starburst galaxy. In comparison with the other two galaxies, NGC 4163 has the lowest amplitude burst of the sample.

NGC 4068. This galaxy is also a BCD and member of the CVn I cloud, although it is significantly farther than NGC 4163 (Karachentsev et al. 2006). There are a number of prominent star forming regions in the image and the SFR shows a ramp in star formation activity from a very quiescent period to a burst at the present day.

IC 4662. This isolated galaxy is the closest blue compact dwarf (BCD) galaxy and has large extended regions of star formation visible in the optical images (Karachentsev et al. 2006). IC 4662 is considered a bursting galaxy based on its Hα EW measurements (Lee 2006) and by the SFRs derived from their Hα spectra (e.g., Hunter & Elmegreen 2004; Kaisin et al. 2007). The SFRs in Figure 2.13 are a composite of star formation activity summed from the regions of differing stellar density in the galaxy.

2.3.2 Measuring the Durations of Three Starbursts

Measuring a burst duration requires defining the beginning and ending points of a burst event. The profile of the SFR across time can be a guiding indicator in determining the characteristic level of a burst and dictate the bursts' temporal limits. However, because of the stochastic nature of star formation, precisely defining these temporal limits is somewhat problematic and potentially very subjective. Quantitatively, a useful parameter to consider is the birthrate parameter, b, which compares the SFR of a given time bin to the average SFR over the life of a galaxy (e.g., $b \equiv$ SFR / $<$SFR$>_{past}$ Scalo 1986; Kennicutt 1998). However, most dwarf galaxies show evidence of an elevated period of star formation early in the history of the universe during initial galaxy assembly. This has been known for some time for the gas poor dwarf spheriodals (e.g., Mateo 1998; Grebel 2001), but recent observations of the gas rich dwarf irregulars also show similar evidence (e.g., Skillman et al. 2003; Dolphin et al. 2005). Thus, for our purposes, a lifetime average star formation is inflated by this early epoch of star formation and is

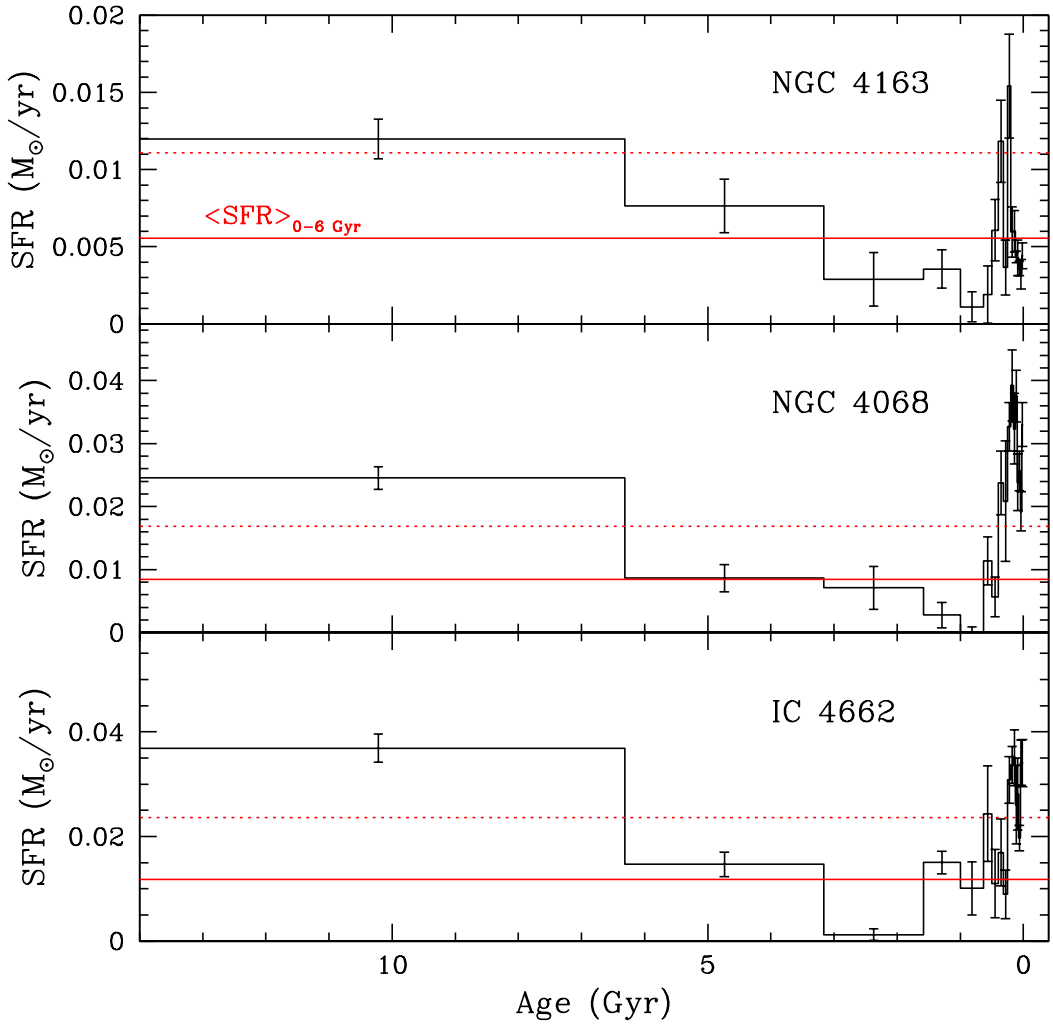

Figure 2.12 Complete SFRs for NGC 4163, NGC 4068, and IC 4662 for the last 14 Gyr. The solid line is the average SFR for the galaxy during the last 6 Gyr as discussed in §2.3.2. The dotted line is twice this average. The final solution for IC 4662 used in the determination of the starburst duration is the summation of the SFRs from the regions of high and low stellar densities.

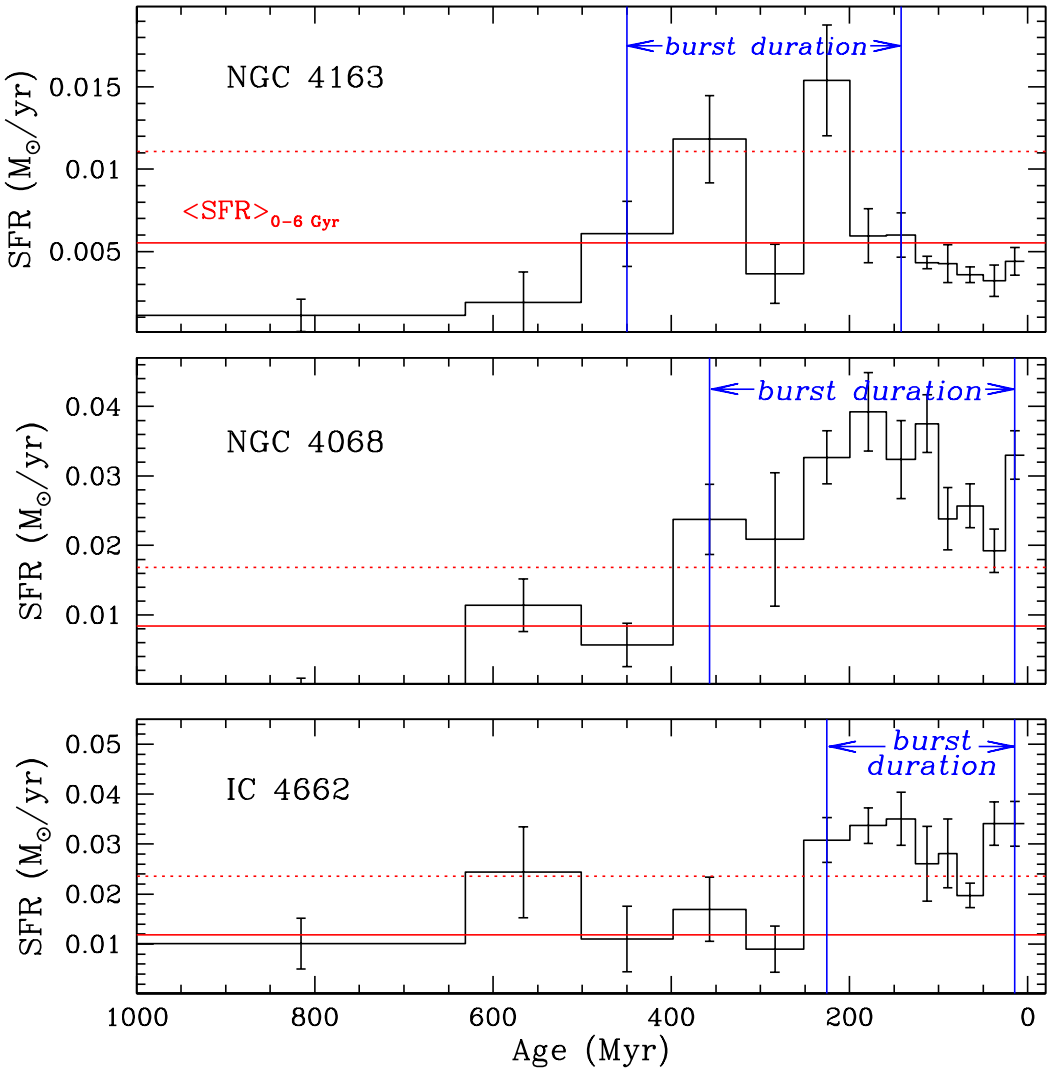

Figure 2.13 SFRs for NGC 4163, NGC 4068, and IC 4662 for the last 1 Gyr. The solid red line is the average SFR for the galaxy during the last 6 Gyr as discussed in §2.3.2. The dotted red line is twice this average. The beginning and end of the starbursts are marked in blue vertical lines. The final solution for IC 4662 used in the determination of the starburst duration is the summation of the SFRs from the regions of high and low stellar densities.

significantly higher than the average star formation rate in the current epoch. Since it is increased star formation in the current epoch that we are concerned with, we introduce a birthrate parameter for recent time epochs $b_{recent} \equiv$ SFR / $<$SFR$>_{6-0Gyr}$ (which excludes our earliest time bin) to study the profile of SFR and restrict our analysis to times after the initial assembly of the galaxy. The SFRs over the last 6 Gyr should be more indicative of the behavior of an unperturbed star forming disk and applies the more recent SFRs as a metric for determining the beginning and ending points of a burst.

An empirical value of $b = 2$ has been suggested as a threshold for dwarf galaxy starbursts by Kennicutt et al. (2005) while Brinchmann et al. (2004) report a range of $b = 0.1 - 30$ for a wider demographic of starburst galaxies. The value of b has a strong redshift dependence (typical values of b for starbursts being lower at high redshift due to the different levels of star formation activity present at those times) which cautions against choosing an absolute value of b to denote starbursts across cosmological scales. Our galaxy sample is restricted to nearby galaxies so we will consider b to be a definite quantity in this limited context. We compare the average SFR over the last 6 Gyr with the SFR in recent time bins (i.e., b_{recent}). Following Kennicutt et al. (2005), we use $b_{recent} \geq 2$ to identify bursts and a threshold of $b_{recent} \simeq 1$ to demarcate the beginning and end of the bursts. The cut-off value of $\simeq 1$ includes the ramp up time to a peak burst SFR and the ramp down to a lower, more sustainable SFR. The SFRs for $b_{recent} = 1$ and 2 are plotted in Figure 2.13 with the beginning and end points of the burst marked for each galaxy. The durations, presented in Table 2.3, range from 225 ± 25 to 385 ± 50 Myr. For NGC 4068 and IC 4662, the durations are lower limits since the starbursts are ongoing at the present day. NGC 4163 may be better described as a post-starburst system with the recent burst ending ~ 65 Myr ago. This system shows a more complete SFR profile of a starburst with an elevated trailing SFR after the peak of the burst.

The uncertainties are driven by the resolution of the time bins shown in Figure 2.13. The maximum value of b for a galaxy listed in Table 2.3 gives a perspective on the relative intensities of the bursts using each galaxy's unique star formation history. The durations measured were not sensitive to the different input parameters to CMD fitting program. The bursts are clearly identifiable from the BHeB and MS branches of the CMDs and are robustly derived for these galaxies. The implications of the lengths of

Table 2.3 Duration of Starbursts in Prototype Galaxies

Galaxy	Peak $SFR_{1\text{-}0\ Gyr}$ ($M_\odot yr^{-1}$)	Peak b_{recent} ($0-1$ Gyr)	$< SFR >_{6\text{-}0\ Gyr}$ ($M_\odot yr^{-1}$)	Duration for b=1 (Myr)
NGC 4163	0.015 ± 0.003	2.7 ± 0.5	0.0055 ± 0.0002	308 ± 50
NGC 4068	0.039 ± 0.006	4.6 ± 0.8	0.0084 ± 0.0006	360 ± 40
IC 4662	0.042 ± 0.004	3.5 ± 0.4	0.012 ± 0.001	225 ± 25[a]

[a]This is most likely a double burst separated by a lower level of SF activity whose rate still exceeds the average.

these burst durations will be discussed in §2.4.

2.3.3 Global Bursts vs. Localized Star Clusters

The starbursts in the dwarf galaxies NGC 4163, NGC 4068, and IC 4662 are not limited to the areas that appear to be bursting at the present day in the optical images (i.e., regions of highest surface brightness and stellar density). Rather, when averaged over the last $200-400$ Myr, the bursts are more global in nature. We studied the regions where bursts *appeared* to be localized in the images (i.e., the regions of higher surface brightness where we applied separate artificial star tests detailed in §2.2.2) and compared these regions' SFR to the rates in the seemingly non-bursting areas (i.e., the regions of lower surface brightness also discussed in §2.2.2) of each galaxy. The comparisons showed that although the low surface brightness regions do not exhibit starburst characteristics in the image, they have indeed been sites of significant star formation activity in the recent past (t< 400 Myr) as shown in Figure 2.14. In two of the three galaxies, NGC 4163 and IC 4662, the elevated star formation in the two regions lag one another, with the most recent high SFRs occurring in the most crowded, highest surface brightness regions, and with the lower surface brightness areas showing higher SFRs in the adjacent earlier time bins. In NGC 4163, the most recent SFR is concentrated entirely in the high surface brightness region of the optical images. However, there has been star formation of burst proportions in the outer regions of the galaxy ~ 300 Myr

ago, just prior to the present day activity (top panel; Figure 2.14). A similar pattern is seen in IC 4662 (bottom panel; Figure 2.14) where the lower stellar density regions show bursting levels of star formation $\sim$ 200 Myr ago. The third galaxy in our sample, NGC 4068, shows bursting levels of star formation in both the concentrated regions of stars and the outer regions of the galaxy in the most recent times bins without any time lag. Elevated levels of star formation do not appear to be limited to areas of high stellar density but can be pronounced in areas of low stellar density as well.

When approached from a 1 Gyr perspective, it appears the bursts have been more global in nature, migrating through different parts of a galaxy. Although the SFR may be unsustainable for the durations of $\sim$ 200$-$ $\sim$ 400 Myr in any particular region of a galaxy due to fuel limitations and possible feedback mechanisms, it appears that the starburst event moves around the galaxy. The burst therefore affects much more of the structure and dynamics of the host galaxy than a local phenomenon could, and is sustainable for longer duration periods of $\sim 10^8$ yr. The idea that starbursts can be more global in nature agrees with what Cannon et al. (2003) found in NGC 625. These authors report that the star formation is widespread over the past 100 Myr. Other authors report a related result that bursting star formation in starburst galaxies is not confined to star clusters but is found throughout the diffuse star formation in NGC 3310 (Meurer 2000) and in field stars outside the central super star cluster (SSC) in NGC 1705 (Annibali et al. 2003).

One of the frequently calculated parameters for starbursts is the intensity of star formation per unit area or Σ ($M_{\odot}yr^{-1}$ kpc^{-1}). It is a useful parameter because it is closely related to the gas surface mass density and because it more closely reflects local disk physics than global quantities like the total SFR (Heckman 2005). However, the intensity also relies on having a well-defined area for a burst. Given that the complete burst event appears to migrate around the galaxy, the intensity depends on the definition of the area, which changes during the burst. Additionally, elevated rates of star formation in the lower stellar density regions contribute to the SFR in even the most recent time bins, making a definition of area even more ambiguous. Thus, while the intensity parameter is useful in quantifying the intensity of *instantaneous* star formation associated perhaps with super star clusters highlighted in the UV and other wavelengths, it could also be misleading for longer, spatially distributed SF events.

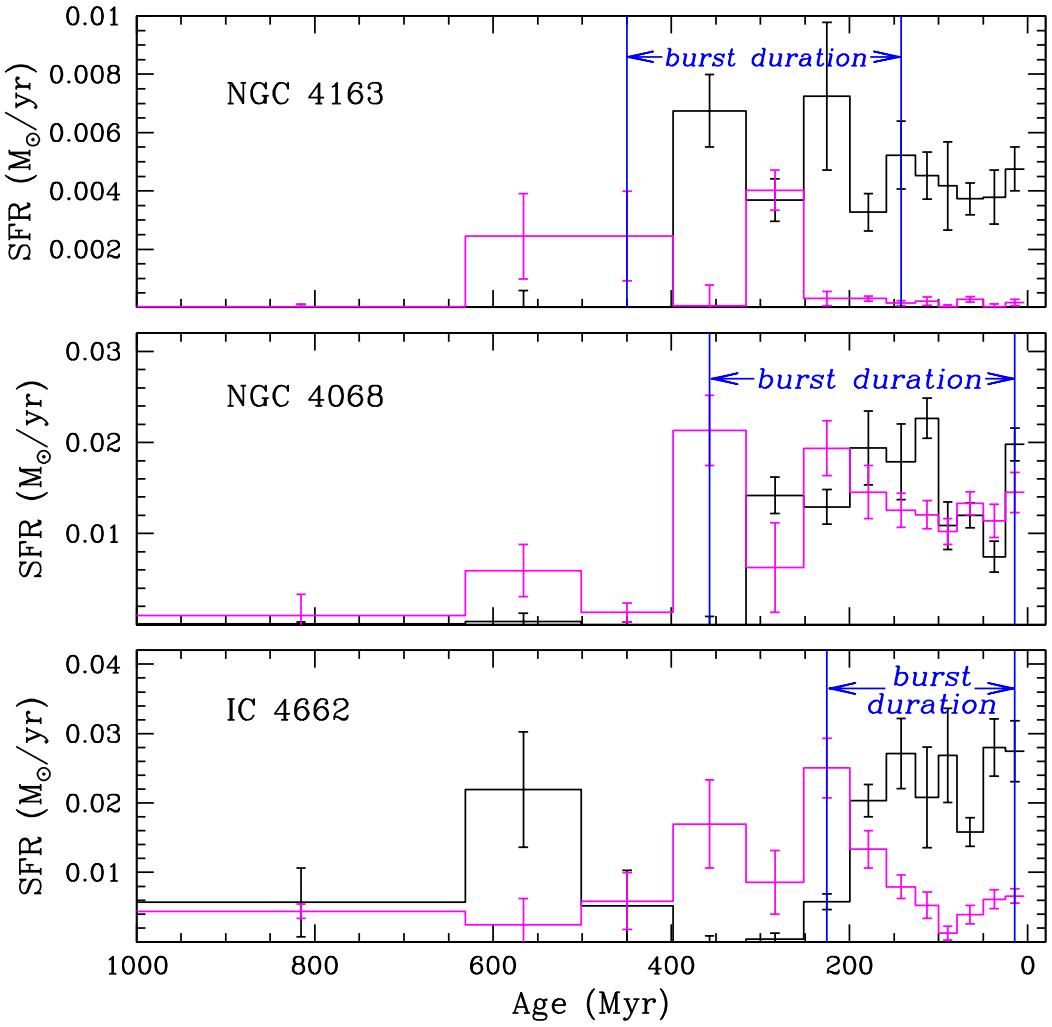

Figure 2.14 SFRs for NGC 4163, NGC 4068, and IC 4662 from the regions of high (black line) and low (magenta line) stellar densities. The beginning and end of the starbursts are marked in blue vertical lines. Note the temporal shift of the peak SFR in the different regions. In NGC 4163 and IC 4662, the areas that appear to be bursting in the optical image show the peak SFR in more recent time bins than the non-bursting regions in the images suggesting that the burst has migrated within the galaxy over the past few hundred million years. NGC 4068 shows star formation with bursting characteristics in both regions of the galaxy in all recent time bins.

2.4 Implications of Longer and More Global Bursts

2.4.1 Flickering Star Formation within a Burst

Previous measurements of $10^6 - 10^7$ yr starburst durations (see references in §2.1) are probably measuring only part of a longer starburst event. Within a starburst galaxy, there are localized regions of intense star formation that are readily studied at many wavelengths due to the intensity of emitted radiation. The duration of star formation measured in such areas can depend on the wavelength observed. For example, timescales derived using Hα or ultraviolet emission measurements will be on the order of the lifetime of the massive stars producing the Hα or UV radiation (i.e., $\sim$ 10 Myr). We briefly summarize some of the durations from the literature and the wavelength from which the duration was derived in Table 2.4. Many studies adopt an instantaneous burst model, assuming that the formation of thousands of massive stars within a short period of time ($\simeq 10^6$ yr), would disrupt any additional significant star formation by the mechanical energy injected into the area (e.g., Mas-Hesse & Kunth 1999; Mas-Hesse et al. 2000, and references therein).

Table 2.4 Previous Methods Used to Determine Durations and Their Results

Wavelength Regime	Object(s)	Duration (Myr)	Authors
Short duration starbursts			
Far-UV Spectra	7 Blue Compact galaxies	<10	Fanelli et al. (1988)
W-R Stars	37 Wolf-Rayet galaxies	$\sim$ a few	Conti (1991)
UV Spectra & Images, FIR	9 Starburst galaxies	<10	Meurer et al. (1995)
Optical Spectra & W-R Stars	17 Starburst objects	< 7	Mas-Hesse & Kunth (1999)
Optical Images, CMD	1 Starburst Galaxy	$10 - 15$	Annibali et al. (2003)
Infrared Spectra	27 Starburst galaxies	~ 10	Thornley et al. (2000)
UV Spectra	NGC 5253	$1 - 8$	Tremonti et al. (2001)
Far-Infrared & Radio	2 Wolf-Rayet galaxies	4 & > 30	Yin et al. (2003)
Long duration starbursts			
Optical Images, CMD	1 Starburst galaxy	$50 - 100$	Cannon et al. (2003)
Optical Images	1 Starburst galaxy	$\simeq 100$	Meurer (2000)
Hα Spectra	$\sim$ 400 SF galaxies	$50 - 100$	Lee (2006)

However, as we have shown, the starburst phenomenon can be a longer and more global event than related by the lifetime of individual stars or pockets of intense star formation. The short duration timescales are instead a measure of the "flickering" created

by currently active pockets of star formation that move around the galaxy. Measuring the characteristics of just one of these flickers reveals much about an individual star formation region but does not measure the totality of the starburst phenomenon in the galaxy. If starbursts are indeed a global phenomenon, then the events are longer than the lifecycle of any currently observable massive star or area of intense star formation and the bursts are *not* instantaneous. An observation that measures currently observable star formation activity will therefore measure the "flickering" associated with a starburst pocket and not the entire phenomenon.

2.4.2 Timescales and Galactic-size Bursts

A basic physical property of a galaxy is the characteristic time needed to communicate an event or disturbance across the entire system. Such a timescale could be a typical rotation period ($t\sim 2\pi R_e/V$) for a disk with solid-body rotation or a crossing time for a spheroidal system such as a star cluster ($t\sim 2R_e/\sigma$). We calculate characteristic timescales of 100 ± 10 to 265 ± 35 Myr for the three galaxies under study, using radii and inclination corrected maximum rotation curve velocities from the HyperLeda database (Paturel et al. 2003), as shown in Table 2.5. The burst durations we report are all greater than the characteristic timescale for the host galaxies.

It is interesting to compare the shorter durations of the "flickering" star formation we associate with localized star formation to the characteristic timescale for a star cluster. We estimate the timescale to be ~ 1 Myr assuming that the effective radius of a cluster is a few pc with a velocity dispersion of ~ 10 km s^{-1} (e.g., Smith & Gallagher 2000; Larsen et al. 2008). This value agrees with the estimation of a few Myr reported by Heckman (2005) using a dynamical timescale calculation $t_{dyn} \sim (G\rho)^{-1/2}$. Given the range of results shown in Table 2.4, the global bursts last on the order of $\sim 1-10$ times the characteristic timescale for a single star cluster. Interestingly, Elmegreen (2000) showed that star formation in small regions (i.e., stellar clusters) occurs within one or two local crossing times while large-scale star formation in a galaxy can proceed at a slower rate with a timescale dictated by the properties of the larger system. Our findings of shorter durations and shorter timescales at the cluster level with longer global starburst durations and timescales at the galactic level support this scenario.

The longer duration, global bursts may be the dominate event shaping dwarf galaxy

Table 2.5 Comparison of Starburst Durations and Dynamical Timescales in Prototpype Galaxies

Galaxy	R_e^a (pc)	V_{rot}^b (km s^{-1})	Time (Myr)	Duration (Myr)	Duration/Time
NGC 4163	710 ± 95	18.3 ± 0.8	240 ± 35	308 ± 50	1.3 ± 0.3
NGC 4068	1165 ± 140	27.0 ± 0.9	265 ± 35	360 ± 40	1.4 ± 0.2
IC 4662	730 ± 75	46.5 ± 3.1	100 ± 10	225 ± 25	2.3 ± 0.3

[a]Major axis measurements and maximum rotational velocities were taken from the HyperLeda database (Paturel et al. 2003). Effective radii were calculated by converting the major axis value to radial size using the TRGB distance by Karachentsev et al. (2006).
[b]Maximum rotational velocity corrected for inclination from the HyperLeda database (Paturel et al. 2003).

internal dynamics, composition, and morphology in isolated environments and certainly may play a significant role in their evolution in galaxy-rich environments where tidal interactions have been thought to dictate the evolutionary history of dwarf galaxies. This longer burst duration coupled with the observation that bursts are not localized events but spread across a significant area of a galaxy suggest that star formation in starburst galaxies may be self-regulating. It appears that the non-equilibrium energy output and mass transfer from an individual pocket of star formation may impact the local star cluster but do not shut-down the burst and the phenomenon to first order is not "self-quenching". A long and global starburst event also has interesting implications from a chemical composition perspective. Starbursts of this magnitude may play a significant role in driving galactic superwinds. Superwinds are thought to be one mechanism responsible for expelling chemically enriched material into the IGM thereby enriching the IGM while simultaneously lowering the metallicity of the host galaxy (e.g., Strickland & Stevens 2000; Strickland et al. 2004; Martin 2007).

2.5 Conclusions

We find the starburst events in NGC 4163, NGC 4068, and IC 4662 are global in nature with durations from 225 ± 25 to 385 ± 50 Myr; longer than the characteristic timescales found for each galaxy. The longer durations suggest that starbursts may not extinguish themselves through energy and mass transfer but may in fact be self-regulating. If these longer duration and more global starburst events are typical of bursting dwarf galaxies, then the starburst phenomenon may have a larger impact on galactic evolution, enrichment of the IGM with heavy metals, and chemical composition of the host galaxies than previously thought. A complete starburst event most likely includes multiple generations of star formation which requires quantifying the star formation history of the past several hundred million years to find the starburst duration. Previously reported duration timescales of ~ 10 Myr measure the "flickering" associated with individual star clusters within a starburst galaxy but do not measure the duration of the heterogeneous star formation present in global starburst events such as found in these three galaxies.

2.6 Acknowledgments

Support for this work was provided by NASA through grants AR-10945 and AR-11281 from the Space Telescope Science Institute, which is operated by Aura, Inc., under NASA contract NAS5-26555. E. D. S. is grateful for partial support from the University of Minnesota. J. J. D. was partially supported as a Wyckoff fellow. K. B. W. M. gratefully acknowledges Matthew, Cole, and Carling for their support. This research made use of NASA's Astrophysical Data System and the NASA/IPAC Extragalactic Database (NED) which is operated by the Jet Propulsion Laboratory, California Institute of Technology, under contract with the National Aeronautics and Space Administration.

We would like to thank the anonymous referee for a prompt and very helpful report.

Chapter 3

SFHs of Nearby Starburst Dwarf Galaxies (McQuinn et al. 2010a)

A slightly modified version of this chapter appears in the published article referenced by Kristen B. W.McQuinn, Evan D. Skillman, John M.Cannon, Julianne J. Dalcanton, Andrew Dolphin, Sebastian Hidalgo-Rodríguez, Jon Holtzman, David Stark, Daniel Weisz, Benjamin Williams, 2010a, ApJ, submitted. Reproduced here with permission.

ABSTRACT

We use archival Hubble Space Telescope observations of resolved stellar populations to derive the star formation histories (SFHs) of eighteen nearby dwarf galaxies that had been previously identified as starbursts. In this first paper we present the observations, color-magnitude diagrams, and the SFHs of the eighteen starburst galaxies, based on a homogeneous approach to the data reduction, differential extinction, and treatment of photometric completeness. We adopt a star formation rate (SFR) threshold normalized to the average SFR of the individual system as a metric for classifying starbursts in SFHs derived from resolved stellar populations. This choice facilitates finding not only currently bursting galaxies but also "fossil" bursts increasing the sample size of starburst galaxies in the nearby (D$<$ 8 Mpc) universe. Thirteen of the eighteen galaxies are experiencing ongoing bursts and five galaxies show fossil bursts. From our reconstructed SFHs, it is evident that the elevated SFRs of a burst are sustained for hundreds of Myr with variations on small timescales. A long $>$ 100 Myr temporal baseline is thus

fundamental to any starburst definition or identification method. The longer lived bursts rule out rapid "self-quenching" of starbursts on global scales. The bursting galaxies' gas consumption timescales are shorter than the Hubble time for all but one galaxy confirming the short-lived nature of starbursts based on fuel limitations. Additionally, we find the strength of the Hα emission usually correlates with the CMD based SFR during the last $4 - 10$ Myr. However, in four cases, the Hα emission is significantly less than what is expected for models of starbursts; the discrepancy is due to the SFR changing on timescales of a few Myr. The inherently short timescale of the Hα emission limits identifying galaxies as starbursts based on the current characteristics which may or may not be representative of the recent SFH of a galaxy.

3.1 A Perspective on the Starburst Phenomenon in Dwarf Galaxies

A starburst is defined as a short-lived intense period of star formation (SF) that is unsustainable over the Hubble time due to the limited supply of gas within a galaxy. Starburst galaxies were first classified by Searle & Sargent (1972) and Searle et al. (1973), based on the blue colors produced by the massive stars formed during the burst. In the local universe, starbursts produce approximately 10% of the radiant energy and 20% of the massive stars (Heckman 1998; Brinchmann et al. 2004). At $z = 1$, starburst characteristics are found in 15% of galaxies (O'Connell 2005), presumably attributable to the greater amounts of gas typically present in young galaxies and increased galactic interactions (e.g., Condon et al. 1982; Kennicutt et al. 1987; Telesco et al. 1988).

The starburst's impact on a galaxy and the surrounding intergalactic medium (IGM) is primarily due to the consumption of gas that fuels the burst and the feedback from massive stars formed in the burst. For example, one of the important mechanisms is the ionizing radiation produced and the mass loss experienced during the lifetime of the massive stellar population and the resulting supernovae (SNe). The mass loss from massive stars alters the chemical composition of the interstellar medium (ISM) and future stellar populations. In addition, the flux of energetic photons escaping the galaxy changes the ionization state of the surrounding IGM. It is possible for starbursts to generate the energy and material to fuel galactic "super-winds" which can escape

from the low potential wells of dwarf galaxies enriching the metallicity of the IGM (Skillman 1997). This has been suggested as an explanation for the continued low metallicity measurements of many local dwarf galaxies (e.g., Spaans & Norman 1997; Romano et al. 2006). Yet, without understanding the SFH of a galaxy, it is difficult to constrain the impact of a starburst.

Starbursts have been observed in gas rich galaxies such as disk galaxies and low mass dwarfs (e.g., Heckman 1998). It is unclear whether most dwarf galaxies experience starbursts during their evolution or whether only a subgroup of dwarf galaxies exhibit bursts (e.g., Marlowe et al. 1997; Mayer et al. 2001b; van Zee et al. 2001b; Pasetto et al. 2003). It is possible that for the dwarf galaxies with starbursts there may be a duty cycle to the bursts (Marlowe et al. 1999; Lee et al. 2009, and references therein) making this a repetitive mode of star formation in these galaxies.

The ionizing radiation flux created during a starburst makes bursting galaxies easily studied at optical, ultraviolet (UV) , far infrared, and Hα rest wavelengths. Numerous studies over the past decade have used these different wavelength observations to study the properties of both nearby and distant actively bursting systems (e.g., Colless et al. 1994; Babul & Ferguson 1996; Meurer et al. 1997; Heckman 2005; Oey et al. 2007; Lee et al. 2009, among many others). The goals of these studies have been many, including characterizing the different properties of a currently observable starburst and quantifying the feedback of starbursts to the different components of the ISM and IGM.

Most studies have been linked to only instantaneous properties of starbursts. However, with resolved stellar populations, we can derive complete SFHs allowing us to study the evolution of starbursts over hundreds of Myr within individual galaxies. Among the many relevant studies on resolved stellar populations in individual galaxies are those of NGC 1569 by Angeretti et al. (2005) who estimate the SFH over the last $1 - 2$ Gyr using synthetic color-magnitude diagrams (CMDs) and by Grocholski et al. (2008) who estimate the SF activity by overlaying metallicity specific age isochrones on the observed CMD of NGC 1569. A similar approach was taken by Cannon et al. (2003) on NGC 625 and Annibali et al. (2008) on NGC 4449 where SFRs were estimated by overlaying age isochrones. In the case of Cannon et al. (2003), the recent SFR estimates were refined in increments of 100 Myr using a model of blue helium burning (BHeB) stars.

The high-resolution data used in such studies presents an opportunity to reconstruct the detailed SFHs over a longer temporal baseline for a sample of starburst dwarf galaxies in a homogeneous and consistent way. To that end, we have gathered the observations of eighteen galaxies from the HST public archive and undertaken a detailed analysis of star formation on these systems. Using information from the CMDs and stellar evolutionary models, we derived SFRs for these galaxies as a function of time taking into account both systematic and statistical uncertainties. Our emphasis on uniformity allows us to consider the strength and importance of a starburst event in the context of the host galaxy's star formation in past epochs, and facilitates a direct comparison between galaxies while minimizing systematic uncertainties.

In this first paper, Paper I, we present the observations and data reduction (§3.2) and CMDs and SFHs (§3.3) for eighteen dwarf starbursts. In §3.4 we discuss the classification of the galaxies as starbursts using a gas consumption timescale, compare our SFRs with existing measurements of Hα emission, and present a SFR normalized to the average SFR of each galaxy. The hypothesis that SF in a burst is "self-quenching" is discussed in §3.5 and a summary of our conclusions in §3.6. In Paper II (McQuinn et al. 2010b) we will present additional analysis on these starbursts, and derive the burst duration for each system. Our third paper in this series (McQuinn et al. in prep) will explore the spatial structure within the starbursts.

3.2 Galaxy Observations and Photometric Reduction

3.2.1 The Galaxy Sample

Our sample of galaxies was selected from observations in the HST public archive and is listed in Table 3.1; a summary of general properties of the galaxy sample is presented in Table 3.2. The majority of the galaxies were previously identified as starbursts in the literature using a number of methods. The different methods all rely on evidence of recent star formation such as the presence of high surface brightness regions, high Hα emission, or the blue color typical of massive, young stars (see Table 3.1 for citations and identification methods used). We explore a new method for identifying galaxies as starbursts based on the presence and distribution of young main sequence and helium burning stars in the optical CMDs. The higher concentration in dwarf galaxies of

these young stars is a sign of recent SF activity that is likely more intense than the average SF experienced in low-mass systems. Using the characteristics of a CMD also has the potential to identify older or fossil bursts which may or may not be producing significant Hα emission at the current epoch. The identification of fossil starbursts potentially greatly increases the number of starbursts in the nearby universe that can be identified and studied. Using this method, we added four additional galaxies to our sample as possible starbursts (Antlia dwarf, ESO 154−023, NGC 784, and UGC 9128). The classification of these systems as starbursts is explored and discussed below in §3.4.

Table 3.1 Observational Parameters for Galaxy Sample

Galaxy (1)	Starburst ID Method (2)	Example Ref. (3)	RA (4)	Decl. (5)	HST ID. (6)	λ_{606} (sec) (7)	λ_{814} (sec) (8)
ANTLIA	CMD	present work	10:04:04.10s	−27:19:52s	GO-10210	985	1170
UGC 9128	CMD	present work	14:15:56.5s	+23:03:19s	GO-10210	985	1170
UGC 4483	μ, morphology	Loose et al. (1986)	08:37:03.0s	+69:46:31s	GO-8769	9500 (555W)	6900
NGC 4163	UBV colors	Gallagher & Hunter (1986)	12:12:09.1s	+36:10:09s	GO-9771	1200	900
UGC 6456	K band, μ, color	Gil de Paz et al. (2003)	11:27:59.9s	+78:59:39s	GTO-6276	4200 (555W)	4200
NGC 6789	K band, μ, color	Gil de Paz et al. (2003)	19:16:41.1s	+63:58:24s	GO-8122	8200 (555W)	8200
NGC 1569	multi-wavelength obs.	de Vaucouleurs et al. (1974)	04:30:49.0s	+64:50:53s	GO-10885	9587	4892
NGC 4068	UBV colors	Gallagher & Hunter (1986)	12:04:00.8s	+52:35:18s	GO-9771	1200	900
SBS1415+437	K band, μ, color	Gil de Paz et al. (2003)	14:17:01.4s	+43:30:05s	GO-9361	35280	35280
IC 4662	multi-wavelength obs.	Heydari-Malayeri et al. (1990)	17:47:08.8s	−64:38:30s	GO-9771	1200	900
ESO154-023	CMD	present work	02:56:50.38s	−54:34:17s	GO-10210	1000	1300
NGC 2366	M_B, emission lines	Thuan & Martin (1981)	07:28:54.6s	+69:12:57s	GO-10605	4780 (555W)	4780
NGC 625	H_α, UBVI images	Marlowe et al. (1997)	01:35:04.6s	−41:26:10s	GO-8708	5200 (555W)	10400
NGC 784	CMD	present work	02:01:17.0s	+28:50:15s	GO-10210	930	1230
NGC 5253	H_α, UBVI images	Marlowe et al. (1997)	13:39:55.9s	−31:38:24s	GO-10765	2400 (555W)	2360
NGC 6822	CMDs of Stellar Clusters	Hodge (1980)	19:44:56.6s	−14:47:21s	GO-6813	3900 (555W)	3900
NGC 4214	multi-wavelength obs.	Huchra et al. (1983)	12:15:39.2s	+36:19:37s	GO-6569	1300 (555W)	1300
NGC 4449	optical and radio data	Hunter et al. (1982)	12:28:11.9s	+44:05:40s	GO-10585	4920 (555W)	4120

Cols. (3) Note that there are multiple citations for many of these galaxies identifying them by different methods as starbursts. We show but one example citation per galaxy. (4) and (5): R.A. and Decl. in J2000 coordinates.

Table 3.2 Properties of the Galaxy Sample

Galaxy (1)	D (Mpc) (2)	m−M (mag) (3)	Ref. (4)	d_{25} (arcmin) (5)	A_R (mag) (6)	M_B (mag) (7)
ANTLIA	1.25 ± 0.1	25.49	13	1.86 ± 0.13	0.212	-9.8^a
UGC 9128	2.24	26.75	13	1.02 ± 0.11	0.065	-12.34^b
UGC 4483	3.2 ± 0.2	27.53	3	1.12 ± 0.12	0.091	-12.53 ± 0.23
NGC 4163	3.0	27.36	10	1.62 ± 0.11	0.052	-13.66
UGC 6456	4.3 ± 0.1	28.19	11	0.79 ± 0.11	0.096	-13.69 ± 0.19
NGC 6789	3.6 ± 0.2	27.78	4	0.98 ± 0.11	0.187	-14.3^a
NGC 1569	3.36 ± 0.2	27.63	7	3.98 ± 0.11	1.871	-14.74
NGC 4068	4.3	28.17	10	1.86 ± 0.11	0.058	-14.87
SBS1415+437	13.6 ± 1.4	30.7	1	0.35 ± 0.12	0.024	-15.07 ± 0.46
IC 4662	2.4	26.94	10	2.09 ± 0.11	0.188	-15.09
ESO154-023	5.76	28.80	13	4.79 ± 0.11	0.045	-16.14^b
NGC 2366	3.2 ± 0.4	27.52	8	4.37 ± 0.11	0.097	-16.17 ± 0.36
NGC 625	3.9 ± 0.4	27.95	2	6.61 ± 0.10	0.044	-16.19 ± 0.18
NGC 784	5.19	28.58	13	4.17 ± 0.11	0.158	-16.5^a
NGC 5253	3.5 ± 0.4	27.88	12	5.01 ± 0.10	0.186	-16.74 ± 0.18
NGC 6822	0.5 ± 0.04	23.3	6	17.38 ± 0.11	0.632	-16.84
NGC 4214	2.7 ± 0.2	27.13	5	6.76 ± 0.11	0.058	-16.93 ± 0.22
NGC 4449	4.2 ± 0.5	28.12	9	4.68 ± 0.11	0.051	-17.94 ± 0.33

[a] de Vaucouleurs et al. (1991)
[b] Local Volume Legacy (LVL) project, Lee et al. (2008)

Cols. (5) Diameter of the projected major axis of a galaxy at the isophotal level 25 mag arcsec^{-2} in the B-band Paturel et al. (2003) HyperLeda database (http://leda.univ-lyon1.fr). Col. (6) Schlegel et al. (1998). Col. (7) Absolute magnitudes uncorrected for Galactic extinction.

References. — (1) Aloisi et al. (2005); (2) Cannon et al. (2003); (3) Dolphin et al. (2001); (4) Drozdovsky et al. (2001); (5) Drozdovsky et al. (2002); (6) Gieren et al. (2006); (7) Grocholski et al. (2008); (8) Karachentsev et al. (2002); (9) Karachentsev et al. (2003); (10) Karachentsev et al. (2006); (11) Méndez et al. (2002); (12) Sakai et al. (2004); (13) Tully et al. (2006);

The dwarf galaxies in the sample cover a range of brightness, morphologies (i.e., SBdm, IAB(s)m, pec, IBm), and spatial extent, facilitating an exploration of the starburst phenomenon in a range of dwarf galaxy properties. While the majority of the galaxies have high Galactic latitudes and low foreground extinction (i.e., $A_R < 0.2$; Schlegel et al. 1998), two of the systems, NGC 1569 and NGC 6822, have high foreground extinction (A_R of 1.9 and 0.6 mag respectively). If we assume that the foreground extinction is uniform across an individual galaxy, the extinction can be easily taken into account. However, it is more likely that the foreground extinction has variations and is not a uniform gray screen (see §3.3.2 and McQuinn et al. 2009). We chose to include these well-studied systems in the sample with the caveat that the high extinction values increase the uncertainties on the SFRs.

Our starburst sample was selected from observations in the HST archive based on three photometric properties. First, we require both V and I band images of a galaxy in the archival observations. Second, we set a minimum photometric depth of the I band observations of $\sim$2 mag below the tip of the red giant branch; a requirement for accurately constraining the recent SFH of a galaxy (Dolphin 2002; Dohm-Palmer & Skillman 2002). Third, the galaxies were required to lie close enough such that their stellar populations were resolved by HST imaging instruments. These properties were chosen to ensure robust reconstruction of the SFH. Seventeen of the eighteen dwarf galaxies in our sample meet these criteria. We include an additional, galaxy to the sample, SBS $1415+437$, even though the photometry stops somewhat short ($\sim$ 0.5 mag) of reaching our required photometric depth despite long integration times (P.I. Aloisi, Program I.D. 9361). While it does not strictly meet our photometric requirements, SBS 1415+437 is a well-studied starburst with an interesting recent SFH. We include it in our sample for comparison purposes and although the ancient SFH derived for this system is uncertain, the recent SFRs are still well constrained. Four other data sets were considered that were at least one magnitude above our photometric depth cut-off (UGCA 290 P.I. Schulte-Ladbeck, Program I.D. 8122; NGC 1705 P.I. Tosi, Program I.D. 7506; NGC 3077 P.I. Seitzer, Program I.D. 8601; I Zw 18 P.I. Thuan, Program I.D. 9400). Testing showed that the recent SFHs on these galaxies were not properly constrained by the shallower photometry and are therefore not included in this work.

The field of view of the HST observations are represented as footprints on DSS images

(Bonnarel et al. 2000) in Figure 3.1. Regions of active and quiescent star formation can be seen in each of the images in these inhomogeneous systems. The galaxies span a large range both in angular size (from NGC 6822 at 15.5′ to NGC 6789 at 1.3′) and in distance (ranging from Antlia at 1.3 Mpc to NGC 784 at 5.9 Mpc with the outlier SBS 1415+437 at 13.6 Mpc). The HST imaging instruments' field of view covers a large fraction of most galaxies in the sample, with the exception of NGC 6822. The HST areal coverage thus includes a sufficient fraction of the stellar populations to profile the SFH although the SFRs derived for NGC 6822 will be lower limits, as noted below. The exposure times and basic data on each galaxy in the sample are listed in Tables 3.1−3.2.

3.2.2 Photometric Processing

Twelve of the eighteen galaxies were observed using the Advanced Camera for Surveys (ACS) Wide Field Channel (WFC) on HST. The observations for three of the galaxies were snapshots taken on a single HST orbit (CRSPLIT = 2) (i.e., NGC 4068, NGC 4163, and IC 4662), while the observations for the remaining objects were obtained across multiple HST orbits. Photometry was performed on the pipeline processed, cosmic ray cleaned images using the ACS module of the DOLPHOT photometry package (Dolphin 2000) for the ACS images that were cosmic-ray split. The other six galaxies observed with the Wide Field Planetary Camera 2 (WFPC2) instrument were reduced using the pipeline developed by Holtzman et al. (2006). Briefly, the WFPC2 images were pre-processed with the standard WFPC2 tasks *mask*, which flags bad pixels as saturated using data quality files and *crmask* which cleans the images. Photometry was performed as part of the pipeline using the HSTphot photometry package (Dolphin 2000) in the PSF mode. Four galaxies, NGC 2366, NGC 4449, NGC 5253, and NGC 6822, were observed with multiple pointings. In these cases, the photometry measurements from each image were combined by geometrically modeling any overlapping regions in the images and selecting the photometry from only one of the images in the overlapping region.

The definitions and derivations of the parameters from the two photometry methods, DOLPHOT and HSTphot, used in the selecting high fidelity point sources are identical ensuring that our final photometry lists from the two HST instruments and photometric packages were homogeneously processed and filtered. The photometry output of

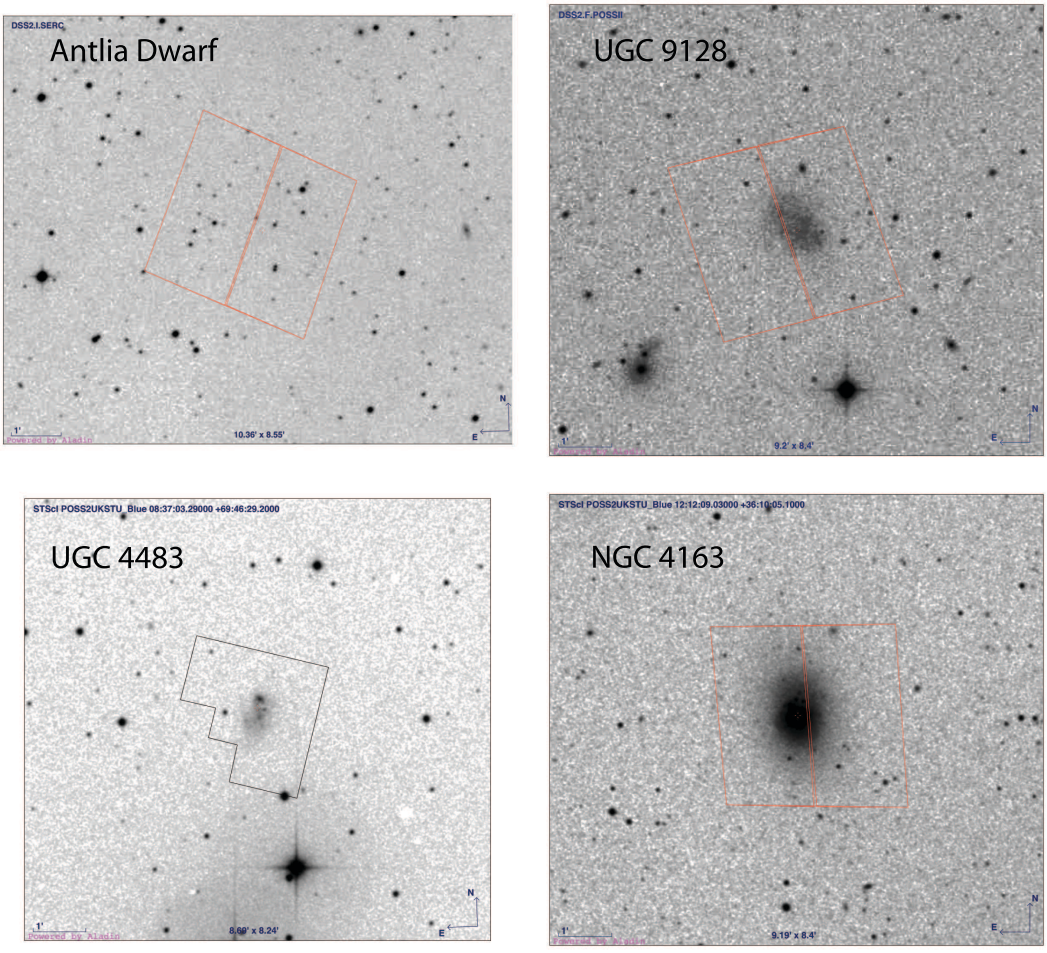

Figure 3.1 The footprints of the HST archival observation fields of view used to derive the SFHs shown on DSS V band images: Antlia, UGC 9128, UGC 4483, NGC 4163 (Bonnarel et al. 2000).

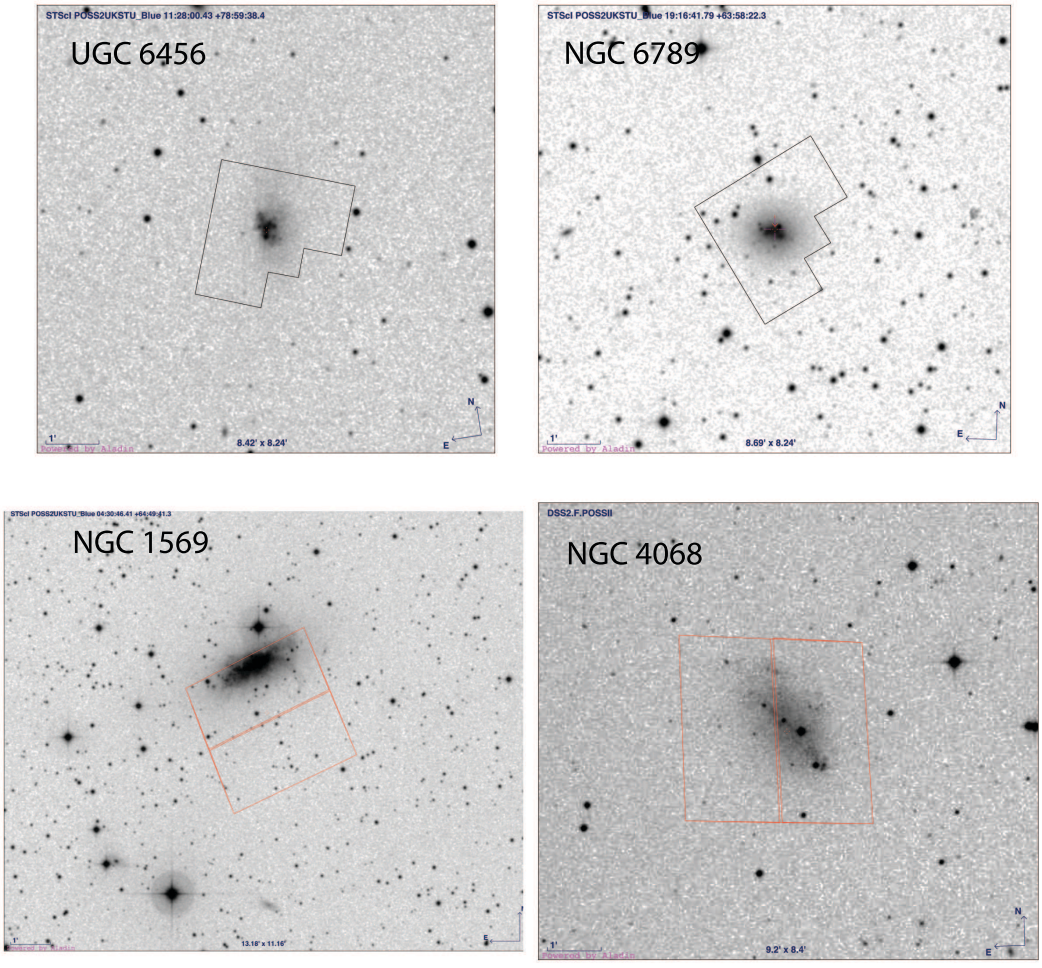

Figure 3.1 *HST footprints continued: UGC 6456, NGC 6789, NGC 1569, NGC 4068*

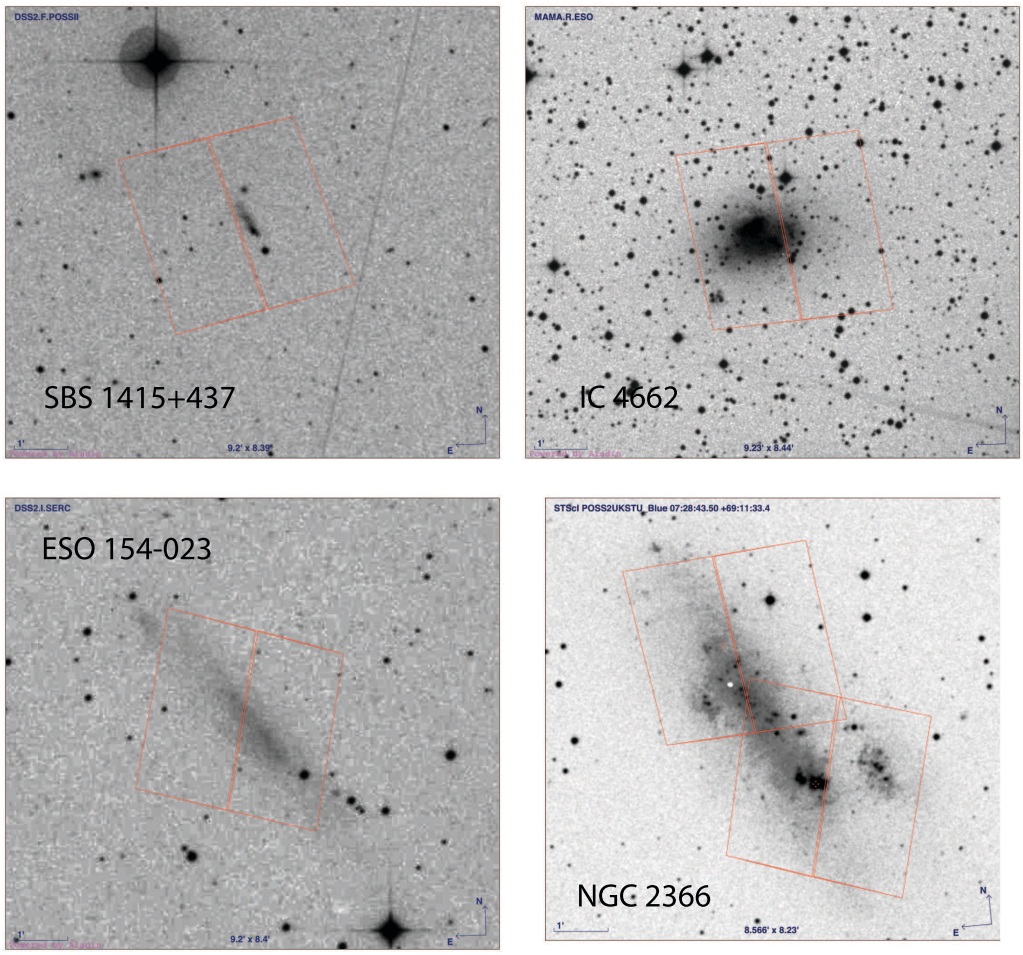

Figure 3.1 *HST footprints continued: SBS1415+437, IC 4662, ESO154−023, NGC 2366*

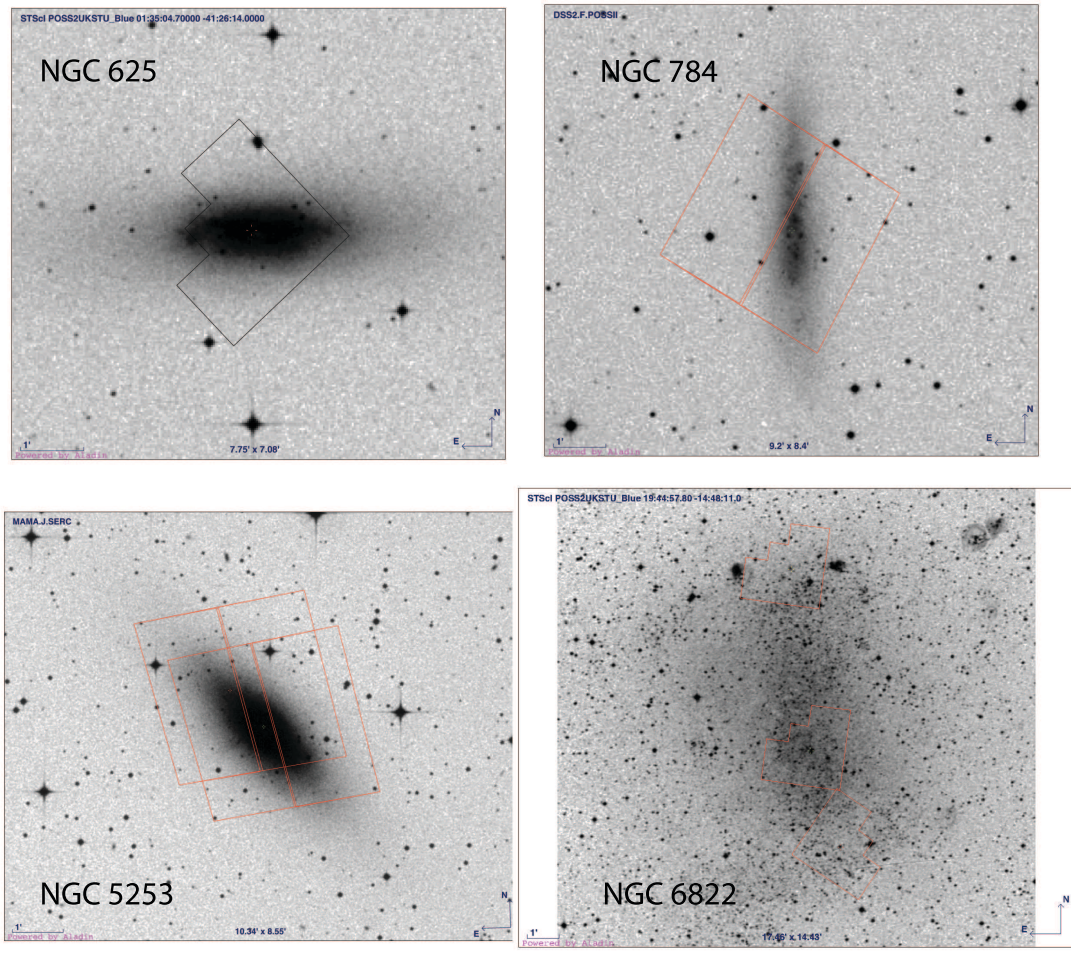

Figure 3.1 *HST footprints continued: NGC 625, NGC 784, NGC 5253, NGC 6822*

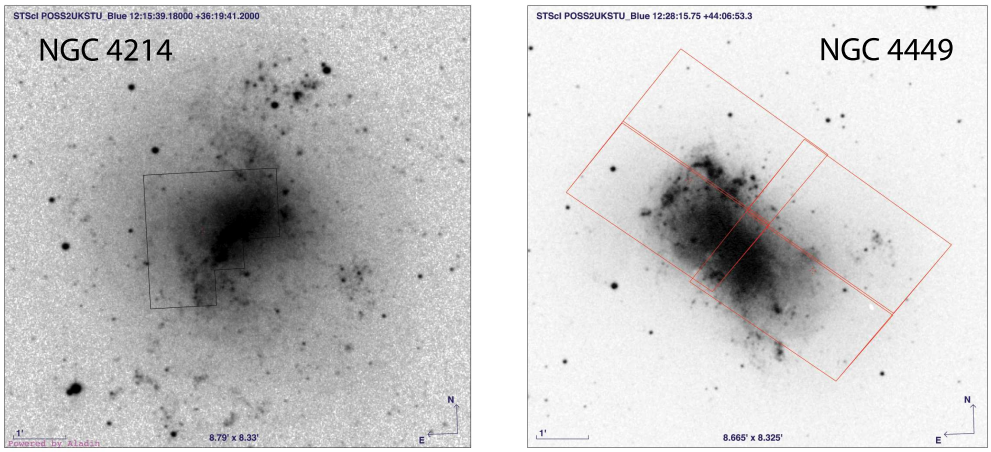

Figure 3.1 *HST footprints continued: NGC 4214, NGC 4449*

DOLPHOT and HSTphot includes a characterization of the quality of each point source including the sharpness of the source, the degree of crowding, and the quality of the fit, etc; a detailed explanation of these parameters can be found in Dolphin (2000). We selected point sources from the photometry that were characterized as well-recovered stars with a minimum signal-to-noise ratio of 5. In addition to these criteria, the sum of the squared sharpness values for the *two* wavelength observations were required to be ≤ 0.39 for an individual point source. We rejected cuts based on crowding, because our tests showed this additional filtering preferentially eliminated bright point sources in areas of active star formation − one of the areas of interest for studying starbursts. Note that while crowding is typically not as significant in low surface brightness galaxies, in regions where crowding is high, the derived SFR may still be a lower limit.

Artificial star tests were performed to quantify the completeness and systematic uncertainty of the photometry in each of the images. The artificial stars were evenly distributed across the field of view at the range of magnitudes and colors that bracketed the measured photometry. We present the percentage of stars recovered across each magnitude bin for one of the shallowest observations (NGC 4214) and for one of the deepest observations (Antlia dwarf galaxy) in our sample in Figure 3.2.[1] The artificial

[1] Note that SBS1415 + 437 has a lower completeness limit than NGC 4214 despite long integration times, but is not representative of our galaxy sample.

star lists were filtered according to the same parameters as the photometry lists. Point sources not meeting the criteria were retained as unrecovered stars.

3.3 Star Formation Histories

3.3.1 Connecting CMDs and Stellar Evolutionary Populations to SFRs

CMDs created from our photometry are shown in Figure 3.3, with galaxies ordered from the faintest to the most luminous. Typical photometric errors per magnitude bin are shown, and include systematic uncertainties derived from artificial star tests. The different photometric depths across all the observations range from an absolute magnitude of $M_I \sim 2.5$ for NGC 6822 to $M_I \sim -2$ for UGC 6456 and NGC 4214. The observations stop short of the depth of the red clump, with the exception of Antlia, NGC 1569, NGC 2366, and NGC 6822. With the exception of SBS 1415 + 437, all photometry reaches ∼2 mag below the tip of the red giant branch (TRGB) in the I band, as needed to provide constraints on the ancient SFRs (t> 8 Gyr) (Dolphin 2002), although our focus remains on the recent SFH.

Multiple stellar evolutionary populations are identifiable by eye in the CMDs in Figure 3.3, including the main sequence (MS), the red giant branch (RGB), the red clump, the asymptotic giant branch (AGB), and the BHeB and red helium burning (RHeB) sequences. While all of these evolutionary populations are used to derive the SFH, the helium burning (HeB) stars offer the clearest differentiation of starbursts, and are thus of the most interest in our study.

Stars on the HeB sequences have masses greater than ∼3 $M_\odot$ and are burning helium in their cores (Bertelli et al. 1994; Dohm-Palmer & Skillman 2002). The ages of stars in this evolutionary sequence is between $5-1000$ Myr during which time the stars will turn off from the MS and migrate across the CMD from the RHeB sequence to the BHeB sequence and back again. HeB stars older than ∼600 Myr merge into the red clump; the actual age is somewhat metallicity dependent (Bertelli et al. 1994). The location of a HeB star on the CMD depends uniquely on age (i.e., Dohm-Palmer & Skillman 2002; Weisz et al. 2008; McQuinn et al. 2009) in contrast to the MS and RGB where multiple aged stars with different metallicities can occupy the same space on a CMD. Because the HeB lifetimes are relatively short, the presence of HeB stars indicates that

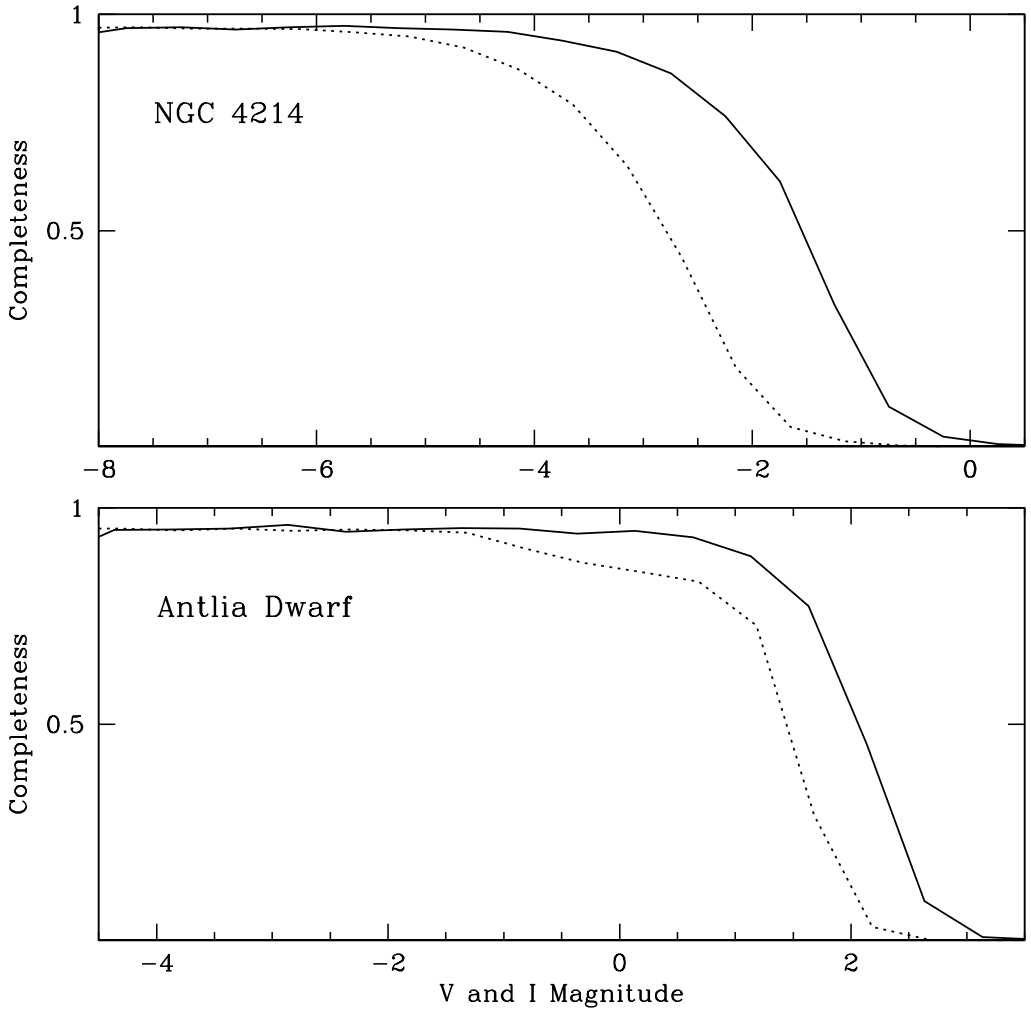

Figure 3.2 The completeness functions for the V band (solid lines) and I band (dotted lines) for the shallowest photometry in our study (top panel: NGC 4214) and the deepest photometry in our study (bottom panel: Antlia). These completeness limits bracket the range in photometry for all eighteen galaxies with the exception of SBS 1415+437 whose completeness is lower than NGC 4214 as noted in the text (§3.2.1).

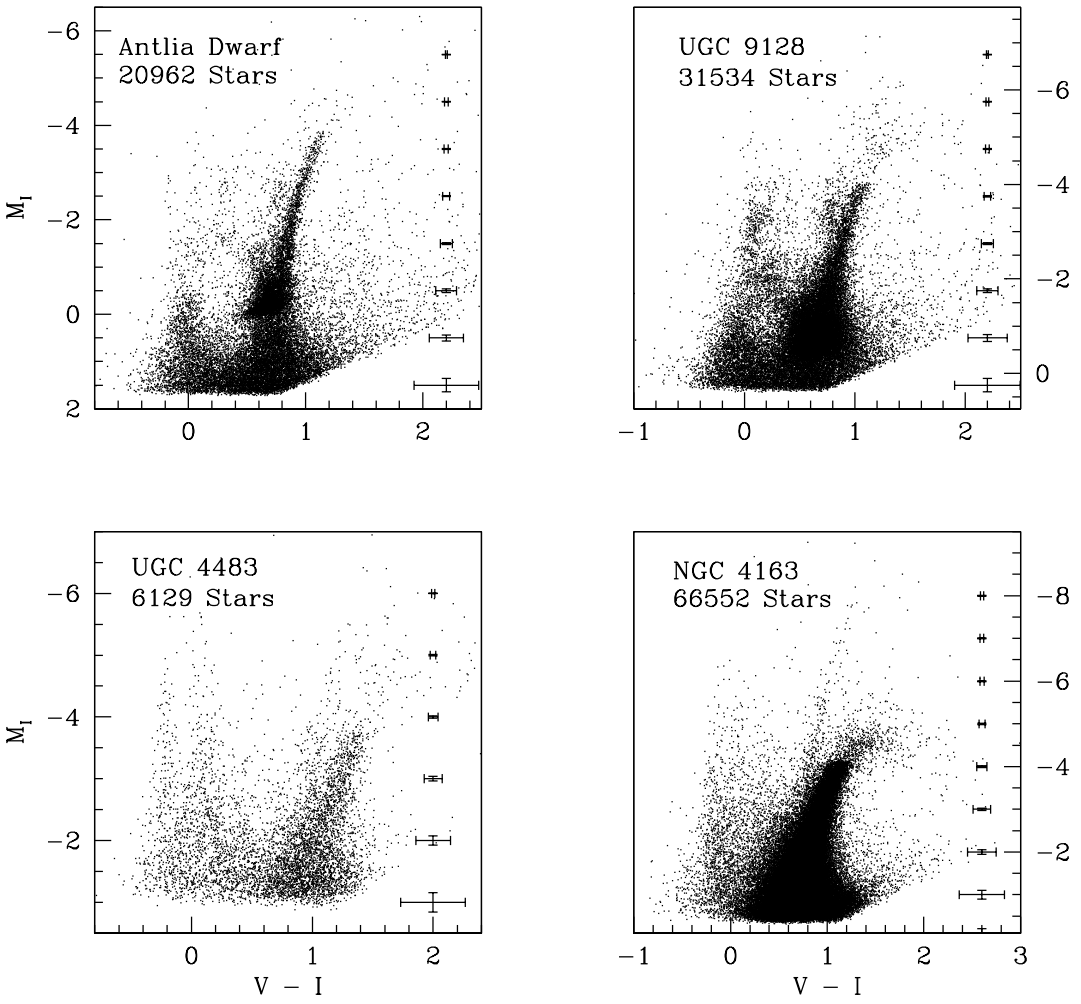

Figure 3.3 Color magnitude diagrams of Antlia, UGC 9128, UGC 4483, NGC 4163 with average uncertainties per magnitude bin. The distances used to calculate the absolute magnitudes are noted in Table 3.2. The TRGB break occurs at $M_I = -4.0$. Note the differences in photometric depth, in the total number of stars observed in each system, and the presence and distribution of BHeB stars.

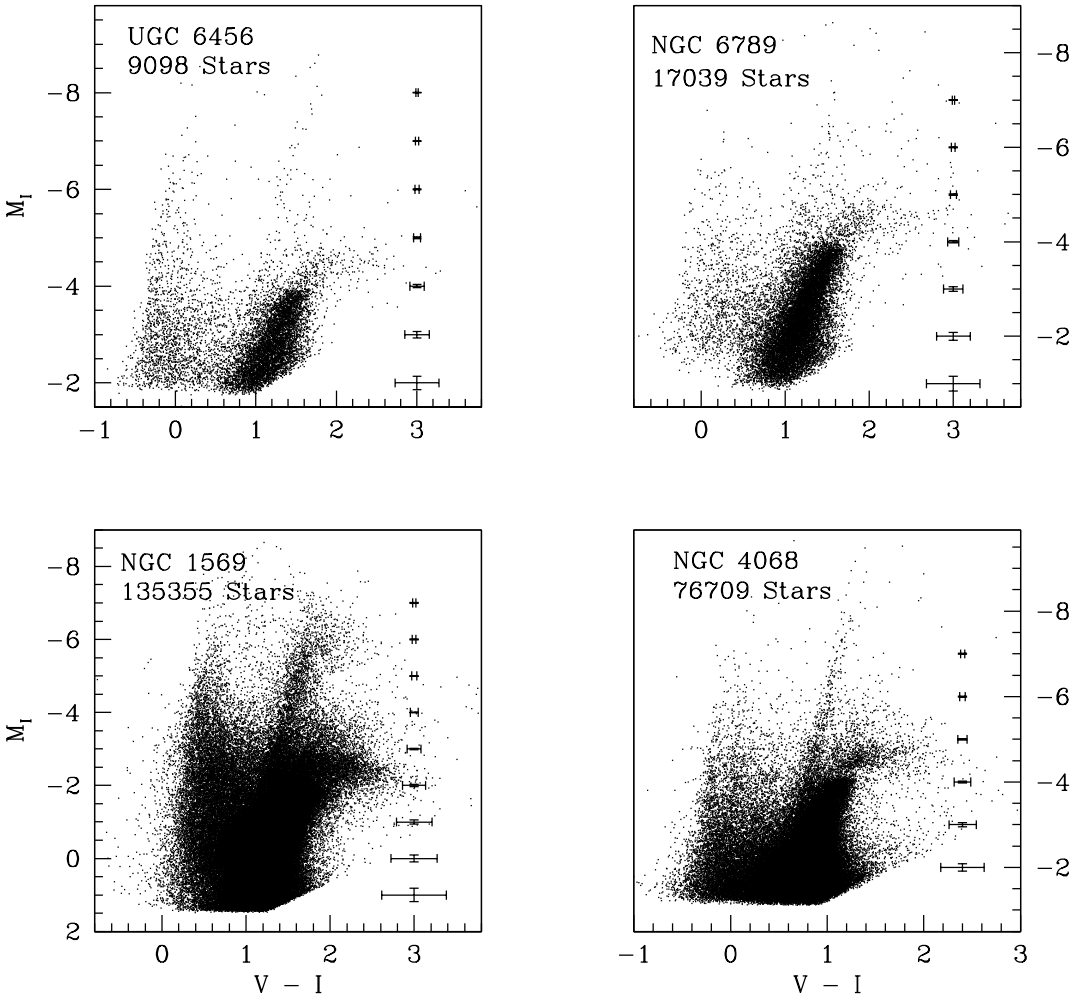

Figure 3.3 *CMDs continued: UGC 6456, NGC 6789, NGC 1569, NGC 4068*

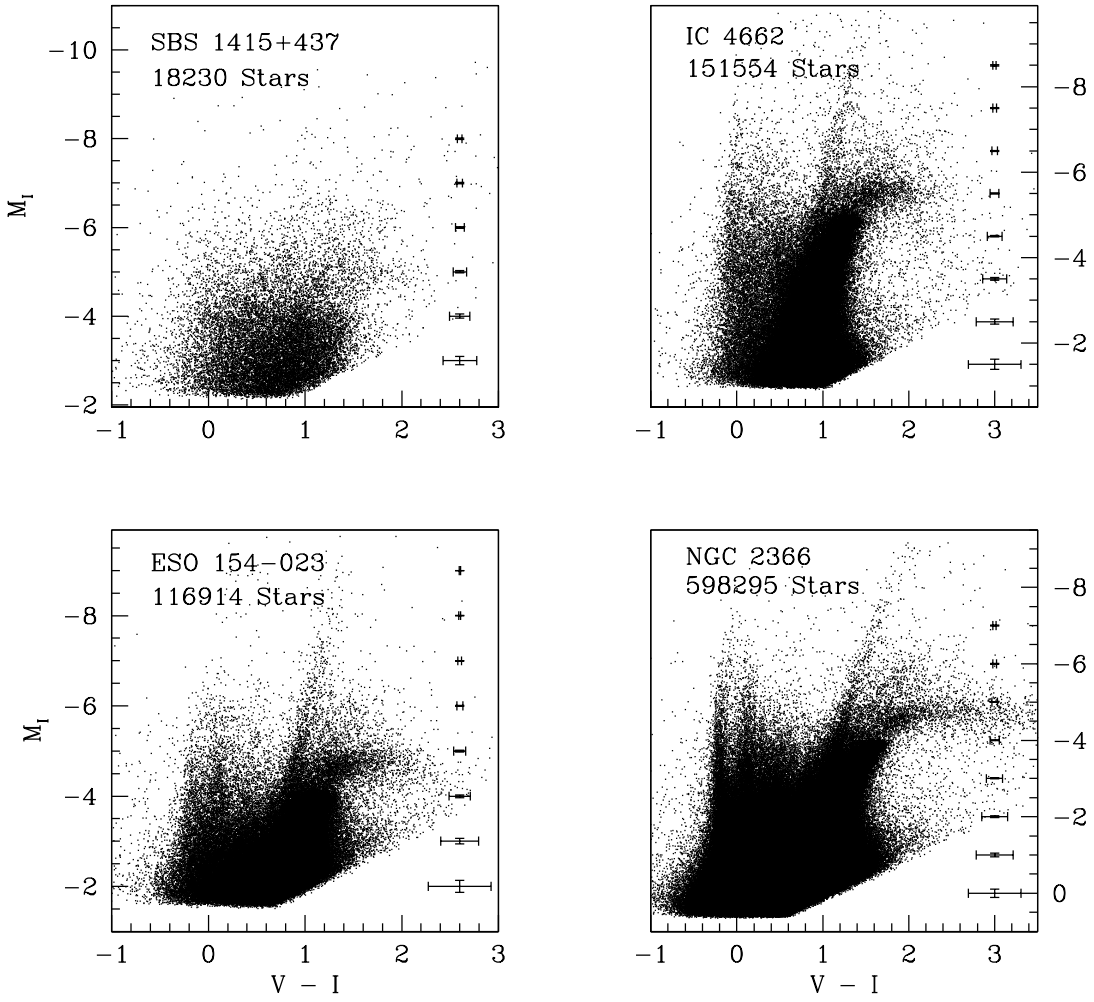

Figure 3.3 *CMDs continued: SBS1415+437, IC 4662, ESO154−023, NGC 2366*

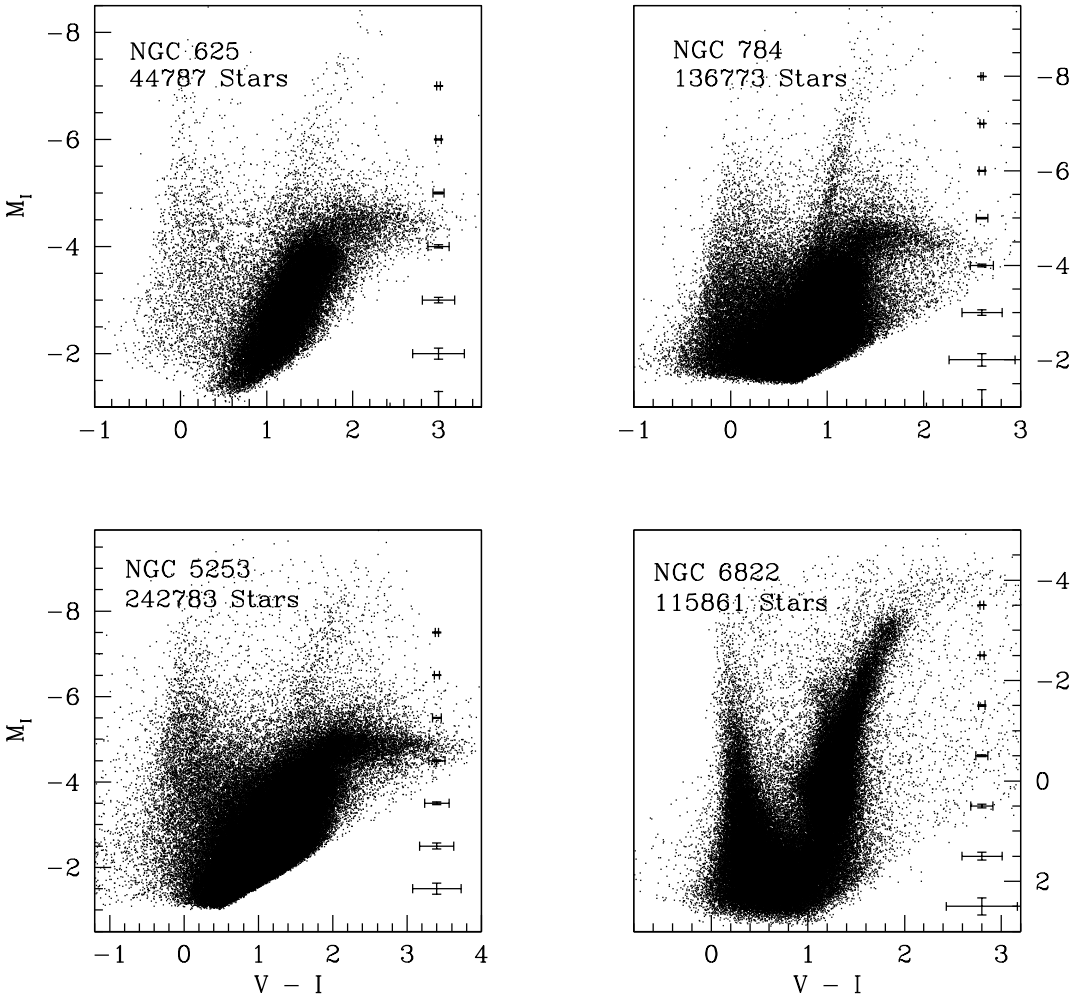

Figure 3.3 *CMDs continued: NGC 625, NGC 784, NGC 5253, NGC 6822*

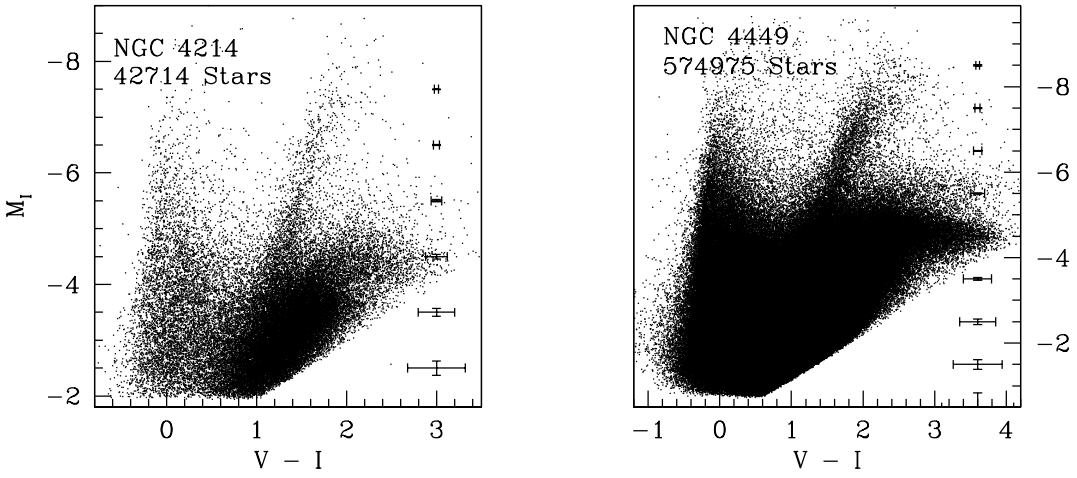

Figure 3.3 *CMDs continued: NGC 4214, NGC 4449*

a galaxy has experienced recent star formation. While this is true for both the RHeB and BHeB sequences, the distribution of the BHeB stars in the CMD is particularly informative due the larger number of BHeB stars (Dohm-Palmer & Skillman 2002, e.g.,). For example, the BHeB distribution will be sparse in galaxy with a low-level constant SFR within a galaxy and will gradually increases from bright to faint magnitudes with a tendency towards redder colors at fainter magnitudes. The BHeB population will be similar but with a heavier density of stars if the SFR has been constant but significantly elevated over the most recent $\sim$ 500 Myr (e.g., IC 4662 in Figure 3.3). The BHeB branch in the CMD will have an uneven distribution in magnitude for a variable SFR typically seen as an over-density of BHeBs at intermediate magnitudes (e.g., UGC 9128 in Figure 3.3). This effect will sometimes be accompanied by a truncation of the MS at bright magnitudes if SF has recently stopped. The properties of the BHeB population in both the distribution as well as the total number of stars can differentiate a galaxy with a constant or low-level of recent SF from a galaxy with bursting levels of SF.

3.3.2 Methodology for Reconstructing SFHs

SFH recovery programs are sophisticated tools that use stellar evolutionary theories to reconstruct the timeline of past SF (e.g., Tosi et al. 1989; Tolstoy & Saha 1996; Gallart et al. 1996; Holtzman et al. 1999; Dolphin 2002; Harris & Zaritsky 2001). These techniques have been maturing over the past decade and are well-established in the literature (see Skillman & Gallart 2002; Skillman et al. 2003; Skillman 2005; Tolstoy et al. 2009, and references therein). The primary inputs in reconstructing the past SFR are the photometry and artificial star recovery fractions (i.e., quantitative observational uncertainties and incompleteness) coupled with the stellar evolutionary models. We employ the numerical CMD fitting program, MATCH (Dolphin 2002) to construct a synthetic CMD based on the observed CMD varying the ages of the stellar populations to find the best fit to the observed CMD, using the stellar evolutionary models of Marigo & Girardi (2007). We assume the Salpeter single sloped power law initial mass function with a spectral index of -1.35 from $0.1 - 100$ $M_{\odot}$ (Salpeter 1955) and a binary fraction of 35% with a flat secondary mass distribution. A recent paper by Gogarten et al. (2009) includes a detailed description of the parameters and method employed here on similar data.

We constrained the metallicity, $Z(t)$, to increase as a galaxy evolves in time. This physically motivated constraint guides the metallicity evolution in the absence of observational constraints that would have been available with deeper photometric depths. We did not constrain the metallicity parameter for three galaxies (Antlia, NGC 2366, NGC 6822)[2] , as the deeper photometry reaches the bottom of the red clump (NGC 2366) or two magnitudes below the red clump (Antlia, NGC 6822) providing enough information at recent times (t<1 Gyr) to constrain the metallicity. We compared the SFHs for both the unconstrained and the constrained solutions and found that both the global SFH solutions and the details of the last 1 Gyr agreed within the uncertainties for all the galaxies. The galaxies that showed the largest deviations were the galaxies with higher extinction or significant stellar crowding. The results of our tests agree with similar tests by Williams et al. (2009).

Photometric errors and differential extinction can broaden features in a CMD. These effects are explicitly accounted for in the CMD fitting programs employed in this study. While these factors must be considered in any SFH derivation, they are of smaller consequence in the deriving recent SFHs for dwarf starburst galaxies. Photometric uncertainties are smaller on the relatively bright stars found in sites of recent SF. Foreground extinction is lower as the galaxies in our study are predominately found at high Galactic latitudes and internal extinction is lower in the low metallicity environments of the sample. Nevertheless, to ensure a robust treatment of these three parameters, we studied different regions of the galaxies with a range in photometric errors, and allowed for foreground and differential reddening when fitting the CMD. We found that the SFRs derived were not significantly affected by varying photometric errors and low extinction levels ($A_V \lesssim 0.5$). Higher levels of differential extinction is more problematic affecting the SFRs derived for galaxies such as NGC 1569 and NGC 6822 with known high Galactic and/or internal extinction. For these systems, our reported uncertainties in the derived SFRs are higher. A complete discussion of these three factors is given in McQuinn et al. (2009). As an additional test of our results, we derived the SFH of one galaxy, NGC 4163, using a different SFH recovery program, IAC−pop

[2] While the photometry of NGC 1569 is nearly as deep, the high levels of internal extinction dictated constraining the metallicity to increase with time.

(Aparicio & Hidalgo 2009). We found the SFHs to be equivalent within the uncertainties between the two methods.

To illustrate the recovery of the SFH, in Figure 3.4 we present a synthetic CMD created by MATCH for ESO $154-023$, alongside the observed CMD on the same scale. The synthetic CMD represents a typical model fit to the data in our sample. The different evolutionary populations are well-reproduced in the synthetic CMD, in both the broad and fine features. The quality of the fit between the observed and modeled CMDs can be quantified with an effective χ^2 parameter (Dolphin 2002). The χ^2 measures the likelihood of the SFH derived from the model CMD to be the true SFH of the observed galaxy given our inputs and models (i.e., Dolphin 2002). The χ^2s per degree of freedom for our analysis are presented in the last column of Table 3.3 and ranged from $1.12-2.67$. The three galaxies with a χ^2 value above two suffer from high extinction (NGC 1569 and NGC 4449) and high crowding (NGC 1569, NGC 5253, and NGC 4449). To match these features, MATCH fits a distance and total extinction value (i.e., foreground plus internal extinction) to each galaxy. In Table 3.3, we compare these modeled values with distances obtained from the literature and Galactic extinction values measured by Schlegel et al. (1998). The distances are well matched within a few tenths of a magnitude. The model extinction values show a wider spread when compared with the Schlegel et al. (1998) foreground extinction measurements. In many cases the modeled value is higher as is expected as the model estimates not only the foreground extinction but also the extinction internal to the galaxy.

Crowding tends to be less in low surface brightness dwarf systems than in spiral and elliptical galaxies. However, regions of higher stellar density presented markedly lower completeness limits than the surrounding lower stellar density regions in four galaxies (IC 4662, NGC 1569, NGC 4449, NGC 5253). We accounted for this disparity by separating these galaxies into regions of higher and lower stellar density. In each region, we conducted the artificial star analysis thus more accurately describing the completeness across the changing condition of the galaxies. The SFHs were derived for each region separately and were summed creating a solution for the entire field of view. As a test, we performed the same analysis with two galaxies that did not exhibit the same extremes in stellar densities (NGC 4068 and NGC 4163) and found that the summed results were equivalent to the SFH derived from the entire field of view within

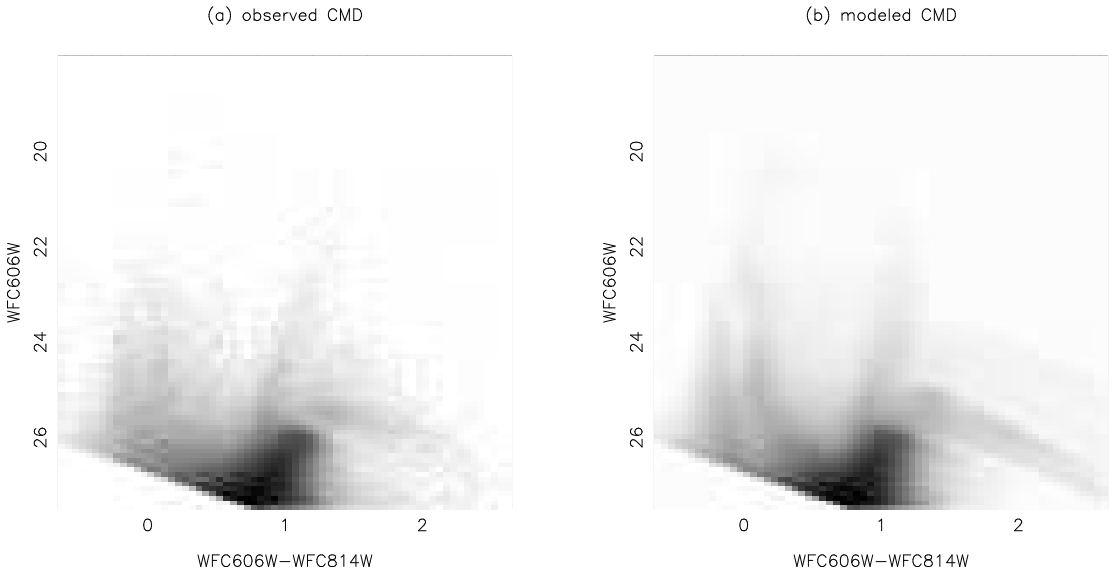

Figure 3.4 The left panel shows the Hess diagrams for the ESO 154-023 observations. The right panel is the best-fit synthetic Hess diagram to the observations representative of a typical fit for the sample galaxies. While there are slight discrepancies, each of the evolutionary populations are well-described in the synthetic CMD.

the uncertainties. We therefore derived the SFHs from the global fields of view for the remainder of the sample which did not exhibit the same extremes in stellar density.

3.3.3 Star Formation Histories

The lifetime SFHs (i.e., SFR(t)) are presented in Figure 3.5. The errors include both systematic and statistical uncertainties derived from Monte Carlo simulations. The average time resolution for deriving the SFH is $\delta\log(t) \sim 0.3$. However, the SFRs at large look-back times are not well constrained without photometry that reaches the oldest MS turn-off. Hence, we averaged the SFR results from the oldest time bins to create one coarse time bin of $6 - 14$ Gyr; loosely constraining the ancient SFH. The uncertainties in this older time bin are relatively small due to averaging over a longer time period. By averaging over a long time interval, we traded temporal resolution for more secure SFRs thus providing a baseline for comparison with current SFRs and a

Table 3.3 Comparison of Distance, Extinction, and Fit Values for Galaxy Sample

Galaxy	Best Fit (m − M)	Lit. Value (m − M)	Total A_V (mag)	Galactic A_R (mag)	χ^2
ANTLIA	25.42±.06	25.49	0.20±.04	0.212	1.18
UGC 9128	26.70±.04	26.75	0.20±.04	0.065	1.36
UGC 4483	27.86±.07	27.53	0.10±.04	0.091	1.12
NGC 4163	27.40±.04	27.36	0.05±.04	0.050	1.31
UGC 6456	28.30±.04	28.19	0.05±.04	0.096	1.08
NGC 6789	27.85±.04	27.78	0.15±.04	0.187	1.29
NGC 1569: HSB[a]	27.53±.06	27.63	1.8±0.1	1.87	1.60
NGC 1569: LSB[b]	27.72±.06	27.63	1.5±.1	1.87	2.14
NGC 4068	28.25±.04	28.17	0.00±.04	0.060	1.59
SBS 1415+437	30.70±.04	30.70	$-.05 \pm .04$	0.024	1.46
IC 4662: HSB[a]	26.80±.04	26.94	0.45±.04	0.190	1.22
IC 4662: LSB[b]	26.75±.04	26.94	0.50±.04	0.190	1.74
ESO154-023	28.80±.04	28.80	0.10±.04	0.045	1.63
NGC 2366: Field 1	27.48±.06	27.52	0.20±.04	0.097	1.33
NGC 2366: Field 2	27.44±.07	27.52	0.15±.04	0.097	1.30
NGC 625	28.05±.04	27.95	$-.05 \pm .04$	0.044	1.40
NGC 784	28.70±.04	28.58	0.10±.04	0.158	1.84
NGC 5253: HSB[a]	27.75±.04	27.70	0.15±.04	0.186	1.26
NGC 5253: LSB[b]	27.65±.04	27.70	0.20±.04	0.186	2.35
NGC 6822: Field 1	23.38±.05	23.30	1.1±.1	0.632	1.31
NGC 6822: Field 2	23.39±.04	23.30	1.1±.1	0.632	1.42
NGC 6822: Field 3	23.45±.06	23.30	0.70±.04	0.632	1.28
NGC 4214	27.20±.04	27.13	0.15±.04	0.058	1.26
NGC 4449: HSB[a]	27.95±.04	28.12	0.25±.04	0.051	3.00
NGC 4449: LSB[b]	28.05±.04	28.12	0.15±.04	0.051	2.41

[a] HSB refers to the high surface brightness region.
[b] LSB refers to the low surface brightness region.

Cols. (2) Distance Modulus best fit by the CMD fitting program. The uncertainties are lower bounds as they include only statistical uncertainties and (3) Distance Modulus reported by various authors in literature. See Table 3.1 for references. (4) Foreground and internal extinction best fit by the CMD fitting program. The uncertainties are lower bounds as they include only statistical uncertainties. (5) Galactic foreground extinction at $\lambda_R = 650$ nm reported by Schlegel et al. (1998). (6) Best χ^2 value of CMD fitting program.

context for the intensity of the recent SF. A finer time resolution is used in deriving the SFH in the most recent $\sim$ 500 Myr leveraging the excellent temporal information from the HeB stars. The SFRs derived for NGC 6822 are lower limits due to the limited spatial coverage of the observations. As noted earlier in §3.2.1, the ancient SFH for SBS 1415+437 is not well constrained due to the shallow photometry.

The uniform photometry and SFH recovery allow us to directly compare the results between galaxies. To first order, the SFHs share some common characteristics. Most show significant star formation in the oldest time bin indicative of galaxy assembly and the formation of stars in systems rich in gas. The galaxies also show elevated levels of recent star formation, as expected for systems previously identified as starbursts or fossil bursts.

Deeper inspection reveals, however, that the details of the SFHs vary from galaxy to galaxy. There does not appear to be a "typical" starburst SFR(t) profile. The most notable differences in the recent SFRs are more readily apparent in Figure 3.6 where we present an expansion of the last gigayear of the SFHs for each of the galaxies. Higher levels of SF are sustained in all the galaxies across some larger interval of time (δt>few 100 Myr) with variations and inhomogeneities on smaller temporal scales (δt$\sim 10-20$ Myr). A number of systems show a sustained SFR over a period of a few hundred Myr (e.g., ESO 154−023, NGC 4068, and UGC 4483) while others exhibit fluctuations in their recent SFR (e.g., UGC 9128, NGC 1569, SBS 1415 + 437, NGC 2366, NGC 625, and NGC 4214). One galaxy, NGC 6822 shows the beginning of a burst with elevated levels of SF in the most recent 50 Myr.

One of the advantages of using resolved stellar populations is the ability to identify and study galaxies whose bursts have ended. Five SFHs show a decline in SFR in the most recent times (i.e., Antlia, UGC 9128, NGC 625, NGC 4163, and NGC 6789) after experiencing elevated levels of SF for a period of a few hundred Myr. These fossil burst galaxies are excellent systems in which to measure the complete duration of a burst event (see Paper II), rather than a lower limit. Fossil burst galaxies also increase the number of nearby systems in which one can study the starburst phenomenon. The resolved stellar populations required for any detailed SFH history limits such studies to galaxies within $5-8$ Mpc. We encountered the limitations of studying farther galaxies even with observations of long integrations times (e.g., SBS 1415+437). Identifying

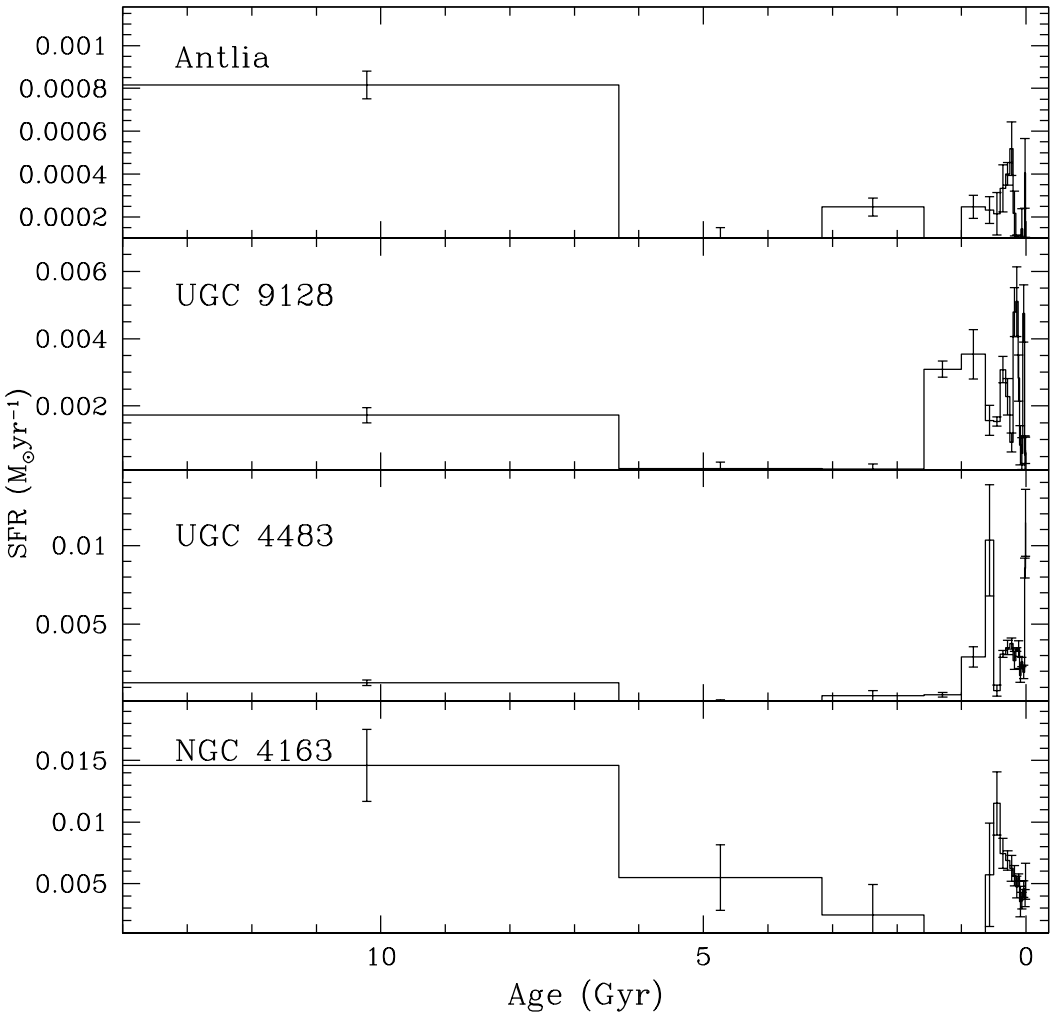

Figure 3.5 The SFHs of Antlia, UGC 9128, UGC 4483, NGC 4163 derived from the HST optical observations of the resolved stellar populations for the eighteen galaxy sample. The oldest time time ($6 - 14$ Gyr) is an average SFR that constrains the ancient SF giving context for the overall SFH yet these numbers are not used in our calculations. The uncertainties in this age bin are underestimated due to averaging over a longer time. The time resolution at more recent times is much finer and makes use of the unambiguous age dating of the HeB stars. Note the elevated levels of star formation in these most recent time bins. Expansions of the last 1 Gyr SFHs are presented in Figure 3.6.

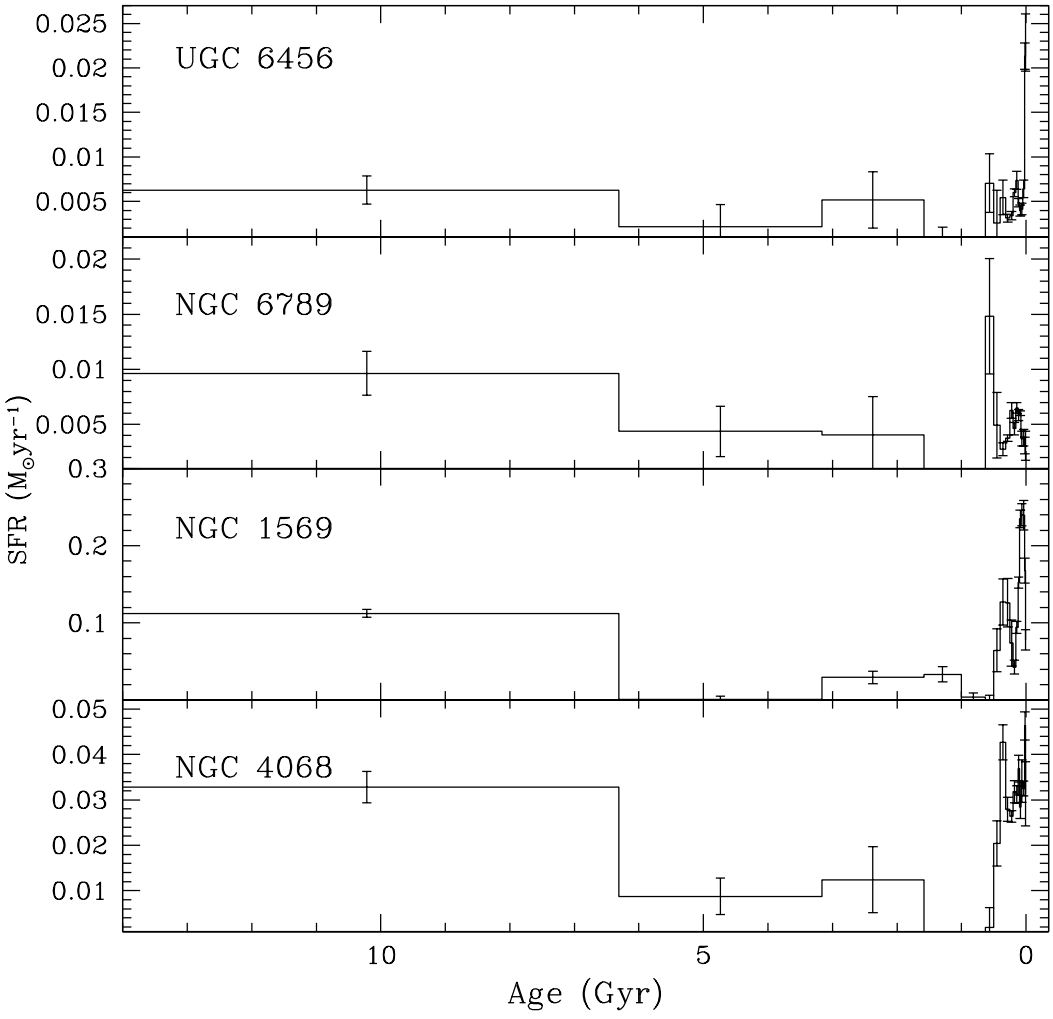

Figure 3.5 *Lifetime SFHs continued: UGC 6456, NGC 6789, NGC 1569, NGC 4068*

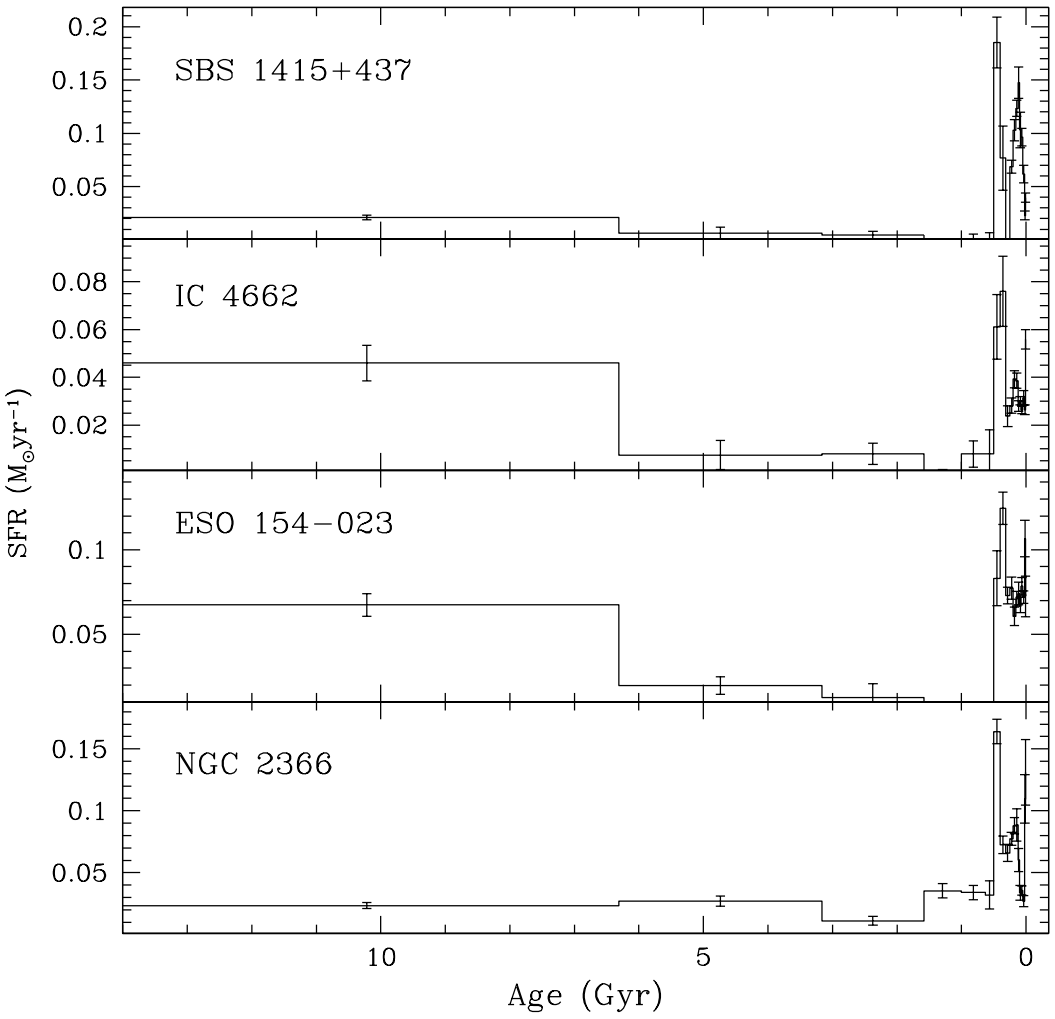

Figure 3.5 *Lifetime SFHs continued: SBS1415+437, IC 4662, ESO154−023, NGC 2366.* Note the ancient SFH for SBS 1415+437 is not well constrained due to the shallow photometry.

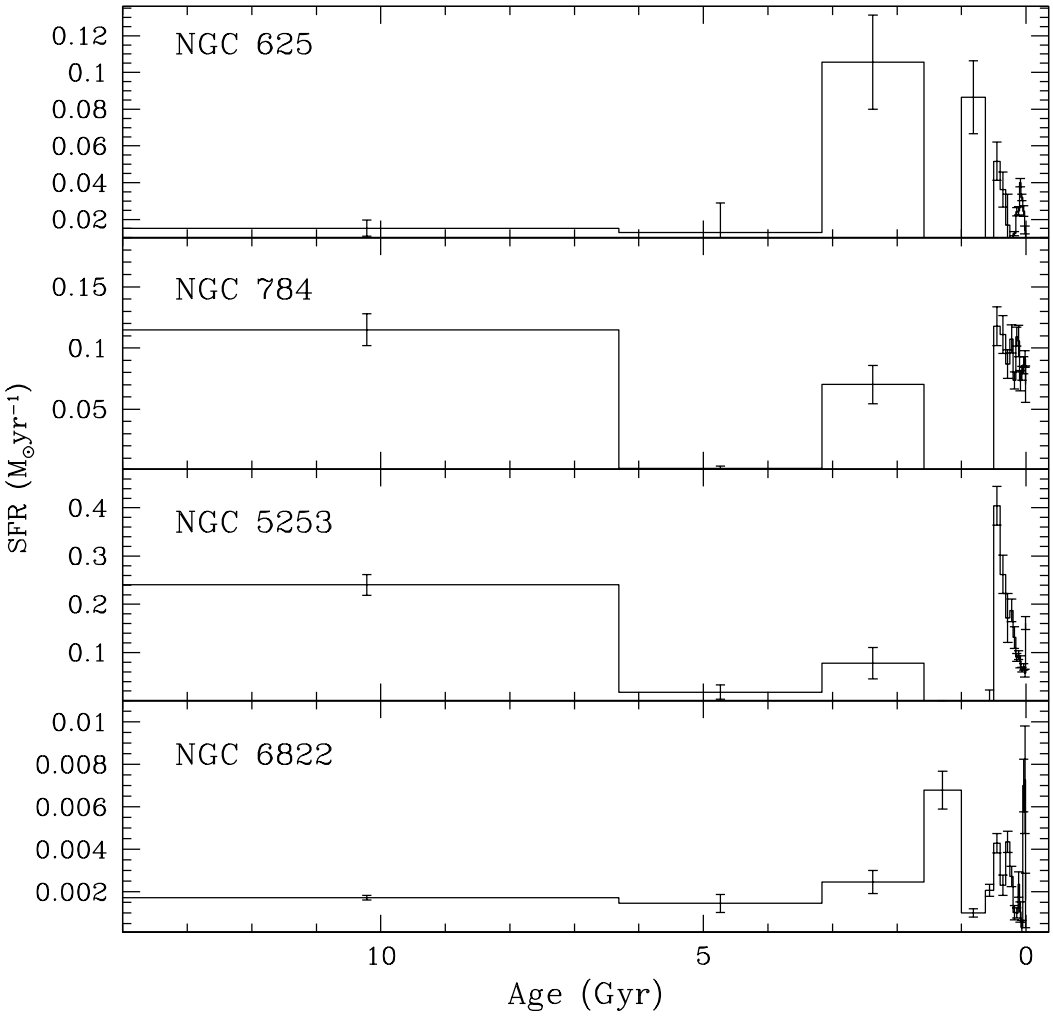

Figure 3.5 *Lifetime SFHs continued: NGC 625, NGC 784, NGC 5253, NGC 6822.* Note the SFRs derived for NGC 6822 are lower limits due to the limited spatial coverage of the observations.

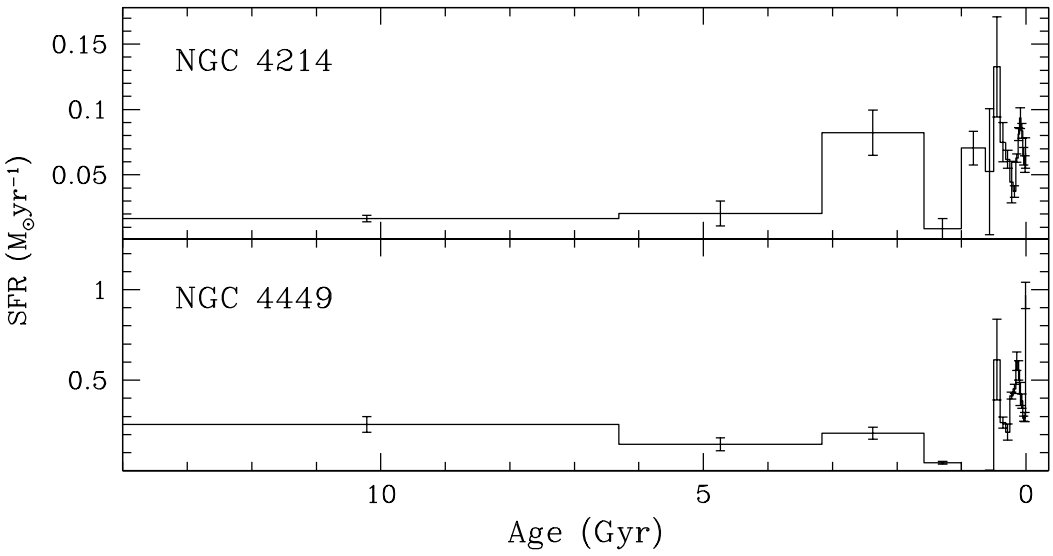

Figure 3.5 *Lifetime SFHs continued: NGC 4214, NGC 4449*

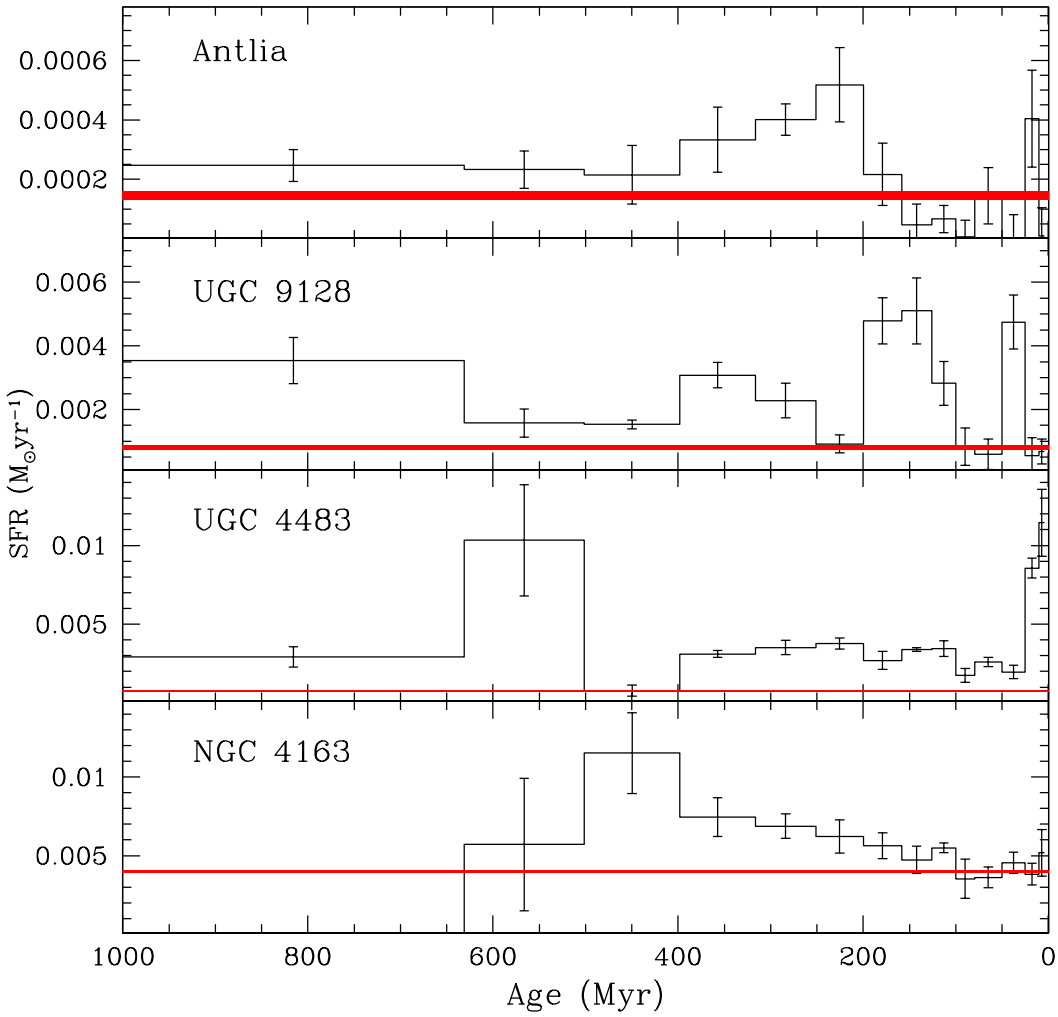

Figure 3.6 The last 1 Gyr of the SFHs of Antlia, UGC 9128, UGC 4483, NGC 4163 presented in Figure 3.5 are shown here in greater detail. The red line represents the average SFR over the past 6 Gyr ($b_{recent} = 1$). The thickness of the red line represents the uncertainties in the average which are affected by the photometric depth, extinction, and photometric crowding. Each profile shows elevated SFRs at recent times yet the SFRs over the past few hundred Myr are diverse. All galaxies exhibit the common characteristic of having SFRs well above the last 6 Gyr average yet there is no specific pattern of SFR that characterizes a burst nor is there an absolute level of SF that sets a threshold for bursting SF.

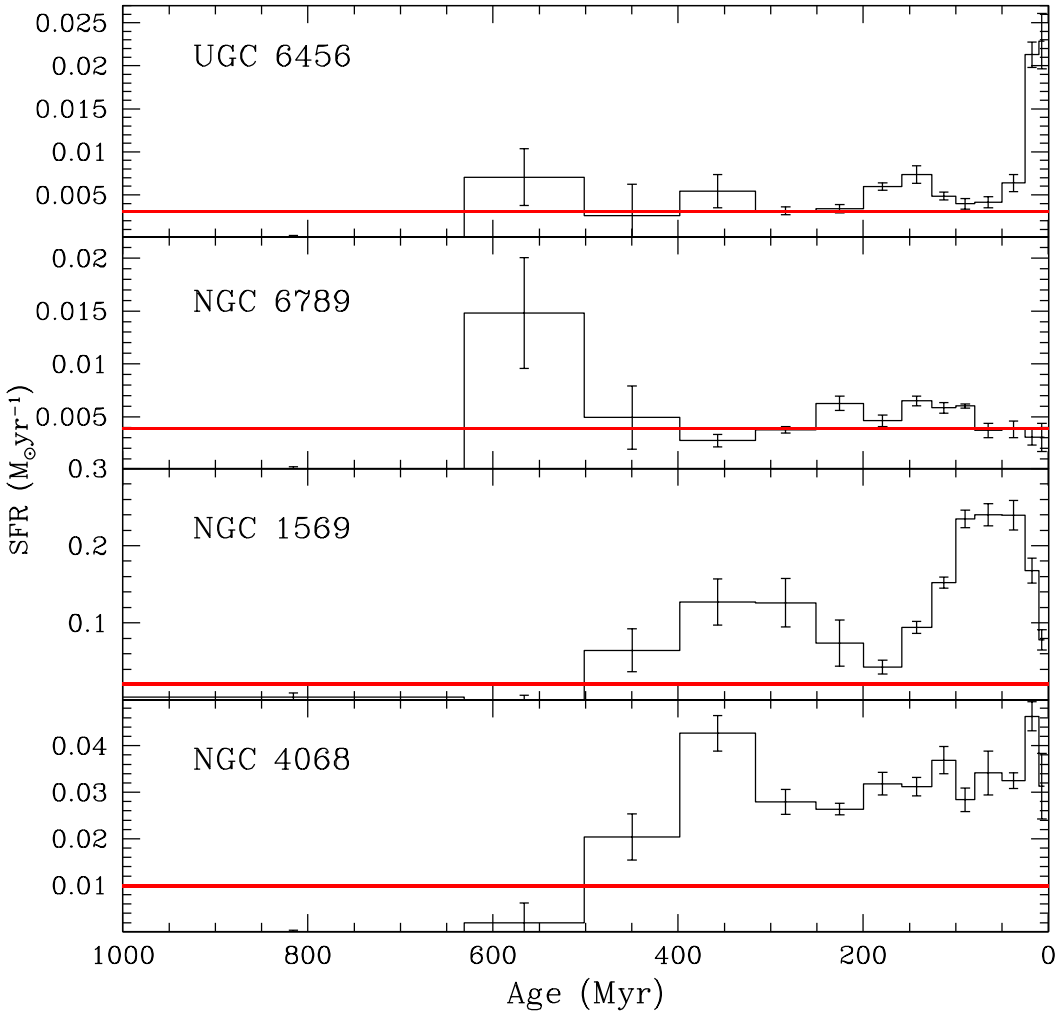

Figure 3.6 *Recent SFHs continued: UGC 6456, NGC 6789, NGC 1569, NGC 4068*

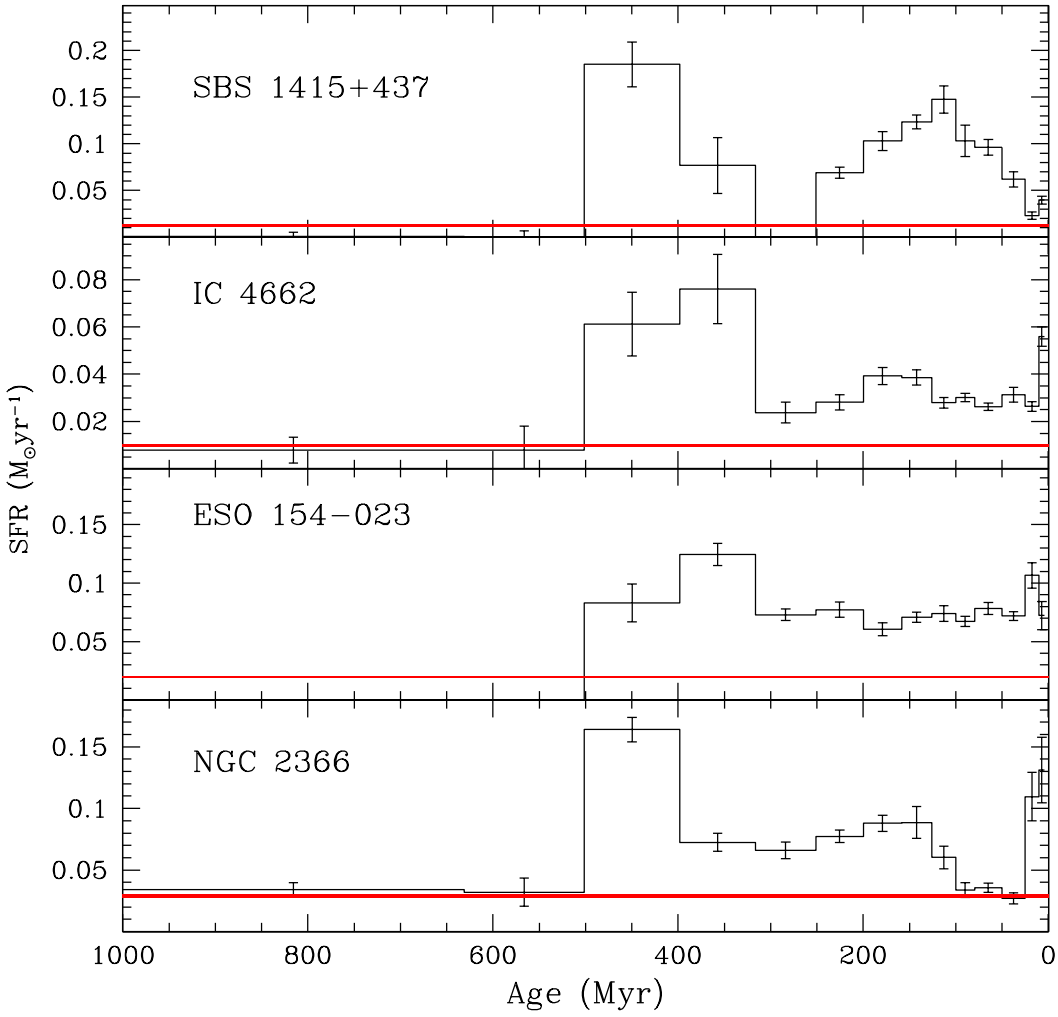

Figure 3.6 *Recent SFHs continued: SBS1415+437, IC 4662, ESO154−023, NGC 2366*

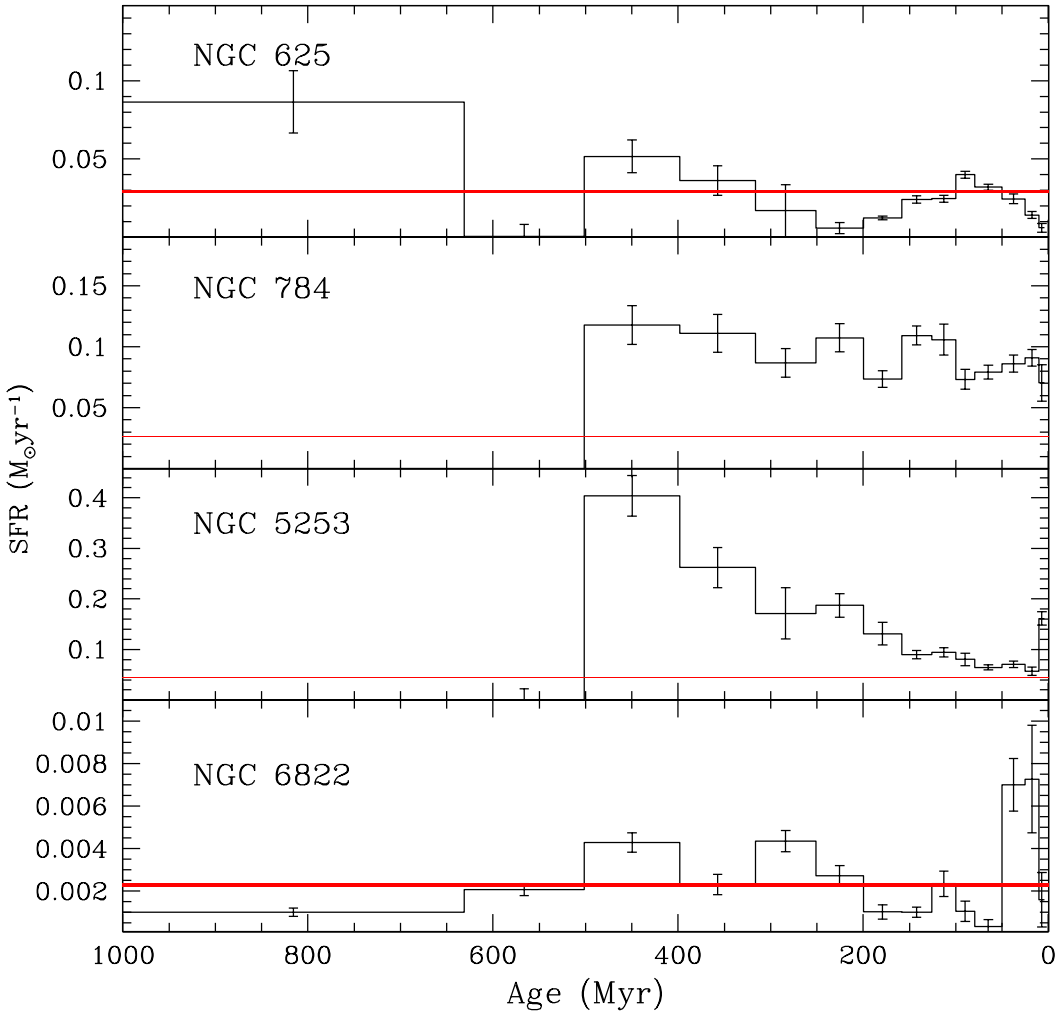

Figure 3.6 *Recent SFHs continued: NGC 625, NGC 784, NGC 5253, NGC 6822*

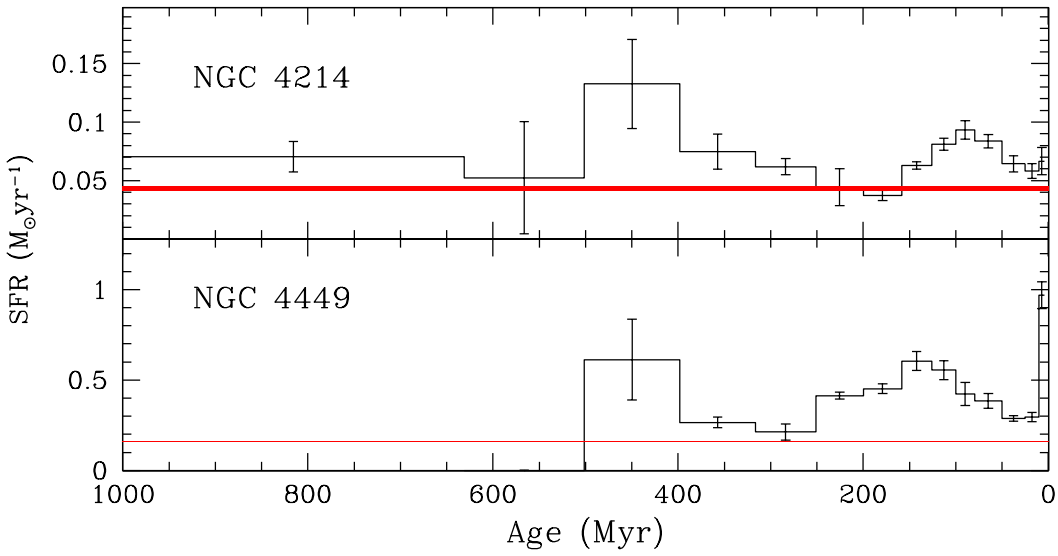

Figure 3.6 *Recent SFHs continued: NGC 4214, NGC 4449*

fossil burst systems increases the sample of starburst galaxies in the nearby universe reducing our dependence on studying systems that push the limit of our observational capabilities.

3.4 When is Star Formation a Starburst?

SF activity within a burst is complex and consequently, there are many definitions in the literature to identify and quantify bursts. Here, we consider three metrics to identify starbursting systems and discuss their applicability/limitations.

3.4.1 Gas Consumption Timescales

The fundamental characteristic of a starburst is that the high rate of SF during the burst is short-lived compared to the lifetime of the host galaxy. A limit for how long this high SFR may be sustained can be determined by calculating how long it would take to turn all the raw material fueling the burst into stars. If this "gas consumption timescale" (τ_{gas}, Roberts 1963) is significantly less than the Hubble time, then the burst must be unsustainable and thus must be short lived on a cosmic time scale, increasing the chance that the elevated SFR is temporary. One can calculate τ_{gas} by dividing the mass of the gas (i.e., the raw material that fuels the starburst) by the peak SFR during the starburst event ($M_\odot$ yr^{-1}).

The total gas mass is not always known for these low mass dwarf systems. The molecular phase of the ISM is rarely detectable in dwarfs (e.g., Israel et al. 1995; Taylor et al. 1998; Barone et al. 2000), and thus is unlikely to contribute significantly to the gas supply, unless the uncertain conversion factor from CO to H_2 is extremely high (e.g., Wilson 1995; Israel 1997; Bolatto et al. 2008). Atomic gas is thus likely to dominate the gaseous ISM. The current best estimates suggest that the ratio of molecular gas mass to atomic gas mass is 0.3 ± 0.05 (Leroy et al. 2005, and references therein) indicating that the atomic gas mass indeed dominates. Therefore, while molecular gas is needed for star formation to proceed, the atomic gas is what ultimately fuels the formation of molecular gas, and is the relevant quantity to consider for the gas consumption times of low mass systems. However, the atomic gas is frequently far more extended than the star forming disk reaching up to several Holmberg radii at a density of 10^{19} atoms cm^{-2}

for dwarf irregular galaxies (e.g., Huchtmeier et al. 1981). Thus, the gas mass available for SF is lower than the measured HI mass in a galaxy making τ_{gas} an upper limit.

We present the resulting gas consumption timescale of the atomic gas in the absence of stellar recycling in Table 3.4. We have calculated τ_{gas} from the peak SFR in the last Gyr for each galaxy (column 3) and atomic mass measurements taken from the literature (columns 4 and 5) after multiplying the HI mass by a factor of 1.4 to account for the mass of helium and heavy elements (e.g., Roberts 1963; Kennicutt et al. 1994). Of the sixteen galaxies for which we have found HI measurements, fifteen show consumption timescales significantly less than a Hubble time (0.44 Gyr$< \tau_{gas} <$ 5.2 Gyr) indicating that the peak SFRs measured in these systems cannot be sustained for the entire history of the galaxy. One galaxy, NGC 6822, has a gas consumption timescale longer than a Hubble time (τ_{gas} = 26 Gyr); however, this timescale is an upper limit, as the optical observations (see observational footprint in Figure 3.1) cover only $\sim$ 17 arcmin^2 of the star forming disk and the atomic gas is known to be unusually extended ($>$ 600 arcmin^2) relative to the optical disk (de Blok & Walter 2000).

Table 3.4 Comparison of Starburst Classification Schemes

Galaxy	Peak b_{recent} of Burst	Peak SFR of Burst (10^{-3} $M_\odot yr^{-1}$)	Atomic Mass ($\times 10^7$ $M_\odot$)	Ref.	τ^a_{gas} Gyr	b_{recent} last $4-10$ Myr	Hα EW Å
Antlia Dwarf	3.5 ± 0.9	0.52 ± 0.01	0.08	8	2.2	0.06 ± 0.65	No Detect.
UGC 9128	6.3 ± 1.4	5.1 ± 1.0	2	7	1.7	0.83 ± 0.49	4 ± 2
UGC 4483	14 ± 3	11 ± 2	4	9	4.9	14 ± 3	144 ± 11
NGC 4163	2.9 ± 0.6	12 ± 3	1.5	13	1.8	1.3 ± 0.4	8 ± 2
UGC 6456	7.6 ± 1.1	23 ± 3	4	1	2.4	7.6 ± 1.1	127 ± 17
NGC 6789	3.8 ± 1.3	15 ± 5	...	...	...	0.78 ± 0.34	23 ± 3
NGC 1569	21 ± 1	240 ± 10	7.5	4	0.44	3.8 ± 0.7	215 ± 12
NGC 4068	4.7 ± 0.3	46 ± 3	10	13	3.0	3.1 ± 0.7	28 ± 5
SBS 1415+437	12 ± 2	150 ± 10	10	12	0.93	3.3 ± 0.6	205 ± 25
IC 4662	7.7 ± 1.6	76 ± 15	13	11	2.3	5.7 ± 0.6	101 ± 10
ESO 154-023	6.4 ± 0.5	120 ± 10	...	...	...	3.7 ± 0.6	40 ± 3
NGC 2366	5.6 ± 0.4	160 ± 10	60	4	5.2	1.5 ± 0.3	149 ± 38
NGC 625	1.4 ± 0.1	$40. \pm 2$	11	2	1.8	0.15 ± 0.07	31 ± 4
NGC 784	4.5 ± 0.6	120 ± 20	38	7	4.5	2.7 ± 0.6	53
NGC 5253	9.0 ± 0.9	400 ± 40	12	10	0.42	3.6 ± 0.3	120 ± 9
NGC 6822	3.1 ± 1.1	7.3 ± 2.5	13	3	26[b]	0.69 ± 0.55	47 ± 12
NGC 4214	3.1 ± 0.9	130 ± 40	41	4	4.3	1.5 ± 0.3	62 ± 7
NGC 4449	6.0 ± 0.5	970 ± 70	110	4	1.5	7.1 ± 0.6	72

[a] The timescale was calculated using peak SFR and the HI gas mass adjusted by a factor of 1.4 to account for helium and heavy elements.
[b] The gas consumption timescale is an upper limit for NGC 6822 as the field of view of the observations used to derive the SFRs does not cover the main optical disk compared with the area from which the gas mass is derived.

References. — (1) Begum et al. 2008 (FIGGS); (2) Cannon et al. 2004; (3) de Blok 2000; (4) Walter et al. 2008 (THINGS SURVEY); (6) van Eymeren et al. 2009; (7) van Zee 2001; (8) Whiting et al. 1997.; (9) Thuan & Seitzer 1979; (10) López-Sánchez et al. 2008; (11) López-Sánchez et al. 2009; (12) Huchtmeier et al. 2005; (13) Bottinelli et al. 1990; (14) Swaters & Balcells (2002)

Our simple calculation supports the gas consumption timescale as a useful first order metric for confirming whether a system is a starburst. Fifteen of the sixteen galaxies considered fit this rubric with higher normalized SFRs generally correlating with shorter gas consumption timescales. However, the τ_{gas} metric provides only a coarse evaluation of these systems as starbursts, due to the dwarfs' spatially extended HI halo that may not be available for SF. An additional drawback of this simplistic gas consumption timescale metric is that is does not provide any additional insight into the nature of the burst.

3.4.2 Starburst Thresholds

Another fundamental characteristic of a starburst is a high absolute level of SF activity. Yet, while a highly elevated SFRs is the common characteristic of any starburst, the exact level that constitutes "bursting" is subjective. Setting an absolute SFR as a threshold to identify bursts would bias any results toward larger galaxies with intrinsically higher SFRs. For an unbiased metric, one must consider the SFR relative to what an individual galaxy has experienced in the past. Previously, Scalo (1986) and Kennicutt (1998) formulated the birthrate parameter (b) which compares the current SFR with the the average SFR over the lifetime of a galaxy (i.e., $b \equiv SFR \; / \; < SFR >$). McQuinn et al. (2009) modified this parameter using the average SFR during the last 6 Gyr,instead of the average SFR over the lifetime of the galaxy (i.e., $b_{recent} \equiv SFR \; / \; < SFR_{0-6 \; Gyr} >$). This calculation decouples any SF activity during the initial assembly period of galaxies from the SF during later epochs providing a more relevant baseline in the current epoch. Note that 6 Gyr is still a substantial fraction of the lifetime of a galaxy, and thus is a robust measure of the average SFR. In addition, the normalized SFRs are more securely anchored with SFRs from the more recent time bins (see §3.3.3).

Using a $b_{recent} > 2$ to identify a burst and defining the beginning and end points of a burst at the time when $b_{recent} = 1$ (McQuinn et al. 2009), the duration of the starburst events in our sample last over a few hundred Myr, with the shortest duration being 450 Myr and the longest being 1.3 Gyr. The accuracy of these measurements depends in part on our inherent time resolution of the affected SFH. The temporal resolution over the last 100 Myr is fine enough that we can discern and measure fluctuations in

the SFR over short timescales and pinpoint the value of b_{recent} with time intervals of $25 - 50$ Myr. In contrast, older bins have coarser inherent time resolution, giving less accuracy on the interval burst duration. Coarse time bins not only reduce the accuracy of the burst duration, but also reduce our sensitivity to bursts. With larger time bins, short duration increases are not detectable if their durations are much shorter than the width of the time bin in our derived SFH. We are therefore most sensitive to starbursts that have occurred in the last 500 Myr where are temporal resolution is the finest.

The average SFR for recent times ($b_{recent} = 1$) are drawn in red across the SFHs in Figure 3.6. We identify starbursts if the birthrate parameter is greater than two (Kennicutt et al. 2005). All galaxies show significant levels of recent star formation that are well above $b_{recent} = 2$ in multiple time bins. In the case of NGC 6822, the high levels of SF occur in the last 50 Myr, indicating that this burst is likely just beginning. The four additional galaxies we included in our sample based on the HeB distributions in their CMDs (Antlia, UGC 9128, ESO $154 - 023$, and NGC 784) are confirmed as starbursts. All show $b_{recent} > 2$ over multiple time bins.

Because of the long temporal baseline available with CMD studies, our analysis also identifies fossil bursts whose *current* SFR is below our starburst threshold (i.e., Antlia, UGC 9128, NGC 625, NGC 4163, and NGC 6789). Four of the five fossil bursts (Antlia, UGC 9128, NGC 4163, and NGC 6789) do not show the typical burst characteristics of intense Hα, UV, or optical emission. For example, looking at a current optical image of the lowest mass galaxy in our sample, the Antlia dwarf galaxy, it is not at all obvious that it has undergone a period of significant star formation in its recent past. The absolute values of the SFR in Antlia are the lowest in our sample, but taken in the context of its own SFH, the recent burst of SF is significant and measurable.

The fifth fossil burst, NGC 625, is unique among our sample. Although NGC 625 produces strong radio continuum and Hα emission often associated with starbursts (Cannon et al. 2003; Cannon & Skillman 2004), the SFRs over the past 500 My fall below our starburst threshold of $b_{recent} = 2$. Yet, NGC 625 shows strong evidence at other wavelengths of a starburst. This discrepancy can be understood if we look at the lifetime SFH in Figure 3.5. The SFH shows the initial onset of SF is suppressed for 11 Gyr, followed by multiple bursts in SF over the past 3 Gyr. Our b_{recent} metric assumes that the initial onset of SF occurs at t>6 Gyr; NGC 625 does not fit this assumption

but we include it for comparison to the others in our sample. Note that suppressed initial SF over a significant period of time is also seen in two other systems in our sample, NGC 2366 and NGC 4214 and reported separately for the dwarf galaxy Leo A (Cole et al. 2007).

Figure 3.7 presents the peak b_{recent} values from each burst against the gas consumption timescale for the systems. There is a general trend that stronger bursts have shorter gas consumption timescales, illustrating the usefulness of τ_{gas} as a simple starburst identification metric. The calculation for NGC 6822 is an upper limit ($\tau_{gas} \sim 26$ Gyr) as the observational field of view does not cover the majority of the optical disk.

3.4.3 Hα Emission from Starbursts

The SF activity in a burst creates a short−lived population of high mass stars that emits copious amounts of radiation. This strong emission can be observed and used as a starburst indicator. Specifically, the high mass stars formed in a starburst create high levels of UV emission (M$>$ 3 M$_\odot$) and Hα emission (M$>$ 20 M$_\odot$) over the lifetime of these stars. Our time-resolved SFHs afford an opportunity to compare to the SFHs derived from their resolved stellar populations with the different timescales of these starburst indicators. We will explore the emission and timescales from the UV emission in a later paper; several of these galaxies are targets for a GALEX legacy program (P.I. Skillman, Proposal number 60026). Here, we compare the Hα emission from Lee et al. (2009) with our SFHs. Since the Hα emission is expected to be emitted over a timescale $\lesssim$ 5 Myr, we compare the Hα fluxes to the SFRs in our most recent time bin of $4-10$ Myr. We do not include younger time bins because the evolution of the most massive stars with lifetimes $\lesssim$4 Myr are not calculated in the stellar evolutionary models employed in the SFH program.

Lee et al. (2009) identify a galaxy as a starburst if it has an Hα equivalent width (EW(Hα)) of greater than 100 Å. They suggest that this corresponds to a birthrate value of 2 or 3 (Kennicutt 1998). This EW(Hα) starburst metric can be directly compared with our starburst indicator b_{recent}, as shown in Figure 3.8. The horizontal dotted line represents the delineation of a starburst in EW(Hα) and the vertical dotted line represent our delineation of a starburst ($b_{recent} \geq 2$). Galaxies presently bursting are plotted as blue points while galaxies with fossil bursts are plotted in thicker, red points.

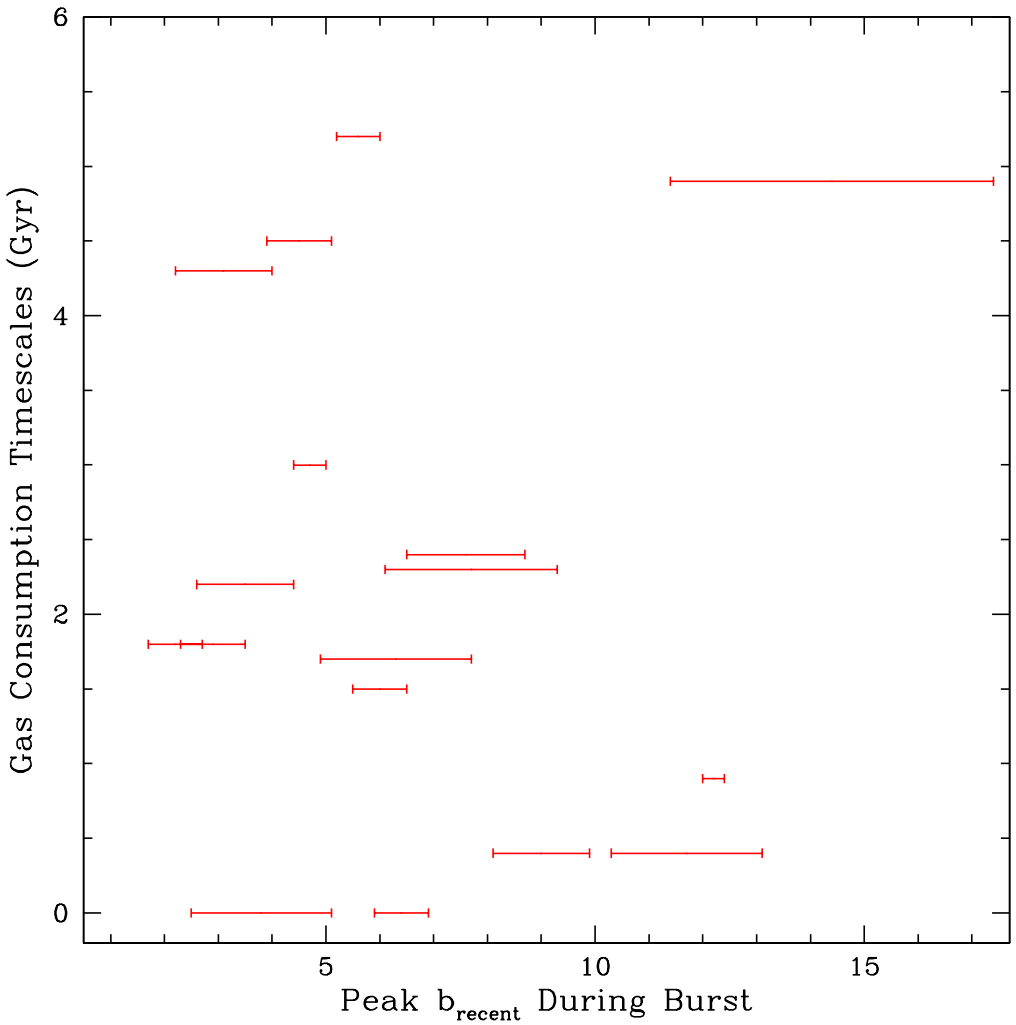

Figure 3.7 The gas consumption timescale is shorter than the Hubble time in sixteen of the sixteen galaxies in our sample for which there are HI mass measurements confirming the short-lived nature of the starbursts on a cosmic timescale. The observational field of view for one galaxy (NGC 6822) did not cover the majority of the optical disk so the gas consumption timescale for this galaxy is an upper limit of $\sim$ 26 Gyr and not plotted as it is off the scale of this figure. Plotted against the peak b_{recent} value for each burst, there is a weak trend that stronger bursts have shorter gas consumption timescales. While the gas consumption timescale does not yield much information about a bursts' properties, it provides a coarse evaluation for identifying starbursts.

The measured EW(Hα) and b_{recent} values are listed in Table 3.4.

The comparison of these two starburst indicators in Figure 3.8 highlights both the usefulness and the limitations of the techniques. Seven galaxies have EW(Hα) > 100 Å classifying these systems as Hα starbursts. These systems also meet our starburst threshold of a $b_{recent} > 2$ in our most closely matched time bin of $4 - 10$ Myr. Eleven galaxies have a measured EW(Hα) below the 100 Å threshold and were not classified as Hα starbursts. These eleven galaxies can be broken into two groups when considering our SFH results. In the first group, seven of these systems had a measured $b_{recent} < 2$ in the last $4-10$ Myr suggesting that the starbursts in these galaxies are currently weak or have ended (red points). This is congruous with lower Hα emission. The second group, however, contains four galaxies (NGC 4068, ESO 154+023, NGC 784, NGC 4449) that show $b_{recent} > 2$ in the last $4 - 10$ Myr. In other words, these four galaxies show recent starburst characteristics from analysis of their stellar populations but do not meet the Hα emission starburst threshold. Note that our most recent time bin overlaps with, but is not coincident with, the timescale of Hα. The SF in this final group of four galaxies must therefore be changing on timescales shorter than a few Myr to explain the discrepancy. Fluctuations of SFR on short timescales are also seen in the SFHs in Figure 3.6 at recent times where our temporal resolution is the finest.

A broader observation can be drawn from Figure 3.8. Analysis of stellar populations gives a longer timescale to consider SF activity within a galaxy. From this perspective, the starbursts are events lasting *at least* a few 100 Myr. If the starburst durations we measure are typical of dwarf galaxies, then short term fluctuations of SF activity are as fundamental as the longer term characteristics of the SFR. The inherently short timescale of the Hα emission is limited to identifying starbursts based only on the most current SF activity which, as we see in Figure 3.8, may or may not be representative of the recent SFH of a galaxy. Hα emission will miss identifying an important number of starburst systems.

3.5 Are Starbursts "Self-Quenching"?

Feedback from massive stars in the form of UV ionizing radiation and SNe impact the surrounding gas cloud from which stars are being formed. The idea that this feedback

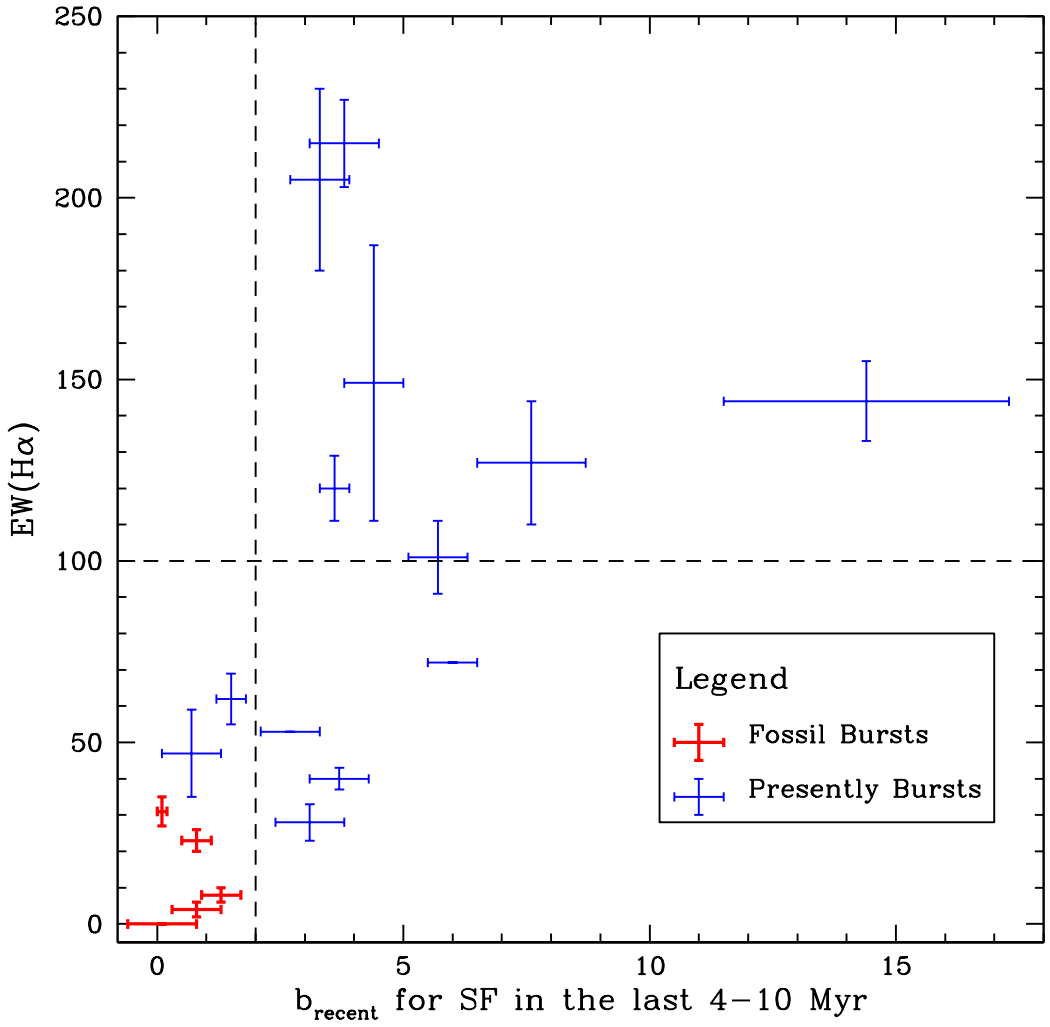

Figure 3.8 The EW(Hα) (Å) (Lee et al. 2009) is plotted against the b_{recent} values from our time bin of $4-10$ Myr; the most closely matched with the Hα emission timescale. The horizontal dotted line represents the 100 Å threshold set by Lee et al. (2009) delineating a starburst galaxy and the vertical dotted line represents our limit of $b_{recent} = 2$ for the same purpose based on resolved stellar population analysis. Seven galaxies classified as Hα starbursts also show bursting levels of SF in our most recent time bin. Seven galaxies that do not meet the Hα starburst threshold, also show lower levels of SF in the past $4-10$ Myr. Four galaxies show discrepancies between the two metrics indicating that the SF is changing on short timescales of a few Myr. These galaxies clearly show bursting SF from a stellar populations perspective but do not show starburst levels of Hα emission.

can regulate or even quench in situ SF via the heating and mechanical disruption of the gas has been put forth by previous authors (e.g., Nishi & Tashiro 2000). Higher metallicity clouds are more effective at cooling so the quenching effect would theoretically be more important in low-metallicity systems (Omukai & Nishi 1999).

The "self-quenching" process has been extrapolated to SF on galactic scales increasing with galaxy mass (Kaviraj et al. 2007). Ferguson & Babul (1998) posit that feedback from a burst limits the burst duration to short timescales of ~ 10 Myr. Numerous other studies have reported that starbursts last $\lesssim 10$ Myr based on: (1) fitting starburst models to UV spectra (Tremonti et al. 2001); (2) studying stellar clusters within starburst galaxies (Harris et al. 2004); and (3) emission from Wolf-Rayet stars (Schaerer, Contini, & Kunth 1999; Mas-Hesse & Kunth 1999), to name a few. These short durations would seem to corroborate the idea of "self-quenching" derived by calculations balancing the kinetic energy output of SNe with the binding energy of the gas (Thornley et al. 2000). If starburst durations are comparable to or shorter than the crossing time, they are self-extinguishing explosions destroyed by their energy output in a non-equilibrium fashion (Meurer 2000).

In Paper II, we measure the durations of starbursts in the sample galaxies from our time-resolved SFHs presented in Figures 3.5−3.6. The durations range from 450 ± 50 to 640 ± 190 Myr in fourteen galaxies and up to 1300 ± 290 Myr in four galaxies. These longer durations are comparable to or longer than the rotational period of the host galaxies and are in agreement with other studies measuring durations on the order of 100 Myr (Calzetti et al. 1997; Meurer 2000; Lee et al. 2009). The SFH show that starbursts events last a few hundred Myr, much longer than the lifetime of O stars. Rapid "self-quenching" does not apply to starbursts in our sample.

The shorter timescales cited in the literature above likely result from measuring only part of a burst event, corresponding to the lifetime of individual star clusters formed. This "flickering" is seen in the dips and variations in the SFHs on timescales of 10 Myr and suggests the small scale SF may be disrupted or quenched via stellar feedback. SF activity on these short timescales is associated with small spatial scales, and can be significantly affected by local conditions, making it a stochastic process. The non-equilibrium energy and mass transfer creating the small scale self-quenching may trigger SF in adjacent areas, creating self-propagating bursts of longer durations.

We will investigate SF propagation within a burst in Paper III of this series using the spatial information of the stellar populations, regional SFHs, and stellar evolutionary time sequences.

3.6 Conclusions

We have used optical data obtained from the HST data archive to reconstruct the SFHs of eighteen nearby starburst dwarf galaxies. The SFHs show large variations from galaxy to galaxy, and, while the galaxies represent a class of objects undergoing significant recent star formation, there is no "idealized" SFR profile that characterizes the starburst phenomenon. Not only are the changes in the SFR during a burst varied but the peak SFRs during the bursts span nearly three orders of magnitude in value indicative of the range in physical conditions present in each of the galaxies studied. Thirteen of the galaxies show ongoing starbursts and five present fossil bursts. The SFRs fall on a continuum between bursting and "regular" with the distinctions between the two dependent on the individualized history of each host system and the complicated feedback mechanisms created during the bursts. With this in mind, we examined three metrics for identifying starbursts with the following results and conclusions:

• The gas consumption timescale provides a coarse evaluation of whether a galaxy's SFR is sustainable over a cosmic timescale. For the sixteen galaxies with HI mass measurements, fifteen systems can be classified as starbursts based on their gas consumption timescales being significantly shorter than the Hubble time. The remaining galaxy (NGC 6822) has an upper limit of the gas consumption timescales of 26 Gyr calculated from SFRs derived from a limited field of view of the optical disk.

• The Hα emission from fourteen galaxies measured by Lee et al. (2009) correlates with the SFR in our most recent time bin of $4-10$ Myr. Four galaxies classified as starbursts in the most recent time bin show non-starburst levels of Hα emission indicating that while the bursts are long-lasting events, the SFR can change on timescales of only a few Myr. If the longer durations of a few hundred Myr for this sample of galaxies is typical of starbursts, this longer lived phenomenon is best studied at wavelengths correlating with comparable emission timescales; the short timescale of Hα emission will miss identifying bursting galaxies experiencing short-lived fluctuations in the SFR.

• We compared how the SFR changes over time within each galaxy normalized with an average SFR from the past 6 Gyr (b_{recent}=SFR /<SFR>$_{0-6\ Gyr}$); avoiding a comparison of absolute values of SFR biased towards larger systems. The recent SFRs are higher than twice the average SFR over the last 6 Gyr ($b_{recent} > 2$) in seventeen galaxies confirming that these galaxies are starbursts by this stellar population metric. The exception is NGC 625 which presents a unique SFH. The initial onset of SF occurred 3 Gyr in NGC 625 and proceeded in three bursts until the current epoch. This galaxy shows evidence of a starburst at other wavelengths although it does not fit our burst metric.

• The starburst events seen in the SFHs last at least 450 Myr on timescales comparable to or longer than the rotational period of the host galaxies ruling out "self-quenching" of these bursts from stellar feedback mechanisms.

3.7 Acknowledgments

Support for this work was provided by NASA through grants AR-10945 and AR-11281 from the Space Telescope Science Institute, which is operated by Aura, Inc., under NASA contract NAS5-26555. E. D. S. is grateful for partial support from the University of Minnesota. J. J. D. was partially supported as a Wyckoff fellow. K. B. W. M. gratefully acknowledges Matthew, Cole, and Carling for their support. This research made use of NASA's Astrophysical Data System and the NASA/IPAC Extragalactic Database (NED) which is operated by the Jet Propulsion Laboratory, California Institute of Technology, under contract with the National Aeronautics and Space Administration. Finally, we would like to acknowledge the usage of the HyperLeda database (http://leda.univ-lyon1.fr).

Chapter 4

Duration of Starbursts in Dwarf Galaxies (McQuinn et al. 2010b)

A slightly modified version of this chapter appears in the published article referenced by Kristen B. W.McQuinn, Evan D. Skillman, John M.Cannon, Julianne J. Dalcanton, Andrew Dolphin, Sebastian Hidalgo-Rodríguez, Jon Holtzman, David Stark, Daniel Weisz, Benjamin Williams, 2010b, ApJ, submitted. Reproduced here with permission.

ABSTRACT

The starburst phenomenon can shape the evolution of the host galaxy and the surrounding intergalactic medium. The extent of the evolutionary impact is partly determined by the duration of the starburst, which has a direct correlation with both the amount of stellar feedback and the development of galactic winds, particularly for smaller mass dwarf systems. We measure the duration of starbursts in twenty, nearby, ongoing and "fossil" starbursts in dwarf galaxies based on the recent star formation histories derived from resolved stellar population data obtained with the *Hubble Space Telescope*. Contrary to the shorter times of $3-10$ Myr often cited, the starburst durations we measure range from $450-650$ Myr in fifteen of the dwarf galaxies and up to 1.3 Gyr in four galaxies; these longer durations are comparable to or longer than the dynamical timescales for each system. The same feedback loop from massive stars that may quench the flickering SF does not disrupt the overall burst event in our sample of galaxies. While five galaxies present fossil bursts, fifteen galaxies show ongoing bursts

and thus the final durations may be longer than we report here for these systems. One galaxy shows a burst that has been ongoing for only 20 Myr; we are likely seeing the beginning of a burst event in this system. Using the duration of the starbursts, we calculate that the bursts deposited $10^{53.9} - 10^{57.2}$ erg of energy into the interstellar medium through stellar winds and supernovae and produced 3.2%−26% of the host galaxy's mass.

4.1 Characteristics of the Starburst Phenomenon

Starbursts refer to periods of intense, massive star formation that persist on timescales much shorter than the Hubble time (Searle et al. 1973). The massive stars formed during a burst can alter the gas dynamics, future star formation, and chemical composition of the host galaxy through the stars' ionizing radiation, mass loss, and nucleosynthesis. The evolutionary effects of starbursts can be dramatic and may be one of the keys to understanding the possible link between the evolution of dwarf irregular galaxies (dIrrs) to dwarf spheroidal galaxies (dSphs) (e.g., Loose et al. 1986; Dekel & Silk 1986; Silk et al. 1987; Davies & Phillipps 1988; van Zee et al. 2004) along with external effects such as ram pressure and tidal stripping from interactions with other systems (e.g., Mayer et al. 2001a,b, 2006). The strength of these feedback processes and their evolutionary impact depend on the SF activity and therefore are largely dictated by both the intensity and the duration of the starburst event.

The duration of starbursts have been previously measured in individual galaxies (e.g., Schaerer, Contini, & Kunth 1999; Mas-Hesse & Kunth 1999; Tremonti et al. 2001) and in larger samples of galaxies (e.g., Thornley et al. 2000; Harris et al. 2004). The most commonly cited timescale for a starburst is $5 - 10$ Myr, comparable to the lifetime of massive stars. It is logical to presume from the similarity of these timescales that bursts might be "self-quenching". In other words, the massive star formation of a burst produces stellar winds and supernovae explosions that could disrupt the gas fueling the star formation and extinguish the starburst on the timescale of a few to ten Myr. The hypothesis of "self-quenching starbursts" has been put forth in a number of papers both observational (Schaerer, Contini, & Kunth 1999; Mas-Hesse & Kunth 1999; Thornley et al. 2000; Tremonti et al. 2001; Harris et al. 2004) and theoretical

(Tosi et al. 1989; Ferguson & Babul 1998; Stinson et al. 2007), all of which derive $\lesssim$10 Myr durations for starbursts. This same short timescale has been adopted in a number of models. Ferguson et al. (1998) use a burst duration of 10 Myr with a star formation efficiency of 10% in modeling the redshift distribution of dwarf galaxies. Krueger et al. (1995) assume a duration of 5 Myr when modeling the spectral energy distributions of bursting dwarf galaxies. The short duration assumed in models by Kauffmann et al. (1994) and by Hogg & Phinney (1997) affects the slope of the faint galaxy count in the galaxy luminosity function.

However, our recent study of three nearby dwarf galaxies (McQuinn et al. 2009) showed both that starbursts can last much longer (i.e., hundreds of Myr) and that starbursts are a global phenomenon that can migrate through a galaxy. The duration of starbursts is not set by the lifetime of massive stars in these galaxies. These results are in agreement with earlier suggestions that starbursts can be much longer than a few to ten Myr (Calzetti et al. 1997; Greggio et al. 1998; Meurer 2000). A complimentary study by Schulte-Ladbeck et al. (2001) reported that although simulations support fluctuations in SFR on short timescales, long periods of quiescence between short bursts produce gaps in the simulated color−magnitude diagrams (CMDs) not seen in observational data.

However, starburst driven winds may feed the intergalactic medium (IGM) altering the internal kinematics and evolutionary path of the host galaxy. The importance of galactic winds and metal−rich gas outflows triggered by supernovae explosions in low mass galaxies has been much debated in the literature (e.g., Dekel & Silk 1986; Skillman et al. 1989; Skillman 1997; Spaans & Norman 1997; Mac Low & Ferrara 1999; Romano et al. 2006; Dalcanton 2007; Martin et al. 2002; Tolstoy et al. 2009, and references therein). If starbursts sustained on timescales of a few 100 Myr for the majority of dwarf starburst galaxies, longer bursts may more readily power galactic winds.

Here, we directly measure the duration of starbursts in twenty nearby bursting dwarf galaxies from their star formation histories (SFHs) reconstructed from archival Hubble Space Telescope (HST) observations. We present the details of observations, data reduction, and method of reconstructing the SFHs in McQuinn et al. (2010a, hereafter, Paper I). In this paper, we provide a summary of the observations and data processing

in §4.2, measure the duration of the burst in each system in §4.3, and compare the durations with the dynamical properties of each host galaxy in §4.4. The bursts' durations are compared in §4.5 with the $5 - 10$ Myr timescale often cited. Finally, we calculate the amount of stellar mass and energy produced in the burst in §4.6. Our conclusions are presented in §4.7.

4.2 The Sample Galaxies and Their Star Formation Histories

Our sample was selected from observations in the HST public archive based on three photometric conditions. First, we require both V and I band images of a galaxy in the archival observations. Second, we set a minimum photometric depth of the I band observations of $\sim$2 mag below the tip of the red giant branch, which is required to accurately constrain the recent SFH of the galaxy (Dolphin 2002; Dohm-Palmer & Skillman 2002). Third, the galaxies are required to lie close enough such that their stellar populations were resolved by HST imaging instruments. These properties were chosen to ensure robust reconstruction of the SFHs and measurements of the duration parameter. The photometry for one galaxy, SBS 1415+437, stopped ~ 0.5 mag short of our depth requirement despite long integration times. We include the results on this well−studied galaxy in our sample for comparison purposes. The resulting sample of twenty galaxies is listed in Table 4.1.

Table 4.1 Duration of Starbursts and Comparison of Timescales in Galaxy Sample

Galaxy (1)	$< SFR >_{6\text{-}0\ \mathrm{Gyr}}$ (10^{-3} $M_\odot$ yr^{-1}) (2)	Peak b_{recent} of Burst (3)	Peak SFR of Burst (10^{-3} $M_\odot$ yr^{-1}) (4)	Duration (Myr) (5)	τ_{dyn} (Myr) (6)	Dur/τ_{dyn} (7)
Antlia Dwarf	0.15 ± 0.01	3.5 ± 0.9	0.52 ± 0.01	640±190	190±20	3.3±1.0
UGC 9128	0.82 ± 0.07	6.3 ± 1.4	5.1 ± 1.0	1300±300	120±10	10.±7
UGC 4483	0.79 ± 0.06	14 ± 3	11 ± 2	> 810±190	200±23	4.1±1.0
NGC 4163	4.0 ± 0.1	2.9 ± 0.6	12 ± 3	460±70	240±20	1.9±0.1
UGC 6456	3.0 ± 0.2	7.6 ± 1.1	23 ± 3	> 570±60	160±30	3.5±0.7
NGC 6789	3.9 ± 0.1	3.8 ± 1.3	15 ± 5	480±70	...	...
NGC 4068	$10. \pm 0.3$	4.7 ± 0.3	46 ± 3	> 450±50	270±20	1.7±0.1
SBS 1415+437	12 ± 2	12 ± 2	150 ± 10	> 450±50	...	...
DDO 165	13 ± 1	6.5 ± 0.5	$80. \pm 5$	> 1300±300	710±40	1.8±0.4
IC 4662	9.8 ± 0.6	7.7 ± 1.6	76 ± 15	> 450±50	100	4.6
ESO 154-023	$20. \pm 1$	6.4 ± 0.5	120 ± 10	> 450±50	460	1.0
NGC 2366	29 ± 1	5.6 ± 0.4	160 ± 10	> 450±50	330	1.4
NGC 625	29 ± 1	1.4 ± 0.1	$40. \pm 2$	450±50	720	1.6
NGC 784	26 ± 1	4.5 ± 0.6	120 ± 20	> 450±50	470	1.0
Ho II	27 ± 1	6.5 ± 0.8	180 ± 20	> 570±70	820±20	0.70±0.13
NGC 5253	45 ± 1	9.0 ± 0.9	400 ± 40	> 450±50	450±20	1.0±.0
NGC 6822	2.3 ± 0.1	3.1 ± 1.1	7.3 ± 2.5	> 20.±13	140	0.14
NGC 4214	43 ± 2	3.1 ± 0.9	130 ± 40	> 810±190	400±10	2.0±0.5
NGC 1569	21 ± 2	12 ± 1	240 ± 10	> 450±50	170±10	2.6±0.3
NGC 4449	160 ± 10	6.0 ± 0.5	970 ± 70	> 450±50	300±10	1.5±.1

Col. (5) Durations are lower limits for ongoing bursts. Col. (6) Timescales were calculated using major axis measurements and maximum rotational velocity corrected for inclination from the HyperLeda database (Paturel et al. 2003) with the exception of NGC 6822 whose maximum rotational velocity was obtained from Weldrake et al. (2003). Uncertainties were not reported on the rotational velocities of five galaxies, thus the dynamical timescale lacks uncertainties in these cases.

All photometry used DOLPHOT or HSTphot (Dolphin 2000) on the standard HST pipeline processed and cleaned images. The details of the observations and photometric processing for eighteen of these galaxies are presented in Paper I and for two galaxies, DDO 165 and Ho II, in Weisz et al. (2008). As a representative example of the data quality and photometry, we present the imaging and corresponding CMD for one galaxy, UGC 9128, in the top two panels of Figure 4.1. The evolutionary features that drive the reconstruction of the SFHs can be readily identified in the CMD including the main sequence (MS) stars, blue and red helium burning (BHeB and RHeB respectively) stars, the red giant branch (RGB) stars, and the asymptotic giant branch (AGB) stars. The upper MS, the BHeB, and the RHeB stars are unambiguous signs of star formation in the past few 100 Myr. The helium burning (HeB) stars are of particular interest as a star in this stage of stellar evolution occupies a unique space in the CMD; the luminosity of a HeB star has a one−to−one correspondence to the mass of the star and, hence, the age of the star. Under the assumption of a universal initial mass function (IMF), this luminosity−mass−age relation of the HeB stars tightly constrains the SFH at recent times.

We reconstructed the past rate of star formation (SFR(t)) for each galaxy by applying a CMD fitting technique (Dolphin 2002) with stellar evolutionary models from Marigo & Girardi (2007) to the stellar photometry. During fitting, the distance and extinction were allowed to vary within limited ranges, and the metallicity was constrained to increase with time except in three cases (Antlia, NGC 2366, and Holmberg II). The metallicity in these three systems could be fully constrained by the metallicity information contained in the deeper photometry reaching a magnitude below the red clump. The lifetime SFH results of the fitting program (i.e., SFR(t, Z)) are presented in Paper I for eighteen galaxies and in Weisz et al. (2008) for two galaxies (DDO 165 and Ho II). As a representative example of our results, we present the complete SFH of UGC 9128 in the bottom left panel of Figure 4.1. Note that we have higher time resolution at younger ages due to the rapid luminosity and spectral evolution of the youngest, most massive stars. At ages older than $\sim$ 6 Gyr, deeper photometry is needed to separate stars of different ages. While the CMD fitting program returns the SFRs in logarithmic time bins varying from one to a few Gyr for these older ages stars, the shallow photometry cannot break the co-variance of the SFR between time bins at these older times.

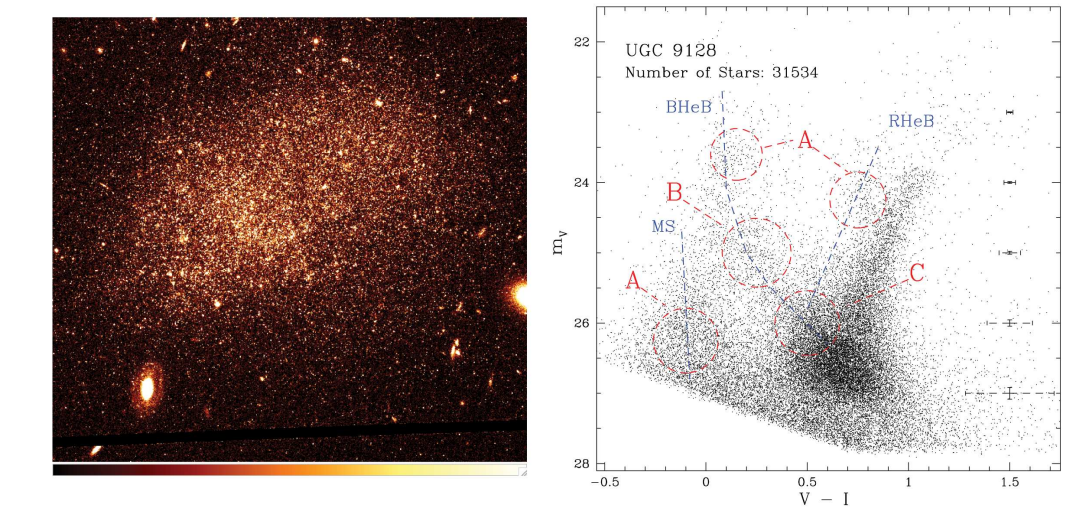

(a) HST V band Image of UGC 9128

(b) Color Magnitude Diagram

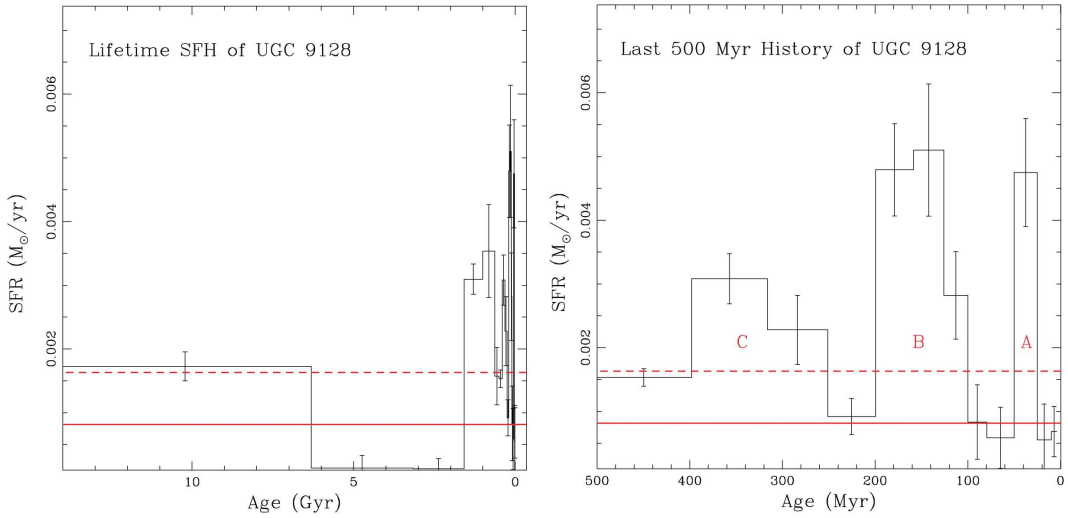

(c) Lifetime SFH of UGC 9128

(d) Most Recent 500 Myr SFH

Figure 4.1 This four panel figure shows the image, photometry, and SFH results for UGC 9128. Panel (a) presents the V band image of UGC 9128 from the HST ACS instrument. Panel (b) shows the CMD with average photometric errors per magnitude bin. The MS and HeB stages of evolution are marked. The regions on the CMD labeled (A), (B), and (C) correspond to three different episodes of recent SF that are not spatially coincident in the galaxy. Event (A) in the CMD includes BHeB stars, RHeB stars, and MS stars. Events (B)and (C) include the BHeB stars highlighted in CMD. The RHeB stars from these events are blended with the red clump while the MS stars born simultaneously with the BHeB stars in regions (B) and (C) lie below the photometric depth in the CMD. The reconstructed SFH for the lifetime of UGC 9128 is presented in panel (c). The solid red line indicates the average SFR over the past 6 Gyr (i.e., $b_{recent} = 1$) and the dashed red line is twice this average (i.e., $b_{recent} = 2$). An expansion of the SFH during the last 500 Myr is presented in panel (d). The SF events (A), (B), and (C) identified in the CMD in panel (b) and the intervening periods of quiescent SF are reconstructed in the SFH.

Therefore, we averaged the SFR in all time bins greater than 6 Gyr trading temporal resolution for more secure SFRs. The averaging eliminates the issue of co-variance thus loosely constraining the ancient SFH.

UGC 9128 provides an interesting example of how the features in a CMD translate into a SFR (see Figure 4.1). The distribution of stars along the helium burning (HeB) sequences is clumpy, suggesting that the SF has been elevated during several distinct episodes interspersed with lower levels of SF. We have highlighted stars produced during three periods of elevated SF labeled as events (A), (B), and (C) in the CMD. The most recent star formation event (A) is traced by BHeB stars, RHeB stars, and MS stars in the CMD. The earlier events (B) and (C) are traced by BHeB stars, as well as by RHeB stars that are blending into the red clump and MS stars that fall below our photometric depth. These three distinct SF events are recovered in the last 500 Myr in the SFH as shown in the final panel of Figure 4.1. Event (C) contains the lowest luminosity BHeB stars in the three events corresponding to the lowest mass (i.e., oldest aged) BHeB stars. This SF event is seen in the SFH as an elevated SFR from $\sim$ 250 Myr ago to $\sim$ 400 Myr ago. More recently (i.e., above the luminosity of event (C) in the CMD) is a period of relative quiescent SF followed by another increase in SFR (the clump of BHeB stars labeled event (B)). This more recent SF event is recovered in the SFH beginning $\sim$ 200 Myr ago and lasting $\sim$ 100 Myr. Similarly, event (B) was followed by a comparative lull in SF before experiencing another increase in SF from $\sim$ 50 Myr to $\sim$ 25 Myr ago, event (A). UGC 9128's unique SFH demonstrates how directly the HeB stars correlate to SFRs at recent time. The excellent temporal resolution clearly achievable with this technique is well suited to measuring the duration of a starburst event.

In Figure 4.2, we show the SFH over the last 1.5 Gyr for all twenty galaxies. These recent SFHs share the common characteristic of elevated SF at recent times, as expected for our sample selection. However, there are differences within the sample. For example, some galaxies show a sustained, elevated rate of SF over a few hundred Myr (e.g., ESO 154−023, NGC 4068, UGC 4483). Others have significant fluctuations in their SFRs on shorter timescales (e.g., UGC 9128, NGC 4214). Importantly, five galaxies show "fossil" bursts, for which the SFR has returned to a lower level in the most recent time bins (e.g., Antlia, UGC 9128, NGC 4163, NGC 625, and NGC 6789). One galaxy, NGC 6822, shows a burst just beginning with elevated SFRs only in the last 50 Myr.

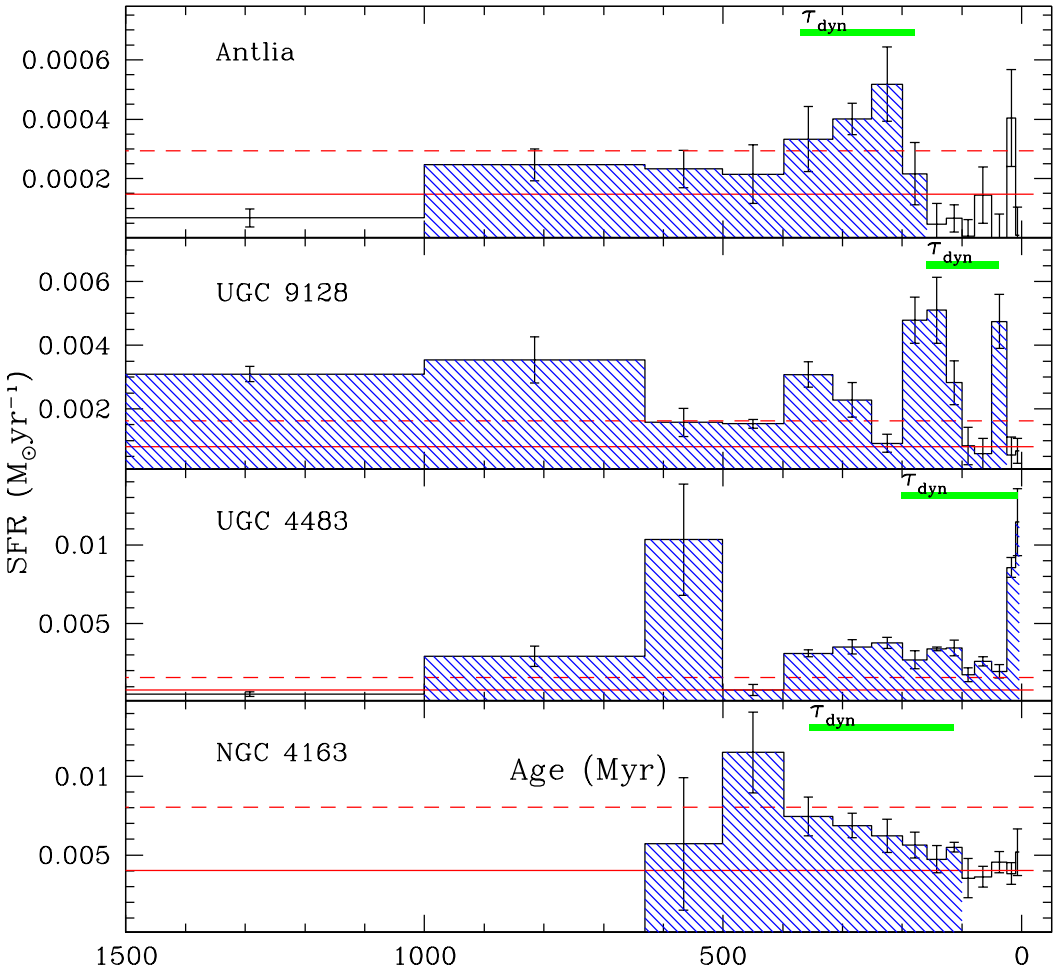

Figure 4.2 The SFH of the last 1.5 Gyr for the twenty galaxies. The durations of the bursts are shaded in blue. The dynamical timescales of the galaxies are plotted in a green bar for comparison. The solid red lines indicate the average SFR over the last 6 Gyr for the galaxy (i.e., $b_{recent} = 1$) and the dashed red line is twice this average (i.e., $b_{recent} = 2$).

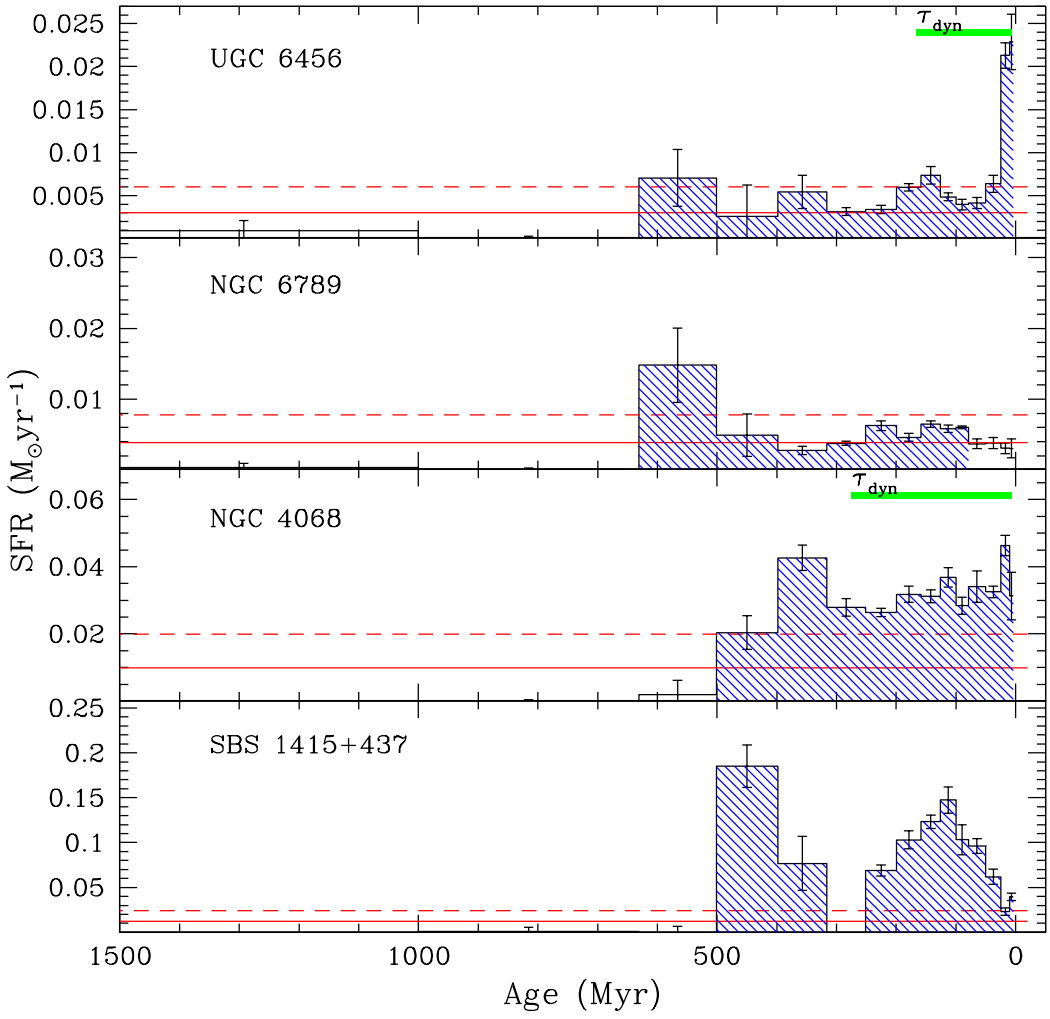

Figure 4.2 *Recent SFHs with durations measurements continued: UGC 6456, NGC 6789, NGC 4068, SBS1415+437*

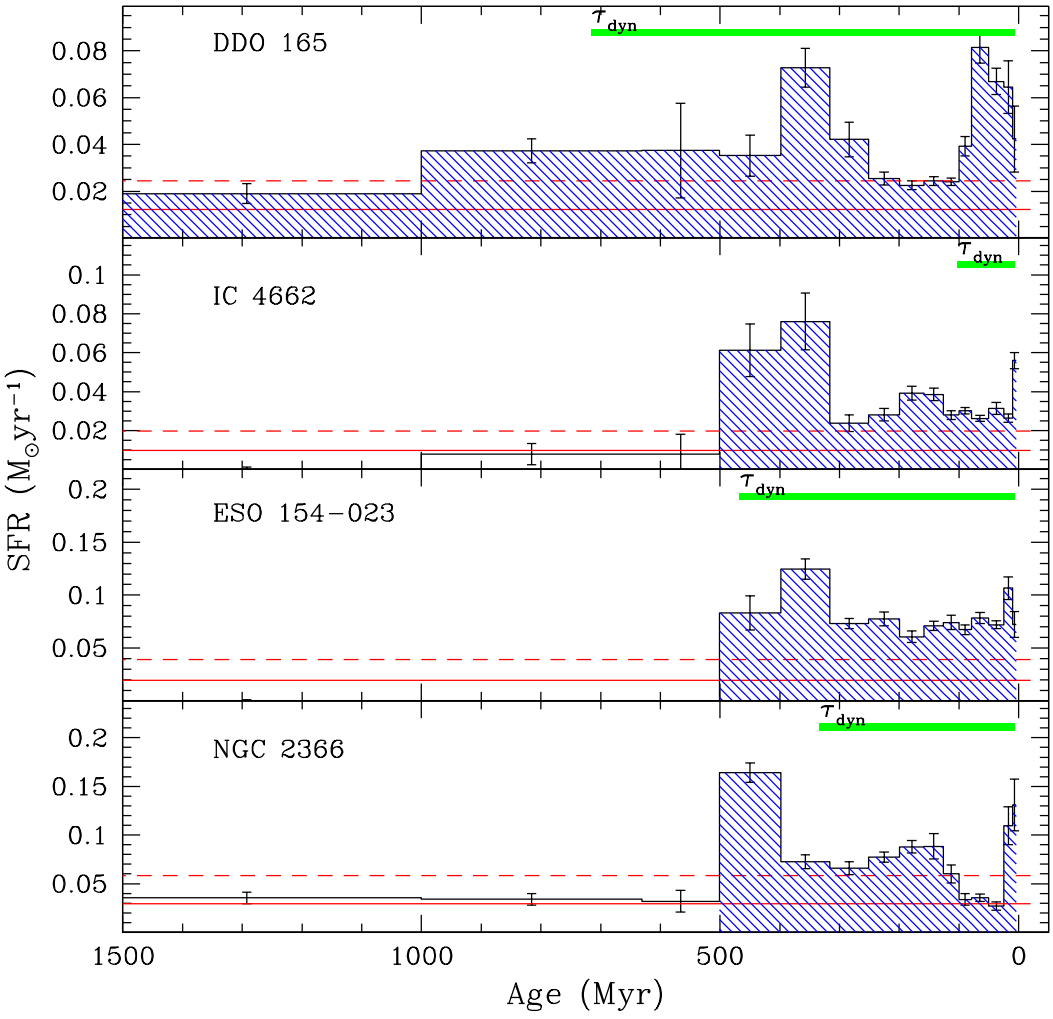

Figure 4.2 *Recent SFHs with durations measurements continued: DDO 165, IC 4662, ESO154−023, NGC 2366*

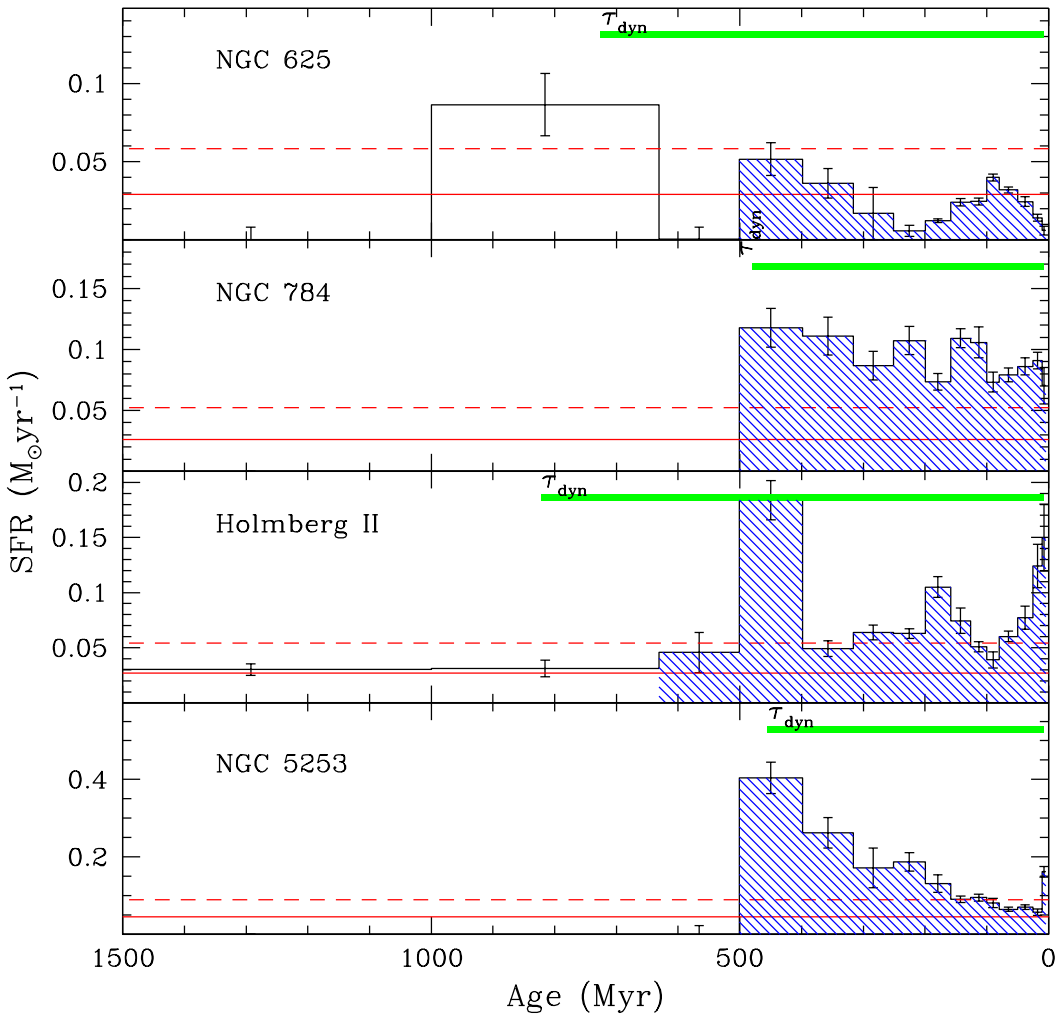

Figure 4.2 *Recent SFHs with durations measurements continued: NGC 625, NGC 784, Holmberg II, NGC 5253*

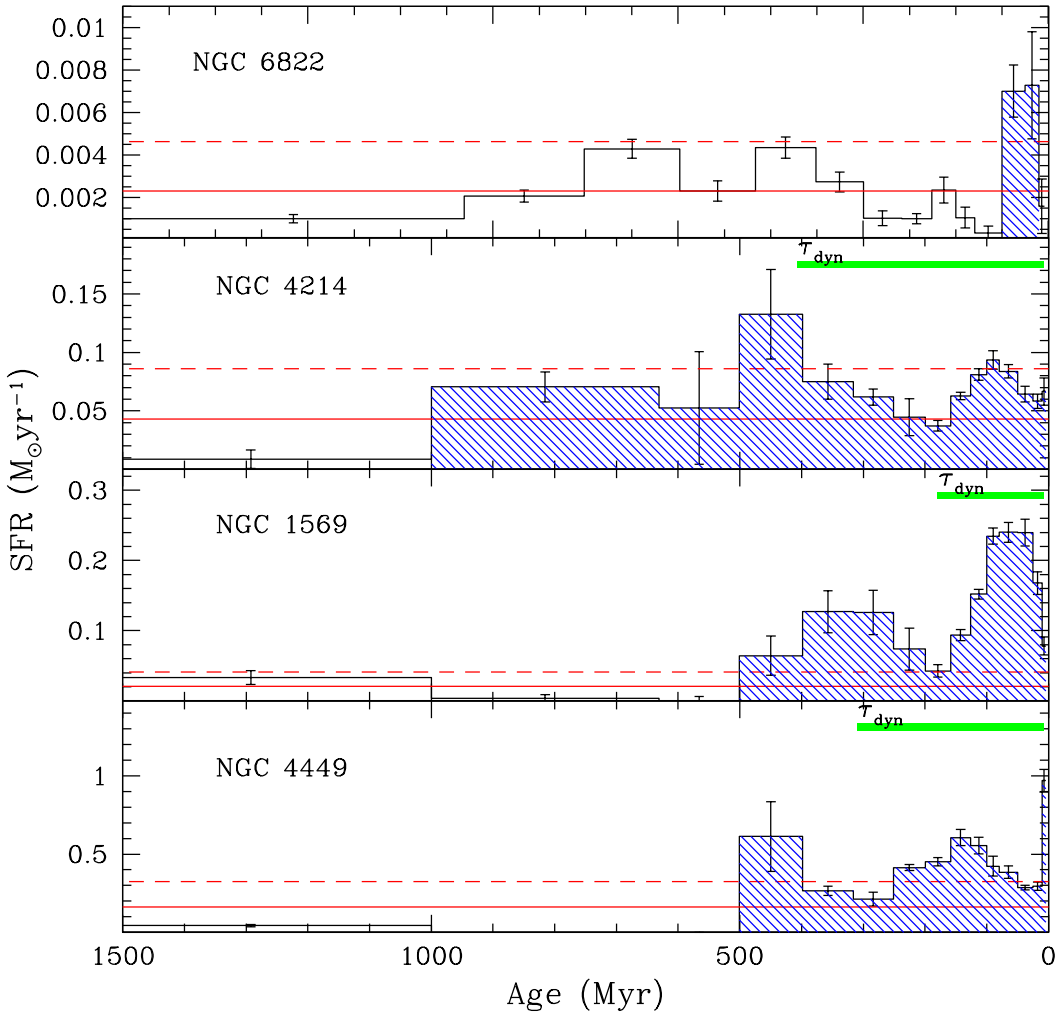

Figure 4.2 *Recent SFHs with durations measurements continued: NGC 6822, NGC 4214, NGC 1569, NGC 4449*

4.3 Durations of Starbursts in Dwarf Galaxies

The measurement of the duration of a starburst event requires a definition of "bursting". To establish such a quantitative threshold, we apply a metric to evaluate the recent SFRs relative to the historical SFRs over the past 6 Gyr within a host galaxy, as discussed in McQuinn et al. (2009). A normalized SFR removes the bias against identifying bursting SFRs in smaller galaxies where the absolute SFR is generally lower than in larger galaxies. We used a birthrate parameter ($b = SFR\ /\ <SFR>$) as defined by Scalo (1986) which compares the current SFR with the lifetime average SFR. However, rather than using the lifetime average SFR as a baseline, we used the average SFR over the last few gigayears, providing a better comparison of the recent SFRs with the more recent evolutionary state of the host galaxy. This choice both avoids suppressing b by excluding the higher levels of SF typically expected during the initial period of galaxy assembly and leverages the most secure part of the SFH. We use our modified birthrate parameter ($b_{recent} = SFR\ /\ <SFR>_{0-6\ Gyr}$) to define a threshold for bursting SFRs; a value of $b_{recent} > 2$ identifies a burst (Kennicutt et al. 2005) and $b_{recent} \simeq 1$ marks the beginning and end of a burst event. In Figure 4.2, we show the average SFR from the last 6 Gyr ($b_{recent} = 1$) as a solid red line and twice this average ($b_{recent} = 2$) as a dashed red line.

The duration of the starburst event can be measured directly as the amount of time $b_{recent} \geq 1$ once the $b_{recent} > 2$ threshold has been reached. The time measurement extends from the midpoints of the beginning and end time bins. The uncertainties on the durations are the width of the longest time bin contributing to the duration. The resulting durations of the burst events are shaded in blue in Figure 4.2. Fifteen galaxies have starburst durations between 450 ± 50 and 640 ± 190 Myr as listed in Table 4.1.[1]

The longest bursts we identify are in UGC 9128 and DDO 165, which show bursts lasting 1300 ± 290. In fifteen cases, the SFR remains above the 6 Gyr historical average in the most recent time bin, indicating that the starburst is ongoing. The durations for these starburst events are thus lower limits. The average SFRs over the past 6 Gyr,

[1] Note: We measure slightly different durations for NGC 4163, NGC 4068, and IC 4662 than previously reported in McQuinn et al. (2009). As discussed in Paper I, we constrained the metallicity of the galaxies to increase with time, which gives improved constraints on the recent SFH. As a result, the SFH of these three systems changed, altering the measured duration of the starbursts by 25% for NGC 4068 and IC 4622 assuming a double burst, and 50% for NGC 4163.

peak SFRs and corresponding b_{recent} value during each burst event are also listed in Table 4.1.

Note that the duration measurement is affected by the inherent time binning of the SFH. The temporal resolution over the last 100 Myr is fine enough that we can discern and measure fluctuations in the SFR over short timescales and pinpoint the value of b_{recent} every $20 - 50$ Myr or so. In contrast, between $650 - 1000$ Myr ago, the inherent time resolution of the data reduces to 350 Myr. One can imagine a burst beginning in the latter half of this time bin but the b_{recent} value is suppressed below unity due to averaging with a lower SFR earlier the same time bin. In such a case, this entire time bin would not be considered part of the burst event and the measured duration would be underestimated. The reverse is also possible. The resolution of time bins has a smaller effect on the final duration measurement for bursts contained in the most recent 650 Myr due to the finer temporal resolution. This effect is quantified in the uncertainties listed for the durations which increase with larger time binning.

Our criteria for defining a starburst serve as a prescriptive guide for measuring a burst duration but we stress that the criteria are guides and the distinction between "regular" and "bursting" SF is subjective in some cases. In thirteen of the galaxies (e.g., ESO $154 - 023$, NGC 784, NGC 5253, among others), the SFR profile increases substantially from one time bin to another and the duration measurement is easily made from analyzing the b_{recent} parameter. In NGC 6822, the burst began ~ 50 Myr ago. We measure the lower limit of the duration in this system to be 20 ± 13 Myr. Given the much longer durations of the other galaxies, this burst is likely just beginning. In six systems the SFH is more complex and thus we discuss each system in turn.

For NGC 2366 and Ho II, the burst is preceded by time bins whose b_{recent} is equivalent to unity within the measured uncertainties (we refer the reader again to the blue shaded regions and red lines in Figure 4.2). By our definition, these time bins should be included in the duration measurement. Yet, these SFRs continue for hundreds of Myr at roughly the historical average SFR. The overall SFR profile suggests that the bursts had not yet begun in these time bins. The lower temporal resolution at these older time also affect the b_{recent} calculation. We chose to exclude these time bins from the duration measurement.

In the third case, NGC 6789, the b_{recent} index drops just below unity approximately

350 Myr ago after which the SFR increases again pushing the b_{recent} close to 2. There is some co-variance between adjacent time bins in the SFHs and this short dip in SFR surrounded by higher levels of SF suggests that the burst is continuing. The SFR profile indicates that the burst event, while weaker than others in our sample, has continued to elevate the SF above the average until our most recent time bins. This conclusion is supported by looking at the overall SFR profile over the past 1.5 Gyr. The period preceding the burst is a quiescent period experiencing very little SF. We chose to include the SF $\sim$ 350 Myr ago as part of the burst event which extends the burst duration measurements from 600 Myr ago until the last $\sim$ 100 Myr. The profile is similar to UGC 6456 where the burst event is clearly defined and extended.

In the fourth case, UGC 4483, the SFR profile experiences a dip $\sim$ 450 Myr ago and the b_{recent} index is equivalent to unity within the measured uncertainties. The time bins on either side are elevated reaching b_{recent} values of 13 and 3.9. This suggests that the burst has continued although the system experienced a period of lower SF during the larger burst event. Likewise, in SBS 1415+437, the SFR dips to zero during one time bin flanked on with side with b_{recent} values of 5.7 and 6.3. We chose to define the burst event inclusive of this period of quiescence based on the overall SFR profile. Note that the photometry of SBS $1415 + 437$ falls ~ 0.5 mag short of our photometric depth requirement, thus the ancient SFH is not well-constrained. However, the recent SFH is well-constrained and the SFR profile in the last 500 Myr clearly defines a burst. We measure the duration of the starburst in SBS $1415 + 437$ despite the uncertainties in the past SFR average and include it for comparison with others in our sample.

Finally, the well−studied starburst galaxy, NGC 625 (Cannon et al. 2003), does not fit our metric for identifying a starburst. The SFH of NGC 625 is similar to that of Leo A in that the initial onset of SF is suppressed (Cole et al. 2007) until $\sim$ 3 Gyr ago. The photometry used to derive the SFH of NGC 625 reaches nearly three magnitudes below the TRGB giving confidence to the low SFRs derived for the 6−14 Gyr time bin. The result of this later onset of SF is that the average SFR over the past 6 Gyr is high and the elevated levels of SF in the last 500 Myr fall below our starburst threshold. Although the unique SFH of NGC 625 does not fit our metric, evidence at other wavelengths classify this system as a starburst reinforcing the premise that the identification of starburst (i.e., the difference between "regular" and "bursting" SF) is

not always clear. Using the elevated SFRs in the recent history of NGC 625 to guide the measurement, the duration of this likely starburst event is 450 ± 50 Myr as seen in Figure 4.2, much like the majority of others measured in this study. We include it in our duration measurements for comparison. Excluding this one unusual system would not change our scientific conclusions.

4.4 Bursts: SF on Timescales > Few 100 Myr

The durations of the burst events fall unambiguously on the scale of hundreds of Myr. The bursts are sufficiently robust that they are not shut off by an individual flicker of a few massive stars. Moreover, the longer durations suggest that a starburst event is a galaxy-wide phenomenon, which likely includes SF in both clusters and in the field regions of the galaxies (McQuinn et al. 2009). In Paper III, will specifically investigate the spatial distribution and possible migration of SF in the stellar clusters and diffuse regions within the starbursts to better characterize the nature of starbursts.

The burst durations can be compared with the characteristic timescale to communicate an event or disturbance across a galaxy. This dynamical timescale can be estimated as the rotation period for dwarf galaxies as these systems exhibit solid−body rotation (Skillman et al. 1988) (i.e., $t_{dyn} \simeq 2\pi Re/V$ where R_e is the effective radius of the galaxy and V is the rotational velocity). We have calculated the dynamical timescale for eighteen[2] of the galaxies using the major axis radii of the galaxies and the inclination corrected maximum rotation curve velocities. The radii and velocity measurements were obtained from the HyperLeda database (Paturel et al. 2003) with the exception of NGC 6822 whose maximum rotational velocity was obtained from Weldrake et al. (2003). The dynamical times calculated are listed in Table 4.1 and are compared with the starburst duration we measured for each galaxy. The ratio of the duration to dynamical timescales for fifteen starbursts range from $0.70 - 4.6$ with a mean ratio of 2.6. Galaxy UGC 9128, with a duration of over 1 Gyr, has a larger duration/dynamical timescale ratio of 10; NGC 6822 has ratio of 0.14 as the burst is just beginning in this system. The dynamical timescales are plotted as green horizontal bars in the SFHs in Figure 4.2 and can be compared to individual galaxy duration measurements. Previous

[2] Rotational velocity data were not available for SBS 1415+437 and NGC 6789.

authors have proposed that if starbursts persist only on the characteristic timescale of a system or shorter, then they would likely be self-extinguishing events destroyed by their own energy output (Meurer 2000). Durations comparable to or longer than the dynamical timescales support our conclusion that these events are not self-quenching as discussed in Paper I.

The starburst durations we measure are clustered around 450 Myr, as shown in Figure 4.3. It is important to note that 75% of these systems have not yet finished; we are measuring lower limits for the burst durations in these systems. The peak of the distribution in Figure 4.3 would likely shift to longer timescales if we had a sample of exclusively fossil bursts. The distribution of the dynamical timescale is plotted as a dashed red histogram in Figure 4.3. This distribution is similar to the distribution of the burst durations but is shifted towards shorter times suggesting the burst process is global in nature. Rapid self-quenching of SF would limit starburst durations to ~ 10 Myr, indicated by the dashed blue line.

4.5 "Flickering": SF on ~ 10 Myr Timescales

Burst durations on the scale of hundreds of Myr differ substantially from the often reported timescale of $5 - 10$ Myr (see references in §4.1). The nearly two orders of magnitude difference between these two scales is the result of measuring two different scales of SF events; i.e., whether one is measuring the duration of a complete starburst event in a galaxy or measuring the duration of a pocket of enhanced SF made up of one or a few stellar clusters within a galaxy. Both scales of SF are evident in our SFHs. We have highlighted the burst events in blue in Figure 4.2. Now we draw the reader's attention to the most recent time bins with the finest resolution (t $\sim 4 - 10$ Myr, t $\sim 10 - 25$ Myr) presented in Figure 4.2. Over these short timescales, there are rapid variations in the SFRs seen in many of the galaxies corresponding to local "flickering" of SF on small scales. This flickering occurs within a larger envelope of enhanced SF on timescales greater than a few 100 Myr. The larger starbursts events are likely comprised of numerous individual pockets of flickering SF in stellar clusters as well as SF in diffuse field regions and the starburst duration is the summation of all these smaller scale events.

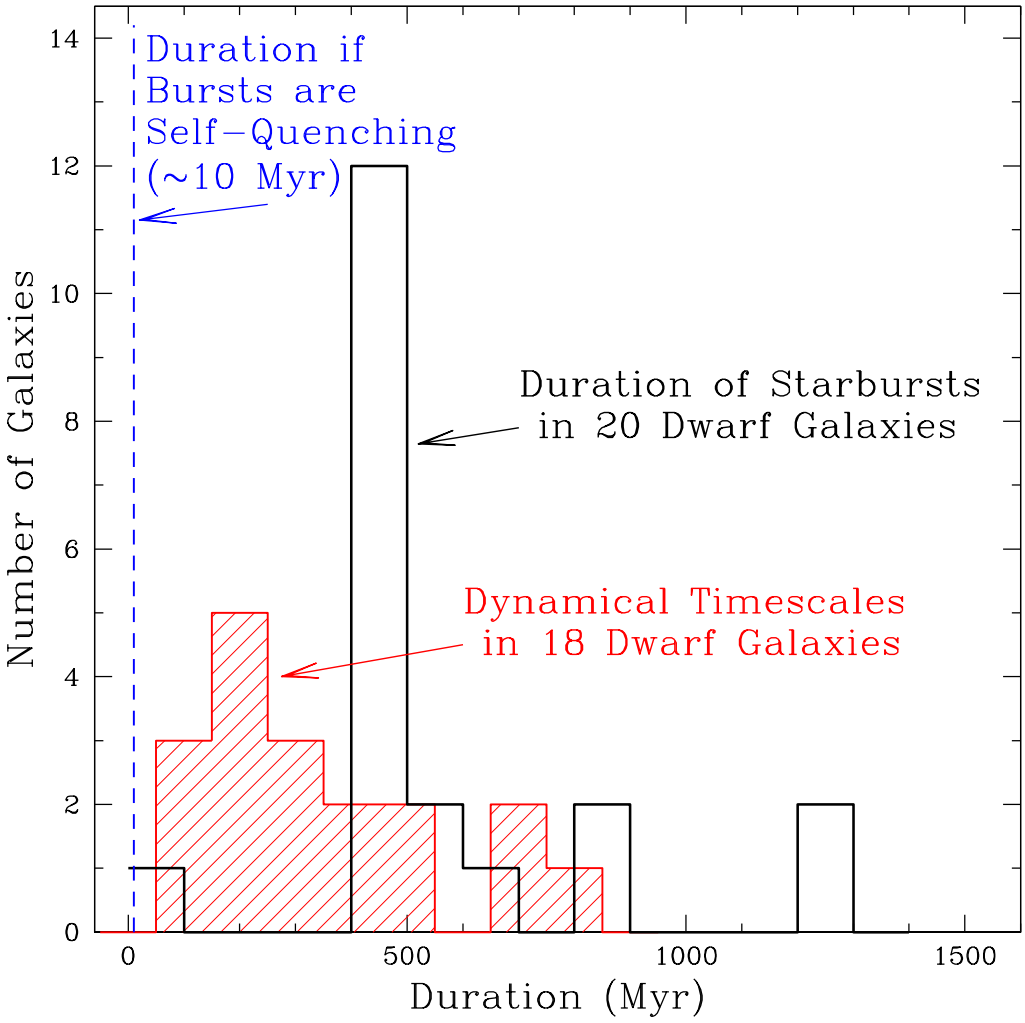

Figure 4.3 The histogram shows the distribution of the starburst durations for the galaxy sample. The histogram bins are a simple scheme with each bin having the width of 100 Myr. The actual uncertainties in the measured durations vary; the shortest durations have the smallest uncertainty (i.e., 450 ± 50 Myr) and the longest durations have the largest uncertainty (i.e., 1300 ± 290 Myr). Also plotted is the distribution of the dynamical timescales for the seventeen galaxies for which rotation speeds are available. Interestingly, the duration of the starbursts for fifteen of the galaxies lie in the range $\sim 450-\sim 650$ Myr with the majority presenting burst duration of 450 Myr. Many of these durations are lower limits as the bursts are ongoing; the distribution would likely shift to even longer timescales with an exclusively fossil burst sample. Two galaxies in the sample show a longer duration greater than 1 Gyr. The timescale for the evolution of massive stars associated with "self-quenching" is plotted to show that the scale of these burst durations far exceed this timescale.

Obviously, small scale increases in the SFR can occur outside of a burst event. In other words, flickering SF and the formation of stellar clusters and associations do not occur solely in starbursts. For example, consider the SFH of the Antlia dwarf galaxy in Figure 4.2. The burst event in Antlia ended nearly 200 Myr ago. Yet, we see elevated SF during one additional time period (t $\sim 10 - 25$ Myr ago) where the b_{recent} index exceeds 2. This increase in SF is temporally isolated from the larger burst event and is likely caused by SF in an individual stellar association or small cluster. We do not include this flickering SF as part of the burst event as the surrounding time bins have lower levels of SF. One of the implications of longer burst durations is that the burst is likely occurring on large spatial scales within a galaxy and small increases in SFR are qualitatively different than bursting SF. We will explore this in detail in Paper III with a spatial analysis of the SF.

The variations of SFR on short timescales (δt $\sim$ 5 Myr) are also seen when the SFR results in our most recent time bin of $4 - 10$ Myr are compared with another starburst indicator, Hα emission, as discussed in Paper I. The timescales for our most recent time bin and Hα emission overlap but do not completely coincide. As one would expect, the results of these two indicators agree in most galaxies in the sample (i.e., where there is significant Hα emission, we find b_{recent} values above two in the $4 - 10$ Myr time bin and vice versa). Yet in four galaxies, the two indicators disagree suggesting that the SF activity has changed rapidly on timescales of a few Myr. This short timescale is the same as what is expected for the evolution of massive stars.

The characteristic timescale to communicate an event or disturbance for "flickering" SF is the crossing time for a typical star cluster ($t_{cross} = 2R_e/\sigma$ where σ is the velocity dispersion of the stars). Assuming a typical radius of a star cluster to be a few pc with a velocity dispersion of $\simeq$ 10 km s^{-1} (e.g., Smith & Gallagher 2000; Larsen et al. 2008), the crossing time is $\simeq$ 1 Myr. This value agrees with the typical dynamical star cluster timescale of a few Myr reported by Heckman (2005) using a timescales defined by $t_{dyn} \simeq (G\rho)^{-1/2}$. These cluster crossing times support the conclusion that the short durations reported for bursts are measuring the SF phenomenon within star clusters, associations, or some equivalently smaller region of SF.

The amplitude of the flickering can be used to estimate the stellar mass created in these smaller scale SF events. Using a range of SFRs from $0.001 - 0.1$ M$_\odot$ yr^{-1} typical

of the sample dwarf galaxies and a timescale of 10 Myr, the total stellar mass produced ranges from $10^4 - 10^6$ $M_\odot$, which are typical masses of stellar associations and clusters. These numbers can be compared to the larger values of $10^7 - 10^9$ $M_\odot$ of stellar mass created during the bursts events of these same galaxies.

The differences in timescales, dynamical times, and amount of stellar mass produced highlight the different physical processes governing local, small scale SF and large scale burst events. The flickering SF is governed by local physical conditions (e.g., gas density, feedback from massive stars, etc.) and is likely to be temporarily suppressed/quenched locally (Omukai & Nishi 1999; Nishi & Tashiro 2000). The same feedback loop from massive stars that may quench the flickering SF does not disrupt/quench the overall burst event in our sample of galaxies. Thus it appears the non-equilibrium energy output and mass transfer characteristic of stellar winds and supernovae that have been proposed to quench SF (Ferguson & Babul 1998; Thornley et al. 2000; Stinson et al. 2007; Kaviraj et al. 2007) cannot be assumed universally on galactic scales.

4.6 Stellar Mass and Energy Created in a Burst

Longer duration bursts have a greater impact on the evolution of the host galaxy than short bursts. Two interesting parameters to quantify are the percent of stellar mass created during a burst and the energy produced by the burst, which can potentially be deposited into the ISM. We have calculated the percent of stellar mass created in each burst relative to the stellar mass created over the lifetime of each galaxy directly from the SFHs. The results range from 3%−26% of the mass being created during the burst; the individual numbers for each galaxy are listed in Table 4.2. The percentage is an upper limit for SBS1415+437 whose ancient SFH remains uncertain due to the limited depth of photometry. The galaxies showing bursts with lower absolute SFRs (i.e., Antlia) or SFRs exceeding the past 6 Gyr average in only one or two time bins (i.e., UGC 6456, NGC 4163, and NGC 6789) lie at the lower end of this range. Galaxies with longer durations and stronger bursts, such as UGC 9128, DDO 165, NGC 4214, lie at the upper end of this range. Additionally, we compare the total amount of stellar mass calculated form the SFH with the luminosity of the galaxies from published absolute magnitudes in the B band, adjusted for extinction from Galactic dust maps (Schlegel et al. 1998). The

mass derived from the SFH does not incorporate all the mass from the optical extent of the galaxies as the field of view in some cases does not extend to the outer optical limits. While this technically makes the mass a lower limit, it is a small effect as most of the optical area is covered in each system and the amount of mass at these outer radii is small compared to the mass in the inner parts of the systems. The one exception is NGC 6822 for which the observations do not cover the main extent of the stellar populations. The mass−to−light ratios (M_*/L_B), in solar units, range from 1.0 ± 0.2 to 8.0 ± 1.0. The highest ratio is for Antlia dwarf galaxy, the lowest surface brightness galaxy with an absolute magnitude of -10.14. These M_*/L_B ratios are consistent with the expected ratios for SF galaxies thus providing an independent check on the derived SFHs.

We calculated the energy produced in each burst using our SFHs and STARBURST99 (Leitherer et al. 1999; Vázquez & Leitherer 2005). STARBURST99 is an evolutionary synthesis code that uses a known SFR and stellar evolution models to predict spectrophotometric properties, the energy distribution, and other related properties of galaxies with active star formation. Of particular interest here is the ability of STARBURST99 to simulate the energy produced by stellar winds and supernovae at a given SFR. Using an instantaneous burst of SF with a fixed mass of 10^6 $M_\odot$ coupled with the same IMF and stellar evolution models employed in the SFH code as done in Weisz et al. (2009), we simulated the energy output of SF for low metallicity galaxies with a time resolution of 5 Myr. This energy output for a 10^6 $M_\odot$ instantaneous burst was scaled by the stellar mass created every 5 Myr for the actual observed bursts and integrated over the duration of the burst. The total energy for the bursts ranges from $10^{53.9} - 10^{57.2}$ erg; individual values are listed in the final column of Table 4.2. There is a clear trend that higher luminosity galaxies have a higher amount of energy produced in a burst. The significant amount of energy deposited into the ISM, particularly in the cases where the energy is $> 10^{56}$ erg, will have an important impact on the gas dynamics and future SF activity of the host galaxy. We will study the spatial distribution of the SF activity in Paper III and explore whether this energy is deposited in concentrated areas or over a significant fraction of the galaxy.

Table 4.2 Estimation of Stellar Mass and Energy Released in Bursts

Galaxy	M_B (mag)	Total Stellar Mass ($10^6 M_\odot$)	M_*/L_B	% Mass Created in Burst	log Energy of Burst (erg)
Antlia Dwarf	-10.14	7.3 ± 0.9	8.0 ± 1.0	3.2 ± 0.5	54.2
UGC 9128	-12.45	19 ± 3	2.4 ± 0.4	24 ± 5	55.5
UGC 4483	-12.68	15 ± 3	1.6 ± 0.4	26 ± 7	55.4
NGC 4163	-13.75	140 ± 40	5.5 ± 1.4	2.8 ± 0.8	55.5
UGC 6456	-13.85	68 ± 27	2.4 ± 1.0	5.1 ± 2.2	55.3
NGC 6789	-14.60	100 ± 30	1.8 ± 0.5	3.9 ± 1.4	55.5
NGC 4068	-14.96	320 ± 50	4.1 ± 0.7	4.8 ± 0.8	56.0
SBS 1415+437	-15.11	240 ± 50	2.7 ± 0.6	$20. \pm 4$	56.5
DDO 165	-15.19	270 ± 50	2.8 ± 0.5	19 ± 4	56.5
IC 4662	-15.39	420 ± 90	3.7 ± 0.8	5.2 ± 1.2	56.2
ESO 154-023	-16.21	650 ± 90	2.7 ± 0.4	6.4 ± 0.9	56.5
NGC 2366	-16.33	370 ± 50	1.3 ± 0.2	12 ± 2	56.5
NGC 625	-16.26	370 ± 140	1.5 ± 0.6	3.8 ± 1.5	56.0
NGC 784	-16.78	1100 ± 100	2.6 ± 0.3	4.7 ± 0.7	56.5
Ho II	-16.92	450 ± 60	1.0 ± 0.1	12 ± 2	56.5
NGC 5253	-16.98	2200 ± 300	4.3 ± 0.6	4.7 ± 0.7	56.9
NGC 6822	-17.86	28 ± 4	...	1.0 ± 0.2	53.9
NGC 4214	-17.02	400 ± 100	1.0 ± 0.2	18 ± 5	56.7
NGC 1569	-17.76	1000 ± 100	1.0 ± 0.1	5.8 ± 0.7	56.6
NGC 4449	-18.02	3000 ± 500	2.3 ± 0.4	7.0 ± 1.5	57.2

Col. (2) Integrated absolute magnitude of the galaxy adjusted for extinction in the B band. Cols. (3) The mass derived from the SFH does not incorporate all the mass from the optical extent of the galaxies as the field of view in some cases does not extend to the outer optical limits. While this technically makes the mass a lower limit, it is a small effect as most of the optical area is covered in each system and the amount of mass at these outer radii is small compared to the mass in the inner parts of the systems. The exception in NGC 6822 where the observations cover less than half of the optical disk. The total stellar mass is a lower limit for the galaxy. The mass-to-light ratio is not calculated for NGC 6822 as the mass and luminosity measurements cover significantly different areas of the galaxy. Col. (4) Uncertainties are derived assuming errors are dominated by uncertainties in mass; uncertainties in luminosity are not included but are negligible at ~ 0.2 mag. Col. (5) The percent of mass created in each burst are likely upper limits. The high SFRs in the galaxies prevent a complete census of the older (t$>$ 6 Gyr) populations. This is particularly true in the case of SBS1415+437 whose ancient SFH remains uncertain due to limited depth of photometry.

4.7 Conclusions

The starburst events in the the twenty dwarf galaxies studied present bursts lasting on the order of hundreds of Myr. The shortest durations measured were $\sim$ 450 Myr, the longest were 1.3 Gyr. The majority of the galaxies display bursts with durations ranging from $\sim$ 450 Myr to $\sim$ 650 Myr but many are lower limits as the SFR is still elevated at the most recent times. The ratio of the durations to the dynamical timescales of the galaxies ranges from $0.70 - 4.6$ for sixteen of the galaxies with one outlier, UGC 9128, having a ratio of duration to dynamical time of 10. These longer duration times rule out the theory that these starbursts are "quenched" by the feedback processes of the massive stellar populations created. Shorter durations often cited on the order of $5 - 10$ Myr are measuring small pockets of enhanced SF or "flickering" that contribute to a burst event but do not represent the extant of a burst. The bursts deposit $10^{53.9} - 10^{57.2}$ erg of energy into the interstellar medium through stellar winds and supernovae and produce 3.2%−26% of the host galaxy's mass.

4.8 Acknowledgments

Support for this work was provided by NASA through grants AR-10945 and AR-11281 from the Space Telescope Science Institute, which is operated by Aura, Inc., under NASA contract NAS5-26555. E. D. S. is grateful for partial support from the University of Minnesota. J. J. D. was partially supported as a Wyckoff fellow. K. B. W. M. gratefully acknowledges Matthew, Cole, and Carling for their support. This research made use of NASA's Astrophysical Data System and the NASA/IPAC Extragalactic Database (NED) which is operated by the Jet Propulsion Laboratory, California Institute of Technology, under contract with the National Aeronautics and Space Administration. Finally, we would like to acknowledge the usage of the HyperLeda database (http://leda.univ-lyon1.fr).

Chapter 5

On the Spatial Structure of Starbursts (McQuinn et al. in prep.)

ABSTRACT

Spatially and temporally resolved SFHs allow us, for the first time, to study the changing distribution of star formation in a galaxy. Here, we present preliminary results on the spatial structure and distribution of star formation in regions of high and low surface brightness for a sample of eighteen starburst dwarf galaxies using SFHs derived from optically resolved stellar populations. The rate of star formation in different regions of the galaxies yields new insights into how much of a galaxy participates in and is directly affected by a starburst. Additionally, connecting SF from different aged blue helium burning stellar populations within a galaxy with their spatial distribution creates a composite picture in space and time of the changing patterns of SF in a galaxy. Here, we present preliminary results on the spatial structure and evolution of star formation in an initial sample of nearby starburst dwarf galaxies. Continuing research will complete this analysis for a sample of nineteen galaxies.

5.1 The Starburst Mode of Star Formation

Starbursts refer to short-lived, intense periods of massive star formation which play an important role in a galaxy's evolution as the feedback from SF can change the gas dynamics, future SF processes, and chemical composition of the host galaxy through the stars own ionizing radiation, mass loss, and nucleosynthesis. While more prevalent in the early universe presumably due to the large gas reservoirs present and increased frequency of starburst triggering galaxy interactions, nearby starburst galaxies offer the opportunity to study this phenomenon in detail.

While starbursts have been observed in gas-rich morphological galaxy types such as disk galaxies and low mass dwarf systems (e.g., Heckman 1998), the most numerous morphological galaxy type experiencing starbursts in the local universe is the dwarf galaxy. In addition to providing a larger sample of starbursts than other morphological types, dwarf galaxies are interesting in which to study starbursts due to the larger amounts of gas and low metallicity of the systems. More significantly, the solid-body rotation of dwarf galaxies (Skillman et al. 1988) prevents the mixing of the stellar populations on short timescales facilitating spatial analysis of the recent SF (Bastian et al. 2009). The starburst phenomenon may have the most significant evolutionary impact on these low mass systems compared with higher mass galaxies. It is poorly understood how the different morphological classes of dwarf galaxies are related, if at all (e.g., Marlowe et al. 1997; Mayer et al. 2001b; van Zee 2001a; Pasetto et al. 2003). Further study is needed to determine if the mass transfer and energy input from a burst into the host galaxy changes the evolutionary path of gas-rich, irregular dwarf galaxies.

The duration of starbursts in dwarf galaxies has recently been reported lasting a minimum of 450 Myr in sample of twenty dwarf galaxies and as much as 1.3 Gyr in two of these systems (McQuinn et al. 2010b). These longer durations suggest that the starburst mode of SF encompasses a significant fraction of the galaxy; it is hard to imagine a burst of SF lasting $\sim$ 500 Myr confined to a small region of a galaxy containing an equally small supply of gas to fuel the burst. Previous authors have reported regions of bursting SF to include areas of lower stellar density in a galaxy as well as the expected stellar cluster regions (e.g., Meurer 2000; Annibali et al. 2003; Cannon et al. 2003). However, both the path the SF takes and the spatial extent a

burst within a galaxy are unclear.

The most common trigger of starbursts is a gravitational interaction with a nearby system. Alternately, a burst might "ignite" due to conducive internal gas conditions within the system. The propagation of the SF may be different in these two scenarios and would likely depend on the initial distribution of gas within the host galaxy. It is also unclear whether bursting SF is a stochastic or self-regulating process. Starbursts lasting longer than the dynamical timescale of the host systems suggest a self-regulating mechanism but no definitive conclusion can be made based on our current understanding of the burst phenomenon. Here, we present the preliminary results from analyzing both the reconstructed star formation histories (SFHs) and the spatial distribution of stellar population of different ages in nineteen starburst galaxies in order to address these unanswered questions.

5.2 The SFHs of Different Parts of Starburst Galaxies

The galaxy sample consists of nineteen starburst dwarf galaxies located within 5 Mpc. Details on the galaxy sample, observations, data processing, photometry, and SFH reconstruction technique are presented in Chapter 3 (see Table 3.1) (McQuinn et al. 2010a). Briefly, a quantitative analysis of the SFH of the lifetime of a galaxy can be derived using a CMD fitting technique. We have previously reconstructed the SFH of the galaxy sample applying a CMD fitting technique (Dolphin 2002) with stellar evolutionary models (Marigo & Girardi 2007). We derived the rate of star formation across time ($SFR(t, Z)$) for each galaxy from the photometry of the stellar populations. Distance, extinction, and stellar ages were the main free parameters in the technique. The metallicity was constrained to increase with time except in two cases where the photometry reached a magnitude below the red clump (Antlia and NGC 2366).

The SFRs in each time bin of a SFH are the spatially averaged SFRs across the observational field of view. However, the SFR in a galaxy generally varies across the disk of the host system. This is evident from the HST images as seen in Figure 5.1. The transfer function in the image highlights regions of high surface brightness corresponding to regions of either higher stellar density, higher SFRs, or both. These high surface brightness regions, enclosed in a green box, are often the historical reason the galaxies

were identified as starbursts. Regions of lower surface brightness are also identifiable in the images (region outside the green box) highlighting the diversity in the stellar populations and SF activity within a galaxy.

The high resolution images and the large number of stars in each field of view make it possible to study these regions independently. We empirically selected areas of high and low surface brightness (HSB and LSB respectively) in each galaxy. The photometry and artificial star lists were separated according to their spatial coordinates. When necessary, additional artificial stars were injected in the regions to fully sample the completeness of an area. We chose to separate the stellar populations guided by surface brightness as areas of different stellar density might have experienced a different SFH. We reconstructed the SFH for each region with the same technique and methodology that we applied to the whole field of view in McQuinn et al. (2010a).

The SFRs over the last 1.5 Gyr are presented in Figure 5.2 for both regions of the galaxies. It is clear from the Figure that most galaxies have experienced bursting SF both in the areas of high and low stellar density. In some instances, the SFRs in each region trace each other in the most recent time bins (i.e., ESO 154−023), while in other systems, the bursting SF starts in the low density regions and migrates over time into areas of high stellar density (i.e., NGC 4068). More analysis is needed to study these patterns in detail.

5.2.1 Calculating a Meaningful SFR/Area

The intensity of star formation per unit area (the "specific SFR" or Σ_{SFR}) has been used to identify and classify starbursts (e.g., Heckman 2005). The areas used in calculating this intensity have primarily been the smaller area of the star clusters within a galaxy. If the starbursts are more global in nature, then another interesting area to consider would be the complete area of the galaxy. The intensity calculated with this larger area is not directly comparable to previous values in the literature using the smaller areas of the star clusters, however it is the appropriate area if the bursts are global in nature.

The observations of the galaxies studied here vary in their areal coverage of the galaxies. In some cases, this area covers the entire galaxy defined by the Holmberg radius (Holmberg 1958). In the other cases, the field of view does not cover the entire galaxy and these values are shown as an upper limit to the SF intensity parameter.

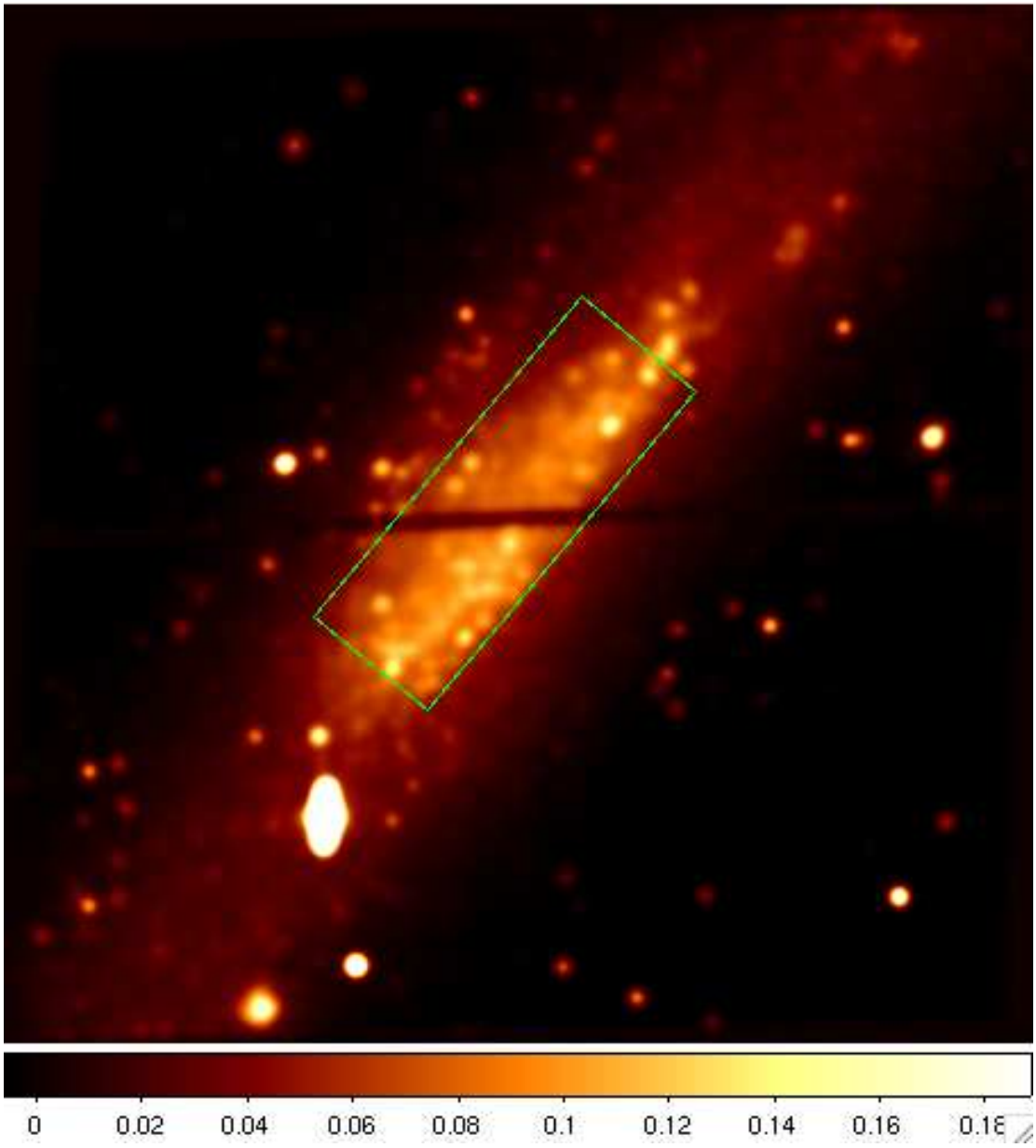

Figure 5.1 A smoothed HST image of ESO 154−023, a typical galaxy in the sample, with regions of higher surface brightness (HSB) enclosed in the green box. The remainder of the field outside the green box constitutes the low surface brightness (LSB) region.

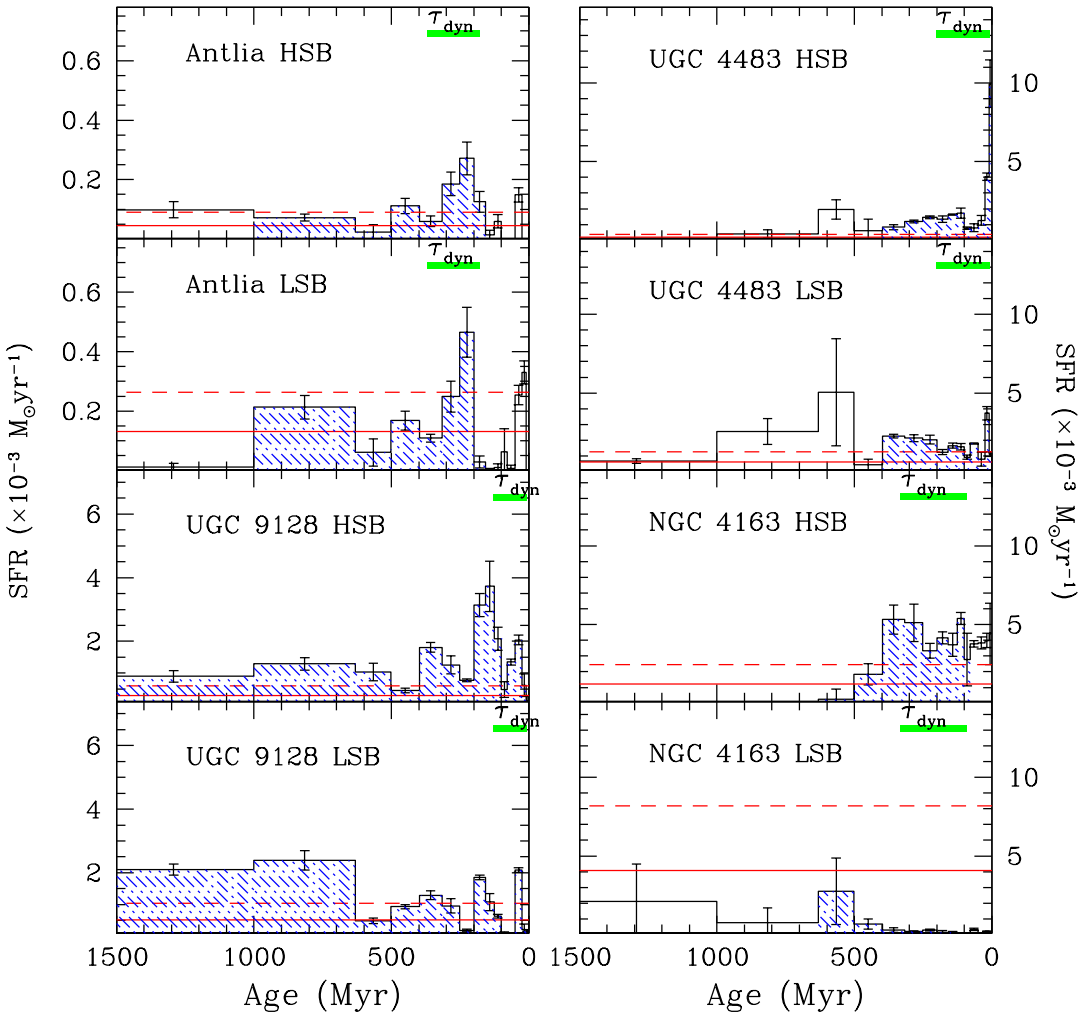

Figure 5.2 The SFHs of high and low surface brightness regions in Antlia, UGC 9128, UGC 4483, NGC 4163. The blue shading represents the burst event in the different regions, the (dashed) solid red line is (twice) the average SFR over the past 6 Gyr, and the horizontal green bar represents the dynamical timescale for the galaxy. Note that the uncertainties measure only systematic uncertainties.

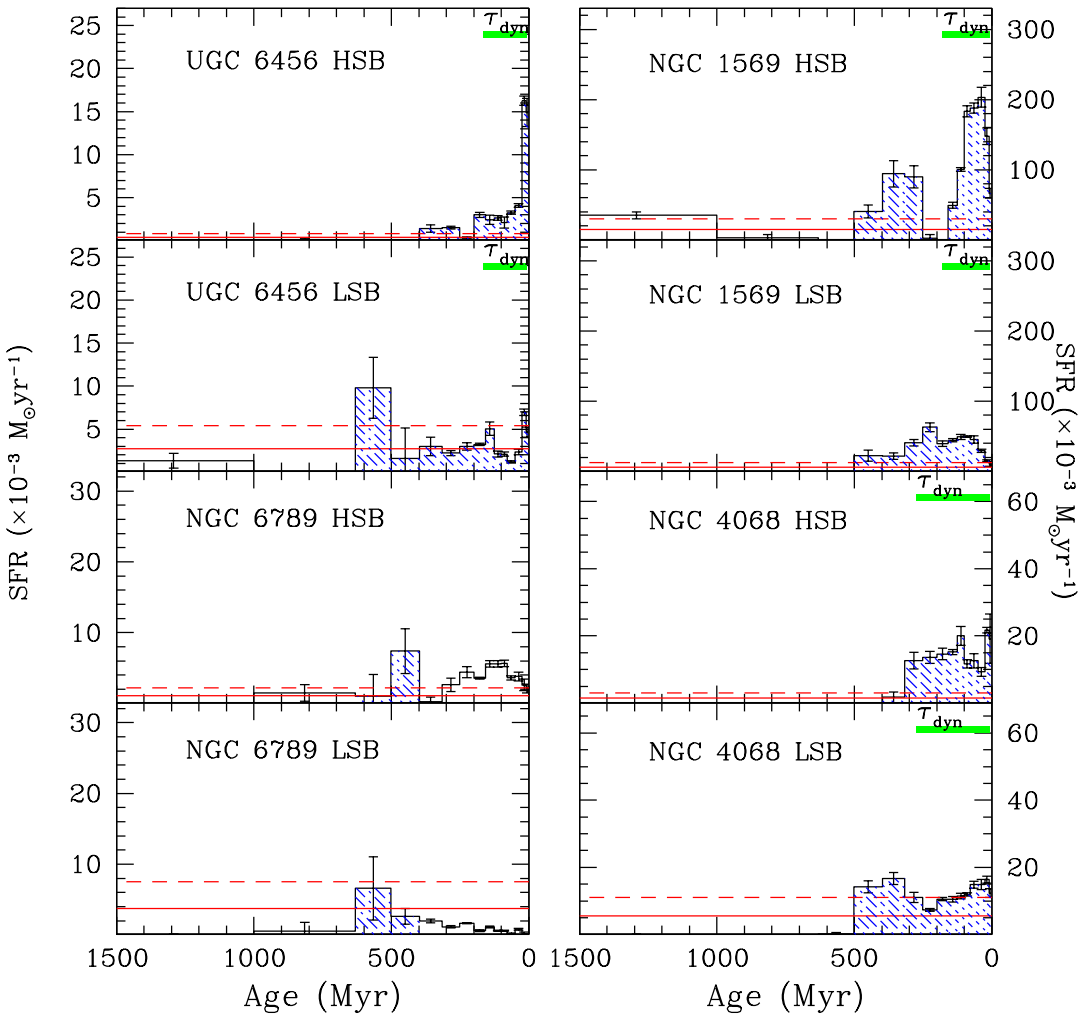

Figure 5.2 *SFHs of high and low surface brightness regions continued: UGC 6456, NGC 6789, NGC 1569, NGC 4068*

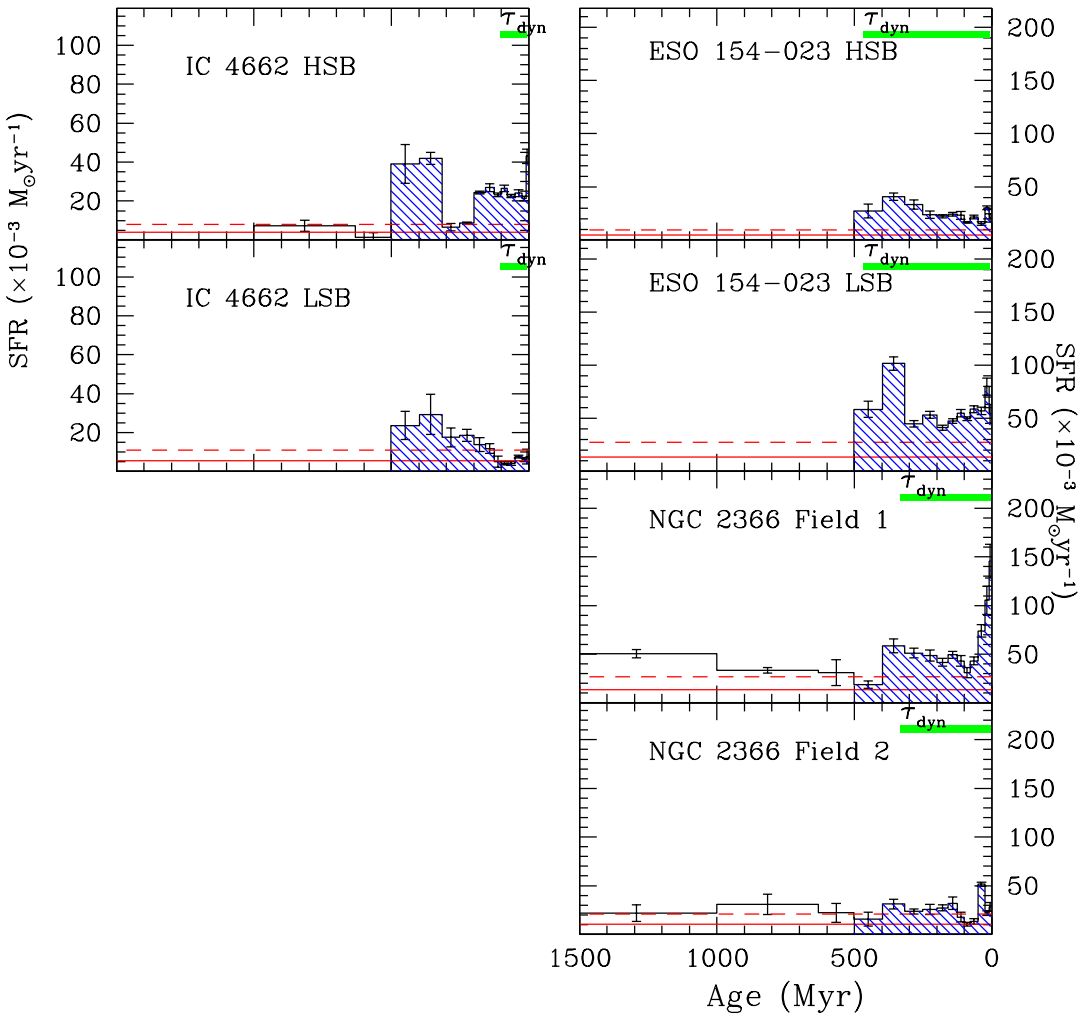

Figure 5.2 *SFHs of high and low surface brightness regions continued: IC 4662, ESO154−023, NGC 2366*

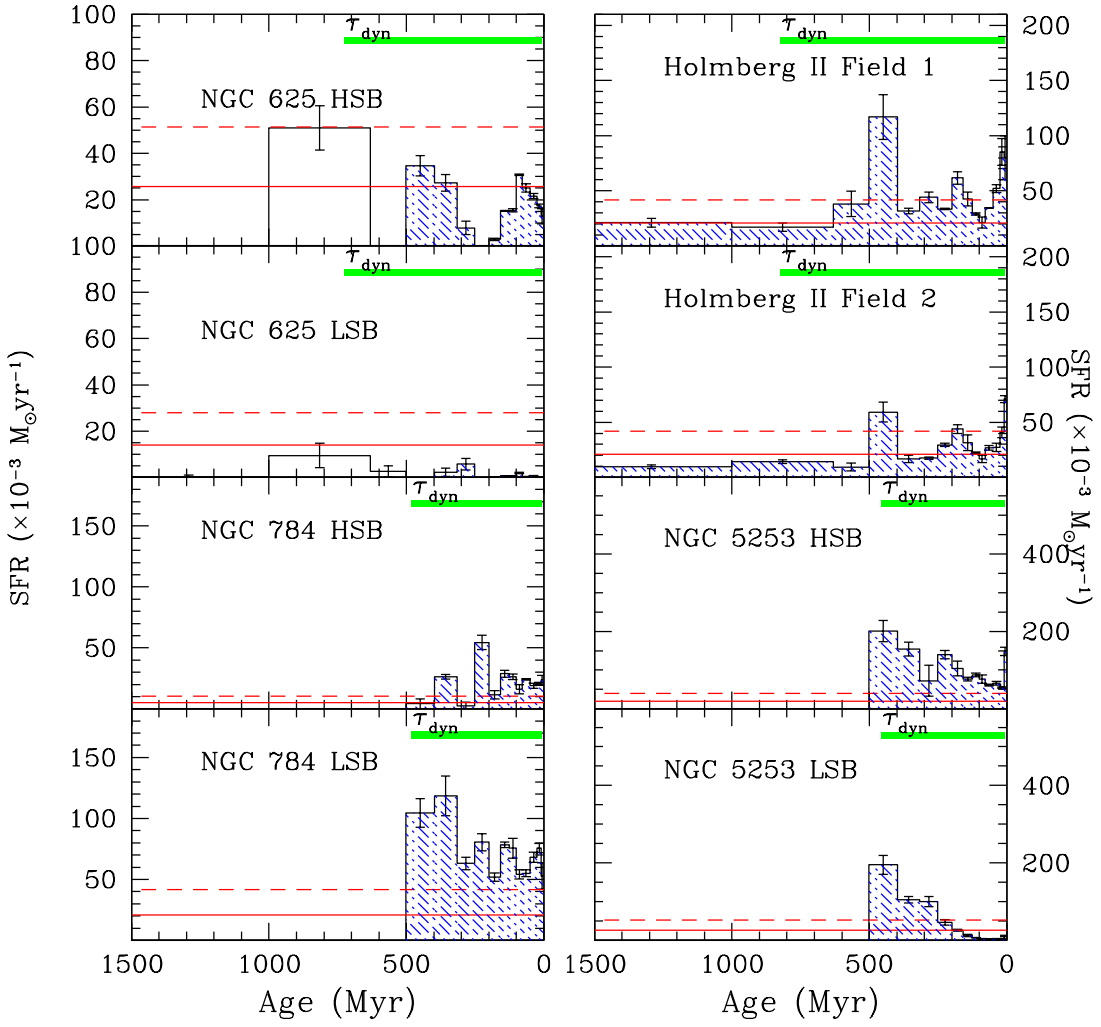

Figure 5.2 *SFHs of high and low surface brightness regions continued: NGC 625, NGC 784, Holmberg II, NGC 5253*

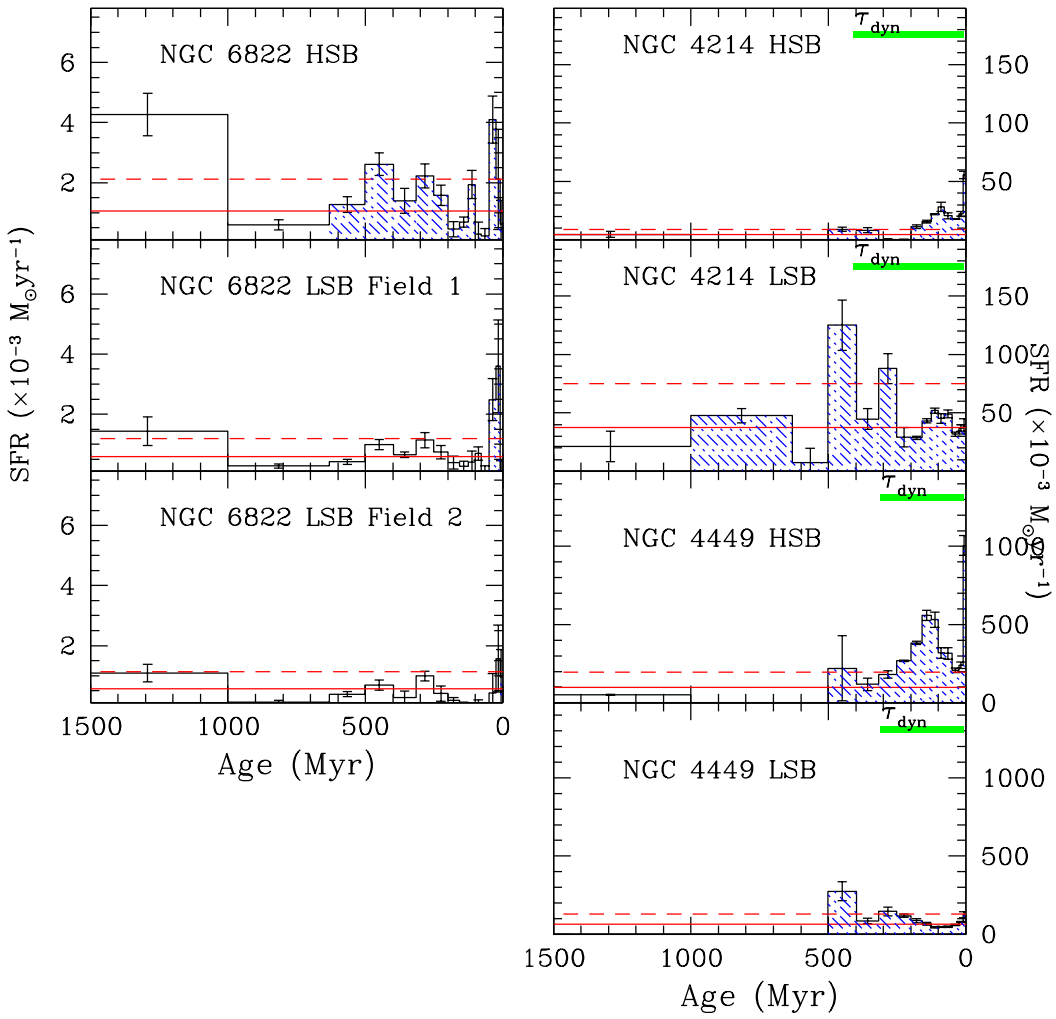

Figure 5.2 *SFHs of high and low surface brightness regions continued: NGC 6822, NGC 4214, NGC 4449*

Planned analysis includes a calculation of the specific SFR using the relevant area and quantifying the fraction of the optical disk subtended by the observations.

5.3 Leveraging Astrometry and the Age Sequence of BHeBs

The evolutionary features that drive the reconstruction of the SFHs can be readily identified in the CMDs including the main sequence (MS) stars, blue and red helium burning (BHeB and RHeB respectively) stars, the red giant branch (RGB) stars, and the asymptotic giant branch (AGB) stars (see Figure 3.3). The upper MS, the BHeB, and the RHeB stars are unambiguous signs of recent star formation. The helium burning (HeB) stars are of particular interest as a star in this stage of stellar evolution occupies a unique space in the CMD for a given metallicity. Specifically, the luminosity of a HeB star has a one−to−one correspondence to the mass of the star and, hence, age of the star. Thus, the HeB stars can tightly constrain the SFH at recent times.

The BHeB stage of evolution can be investigated in detail using stellar evolution isochrones fit to the stellar populations of each CMD. The evolutionary tracks we will use are detailed in Marigo et al. (2008, and references therein) and assume a Salpeter IMF. No circumstellar dust models will be used as this primarily effects the AGB stage of evolution. The isochrones will be adjusted using interstellar extinction estimates that include both external foreground extinction and internal extinction derived from the CMDs (see §3.3). The metallicities for the isochrones will be obtained from measurements of H II region abundances in the literature wherever possible. In cases for which there are no measured H IIregion abundances, we will use the position of the MS stars to determine the appropriate isochrone metallicity as the MS provides the best anchor to metallicity estimates in the absence of abundance measurements. These isochrones can be compared to the metallicity values derived from reconstructing the SFHs.

As an example of fitting stellar evolution isochrones to a CMD, we present the CMD of UGC 9128 with isochrones of various ages over-plotted on the stellar populations in Figure 5.3. The unambiguous age sequence of HeB stars is apparent from this figure; each isochrone plotted represents a unique age in the HeB stage of evolution corresponding to a unique population of BHeB stars.

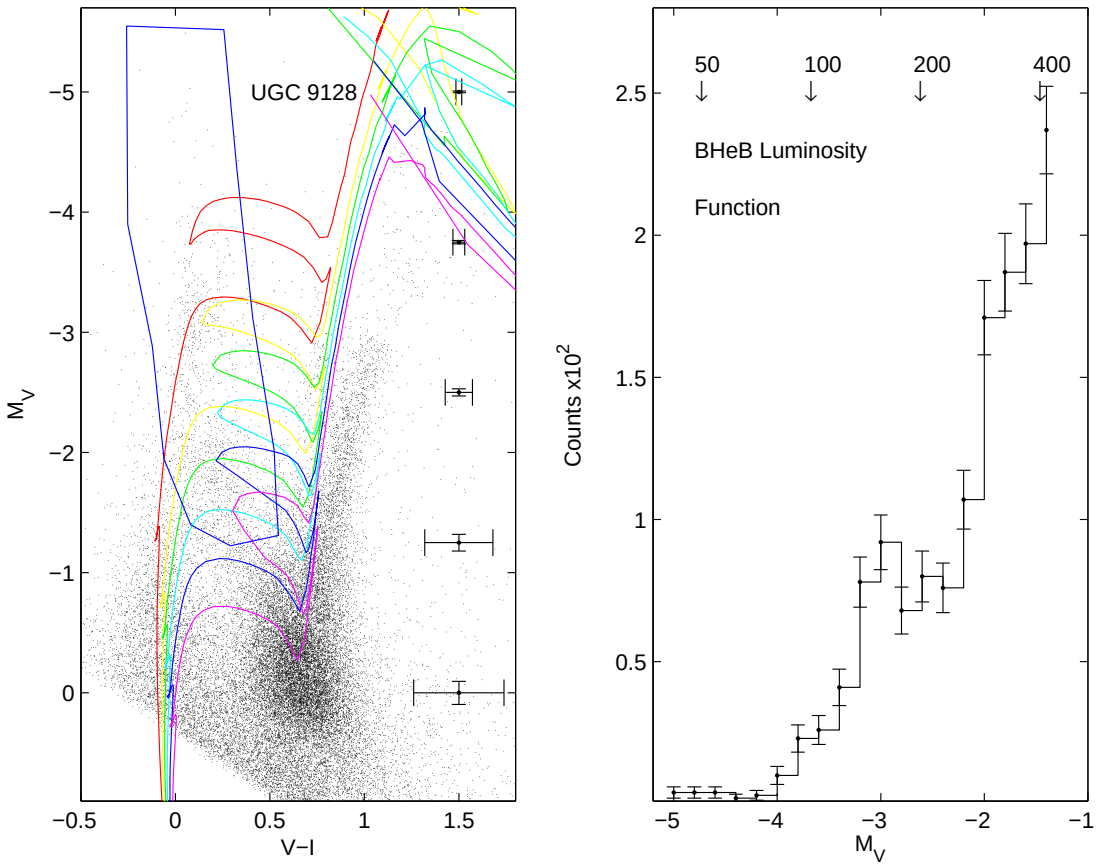

Figure 5.3 Note the isochrones match the MS locus of points on the CMD and both the blue and red extremes of the blue loop sequence. Uncertainties in the luminosity function include both Poisson errors and incompleteness measurements. The colored isochrones correspond to different ages according to the color key: red=100 Myr, yellow=150 Myr, green=200 Myr, cyan=250 Myr, blue=300 Myr, and magenta=400 Myr.

The age sequence of the isochrones provides a reference for selecting the BHeB population from the CMD. In our example case in Figure 5.3, the BHeB stars selected based on the isochrones are enclosed by the blue polygon in the CMD and are used to populate the luminosity function in the second panel of the same Figure. The BHeB luminosity function in Figure 5.3 extends from the brightest luminosities to the magnitudes at which the BHeB stars merge into the red clump. The magnitude of the stars are labeled on the bottom axis of the luminosity function with the age of the stars marked near the top axis linking the ages from the stellar evolutionary isochrones with the BHeB stars' magnitudes. A qualitative description of the recent SFH can be made directly from the luminosity function of BHeB. Increases in the SFR can be seen from the luminosity function at ~ 120 and ~ 220 Myr as well as periods of relative quiescence in the SFR at $50 - 100$ Myr or from $150 - 200$ Myr.

The ages of the BHeB population can be combined with high fidelity, astrometric spatial coordinates of each BHeB star to explore the spatial and temporal distribution of the starburst. As an example of this analysis, we present the distribution of four different age groups of BHeB pulled from the CMD plotted over a smoothed HST image of UGC 9128 in Figure 5.4. The SF appears to cover a large areal fraction of the galaxy and is not limited to the central, bright SF regions often associated with starbursts. In the oldest time bin ($300 - 400$ Myr), the BHeB are concentrated more in the upper right area of UGC 9128 moving towards the lower left of the galaxy in the more recent time bins of the last 200 Myr.

We have performed this same analysis on a second galaxy in the sample, NGC 1569. Preliminary results show the the SF in this system is widespread $100 - 150$ Myr and concentrates in the central regions more recently (t<25 Myr) as seen in Figure 5.5. The timescales of SF and the spatial patterns are different in these two galaxies; a complete analysis of the galaxy sample promises to reveal much about the spatial structure of bursting SF.

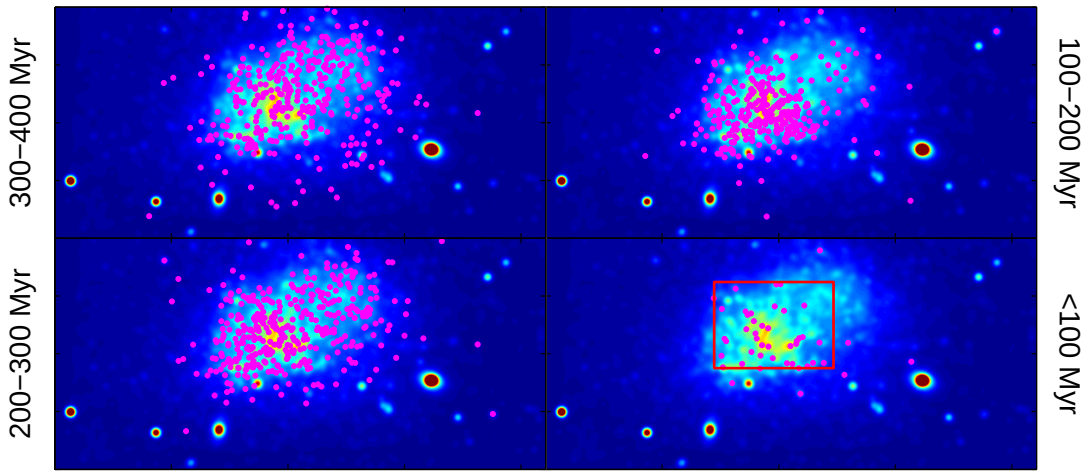

Figure 5.4 The smoothed images were made by applying a 25 pixel radius Gaussian kernel to the original HST observations. The location of the BHeB stars are plotted for the time time bin $300-400$ Myr in the top left panel, $200-300$ Myr in the bottom left panel, $100-200$ Myr in the top right, and <100 Myr old in the bottom right. Note the movements of the star formation from the upper right in the oldest time bin to the lower left in the two most recent time bins.

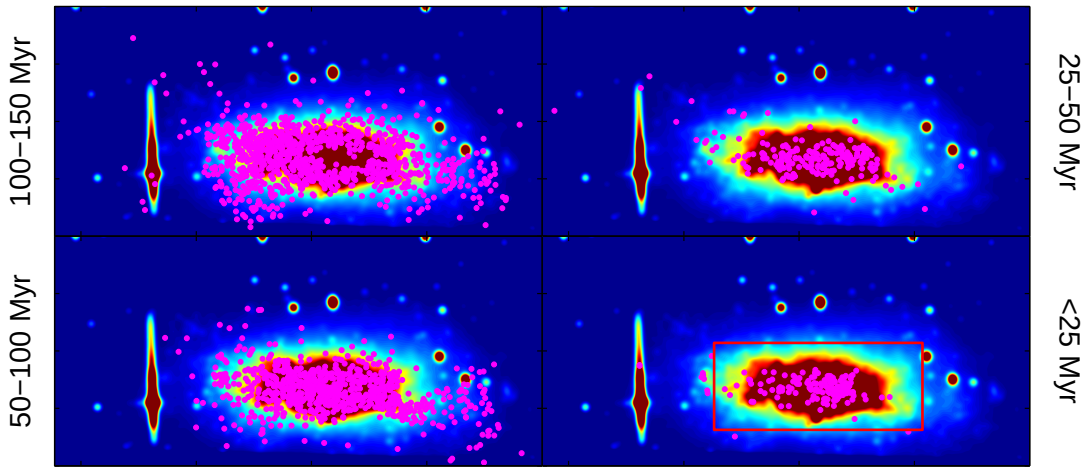

Figure 5.5 The smoothed images were made by applying a 25 pixel radius Gaussian kernel to the original HST observations. The location of the BHeB stars are plotted for the time time bin $100 - 150$ Myr in the top left panel, $50 - 100$ Myr in the bottom left panel, $25 - 50$ Myr in the top right, and < 25 Myr old in the bottom right. At earlier times, the SF was widespread. In the most recent time bins, the SF in more centrally located.

5.4 The Combined Spatial and Temporal Characteristics of a Starburst

We will combine the regional SFHs with the spatial and temporal distribution of BHeB for each individual galaxy providing a more complete picture of the spatial characteristics of each starburst galaxy. As an example, we present preliminary results for UGC 9128 in Figure 5.6 with the CMD, BHeB luminosity function, regional SFHs, and the spatial distribution of BHeB of different ages. Combining the regional SFHs with the spatial distribution of BHeB stars of different ages, the spatial and temporal nature of a starburst event can be understood. The combined plots promise to reveal much about an individual galaxy's starburst history. When complete for the galaxy sample, these analyses will allow us to probe deeply into how star formation proceeds on galactic scales and whether starbursts are self-regulating or stochastic in nature.

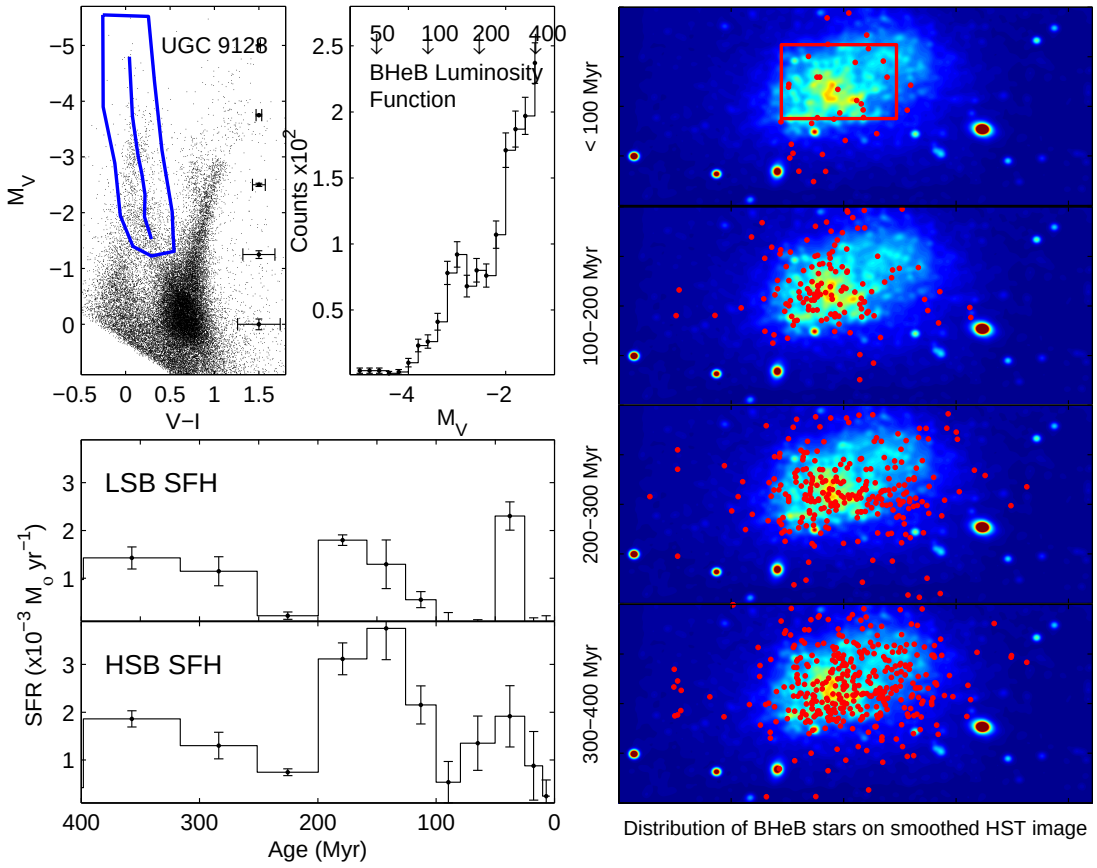

Figure 5.6 The combined spatial analysis results for UGC 9128 combining results from Figure 5.2−5.4. This example plot will be generated for the complete galaxy sample allowing us to probe deeply into the spatial structure and nature of the starburst mode of star formation in the nearby universe.

Chapter 6

SFRs and Emission Timescales in the UV and IR Wavelengths

The next stage of research into the nature of starbursts has been mapped out in two recently accepted proposals (funding provided through a NASA ADP grant and GALEX GI observation grant). The science goals of the two proposals are interconnected; a merged summary is presented here.

ABSTRACT

The rate of star formation (SFR) is a fundamental parameter shaping the evolution of a galaxy. In the extreme environments of starburst galaxies, the elevated levels of star formation can have a dramatic impact on the chemical composition and dynamics of the galaxy, on the future star formation within the galaxy, and potentially drive enriched material into the intergalactic medium surrounding the galaxy. While starbursts are a very important phenomenon with many aspects still not well understood, there has been no GALEX survey dedicated to the study of the nearest starburst galaxies. Starburst dwarf galaxies are ultimately an ultraviolet (UV) phenomenon due to their low dust content and as such warrant a legacy project of deep observations with Galaxy Evolution Explorer Space Telescope (GALEX) that will produce a homogeneous archive. We propose a comprehensive comparison of the SFRs and spatial structure in twenty nearby, spatially resolved starburst galaxies derived from new and existing GALEX

observations and Spitzer Space Telescope (Spitzer) mid-infrared (MIR) data. Our sample of nearby starbursts is composed of galaxies for which we have reconstructed star formation histories (SFHs) from resolved stars using archival Hubble Space Telescope (HST) observations. The spatial analysis possible with these data sets combined with the temporally resolved SFHs and SFRs derived at different wavelengths will allow us to understand the true nature of starbursts in dwarf galaxies for the first time. Using the multi-wavelength suite of observations, we will be able to determine how the bursts propagate within a galaxy and whether they are causally connected or of a more stochastic nature, and whether starbursts are indeed "self-quenching". Further, we will be able to probe the timescales of star formation responsible for the emission at the UV and MIR wavelengths while considering the spatial migration of a starburst. Finally, these fully reduced data sets will populate a new public archive of multi-wavelength observations of great use to a large community of researchers. Our proposed work will build our understanding of how galaxies change over time, one of NASA's strategic goals, and is a direct successor to the accomplishments and results of a project supported by a NASA HST archival grant.

6.1 On the Importance of Studying Nearby Starbursts

Starbursts are short-lived periods of intense star formation whose energy output dominates the total luminosity of their host galaxies. The ionizing radiation, mass loss, and nucleosynthesis of the massive stellar populations formed in a burst can alter the gas dynamics, future star formation, and chemical composition of the host galaxy. Local starbursts ($z << 1$) provide 10% of the radiant energy production and $\sim 20\%$ of all the high mass star formation (e.g., Heckman 1998; Brinchmann et al. 2004). In the small potential wells of low-mass systems, such as dwarf galaxies, the star formation that takes place within a starburst can also power energy and mass transfer from the host galaxy to the intergalactic medium (IGM) (e.g., Dekel & Silk 1986; Strickland & Stevens 2000; Martin et al. 2002) linking galactic evolution with the chemical enrichment of the IGM (e.g., Spaans & Norman 1997; Romano et al. 2006).

Understanding the starburst mode of star formation in dwarf galaxies is critical in the exploration of galactic evolution in the local and the early universe (Heckman 2005). In

the early universe, starbursts were more common due to the larger amount of gas present in galaxies to fuel starbursts and the increased frequency of burst-triggering galactic interactions and mergers. The nearby dwarf starburst galaxies offer us an opportunity to study this powerful phenomenon in detail not only as proxies to the numerous starbursts that shaped galactic evolution in the distant past, but also to help answer questions about the physics of star formation. Previous authors have suggested bursting star formation continues for less than 10 Myr and would be "self-quenching" meaning the supernovae and stellar winds prevalent in starbursts would disrupt the star-forming environment and shut-down the burst (e.g., Thornley et al. 2000; Ferguson & Babul 1998). However, our recent results on starbursts (McQuinn et al. 2009) show elevated SFR lasting hundreds of Myr suggesting "self-quenching" may not be the case.

We propose a comprehensive comparison of the star formation rates (SFRs) and spatial structure in twenty-one nearby, spatially resolved starburst galaxies (see Table 6.1 for a list of the galaxies and their basic properties) derived from archival and new GALEX UV data and archival Spitzer MIR data coupled with ground based Hα data. Our sample of nearby starburst galaxies is composed of galaxies for which we have reconstructed star formation histories (SFHs) from resolved stars using archival Hubble Space Telescope (HST) observations (McQuinn et al. 2009, 2010a,b). Our analysis will address unanswered questions concerning the physics of star formation in bursts such as how starbursts propagate within a galaxy, whether the star formation regions are causally connected, and if there is any physical evidence for "self-quenching". We will compare the SFRs derived from the UV, MIR/Hα, and resolved star observations while probing the timescales of emission at these different wavelengths. Our spatial and temporally resolved SFHs will be used to predict the emission at the UV, MIR, and Hα wavelengths facilitating a comparison with measured emission at these wavelengths further testing the assumptions used when constructing holistic pictures of galaxies in the nearby and distant universe.

Table 6.1 Properties of Proposed Galaxy Sample

Galaxy	M_B (mag)	D (Mpc)	$m-M$ (mag)	A_R (mag)	(10^{-3} $M_\odot yr^{-1}$)
ANTLIA	-9.8	1.25 ± 0.1	25.49	0.212	0.5 ± 0.03
UGC 9128	-12.34	2.24	26.75	0.065	5 ± 1
UGC 4483	-12.53 ± 0.23	3.2 ± 0.2	27.53	0.091	8 ± 1
NGC 4163	-13.66	3.0	27.39	0.052	11 ± 2
UGC 6456	-13.69 ± 0.19	4.3 ± 0.1	28.17	0.096	22 ± 1
NGC 6789	-14.3	3.6 ± 0.2	27.78	0.187	13 ± 7
NGC 1569	-14.74	1.9	26.39	1.871	90 ± 10
NGC 4068	-14.87	4.3	28.16	0.058	42 ± 3
SBS 1415+437	-15.07 ± 0.46	13.6 ± 1.4	30.7	0.024	158 ± 71
IC 4662	-15.09	2.4	26.90	0.188	71 ± 11
DDO 165	-15.09	4.6	28.30	0.065	68 ± 5
ESO154-023	-16.14	5.76	28.80	0.045	127 ± 6
NGC 2366	-16.17 ± 0.36	3.2 ± 0.4	27.52	0.097	47 ± 16
NGC 625	-16.19 ± 0.18	3.9 ± 0.4	27.96	0.044	63 ± 22
NGC 784	-16.5	5.19	28.58	0.158	110 ± 5
Ho II	-16.72	3.4	27.65	0.086	112 ± 22
NGC 5253	-16.74 ± 0.18	3.8 ± 0.2	27.90	0.186	200 ± 25
NGC 6822	-16.84	0.5 ± 0.04	23.3	0.632	4 ± 0.2
NGC 4214	-16.93 ± 0.22	2.7 ± 0.2	27.16	0.058	92 ± 8
IC 2574	-17.46	4.0	28.02	0.084	109 ± 19
NGC 4449	-17.94 ± 0.33	4.2 ± 0.5	28.11	0.051	1000 ± 1

Basic properties of the starburst galaxy sample. The distances are taken from various sources in the literature. A_R is the foreground extinction values taken from Schlegel et al. (1998). The peak SFRs during the starburst are from McQuinn et al. (2010a). Note that many of these systems are not generally regarded as starburst galaxies because they are not currently experiencing a starburst. In five cases, we have captured a "fossil" starburst within the last 200 Myr in our HST observations.

6.2 SFR Indicators, SFHs, and Spatial Structure from Resolved Stars

The rate of star formation in galaxies is one of the fundamental parameters in understanding the evolution of galaxies (Kennicutt 1998). The SFR governs the chemical enrichment processes in the interstellar medium (ISM) and the intergalactic medium (IGM) while simultaneously impacting the energy feedback mechanisms in the galaxies. The studies at high-redshift (z > 3) that measure SFRs at rest-UV, MIR (24 μm), and Hα wavelengths make assumptions about how these star formation indicators are related. The indicators are based on measuring one form of the radiation produced by massive stars and applying an assumption about the stellar initial mass function (IMF). One of the main differences between the indicators is that the measured UV radiation is emitted directly by the massive stars produced in a starburst with a continuum intensity that evolves over a timescale of a few hundred million years. The MIR radiation, in contrast, is from dust heated by the ionizing stellar radiation of a more massive stellar population that evolves over a timescale less than ten million years. The flux of this ionizing stellar radiation field can be measured in the non-dust obscured regions at the Hα wavelength giving a more complete energy budget.

Interest in SFRs found from UV emission has increased dramatically due to the quality and quantity of data obtained in the FUV and NUV wavelengths from GALEX. However, the longer timescale associated with UV derived SFRs can be problematic in determining how the SFR *changes* over time as an instantaneous burst event is indistinguishable from a lower level of constant star formation. Our proposed work will aid in the interpretation of these SFRs as we have the additional time-resolved information on the galaxies from the HST observations in hand. The high quality data from *Spitzer* are yielding more results on the SFRs in large statistical samples of galaxies and indicate not only the timeliness of our proposed study but also the usefulness of studying and understanding the SFRs indicators in resolved systems.

Nearby galaxies are the only systems that afford an opportunity to study the timeline and spatial structure of star formation and galactic evolution. We can probe the timescales of the UV and MIR/Hα SFR indicators by using our time-resolved histories of these nearby galaxies. Rigorously defining the timescales for each wavelength

is critical to the correct interpretation of the SF processes occurring locally and at high-redshift and will test the assumptions used when finding the SFRs in the more numerous starburst galaxies at high-redshift. For example, the coupling of the SFRs derived from the UV and MIR/Hα wavelengths with the time resolved SFHs will likely resolve the tension between the classification of a galaxy as a starburst at one wavelength but not at another. For example, NGC 4068 is classified as a starburst galaxy by Karachentsev et al. (2006) based on HST imaging but the galaxy does not meet the starburst Hα equivalent width criterion of Lee et al. (2009). This double classification is most likely due to the SFR changing on timescales shorter than the Hα emission timescales. Our proposed work would resolve the inconsistent classification of galaxies by developing a more detailed understanding of the physics of a starburst.

6.3 The Need for New GALEX UV Observations

While starbursts are a very important phenomenon with many aspects still clearly not well understood, there has been no GALEX survey dedicated to the study of the nearest starburst galaxies. The existing GALEX observations on this class of objects are a mismatched data set taken piecemeal with one orbit observations obtained through the Nearby Galaxy Survey (NGS) and a few longer exposure time by Guest Investigators (GII). The galaxies in our sample are of great interest to the research galaxy reflected by the number of citations listed for each system. For example, NGC 5253 returns 620 separate citations, NGC 4449 registers 498, and NGC 4214 lists 424 when queried in the NASA/IPAC Extragalactic Database. Starburst dwarf galaxies are ultimately an ultraviolet (UV) phenomenon due to their low dust content and as such warrant a legacy project of deep observations with GALEX that will produce a homogeneous archive. We propose to do just that by assembling a uniform set of seven orbit observations of twenty nearby starburst dwarf galaxies. Deep observations are necessary as starbursts are best understood as a global phenomenon with star formation occurring throughout the galaxy, including in regions of current lower surface brightness. Previous authors have reported that bursting star formation in starburst galaxies is not confined to star clusters but is found throughout regions of diffuse star formation Meurer (2000); McQuinn et al. (2009) and in field stars outside the central super star clusters (Annibali et al. 2003). A

complete census of the star formation in these starburst galaxies must therefore include the currently fainter regions of the bursting galaxies that are not clearly imaged in shorter exposure times.

As an example of the S/N we want to achieve, we present a GALEX archival 2-color image (blue:FUV; yellow:NUV) of the starburst galaxy IC 2574 in Figure 6.1(a) obtained with an exposure time of 12.9 ksec; slightly greater than the 10.5 ksec we propose to achieve. The sub-structure and emission seen across the the extent of this starburst galaxy allows for detailed analysis on the starburst mode of star formation both spatially and, when combined with the SFHs we have derived from HST observations, temporally. Existing piecemeal observations of the galaxies for which we are requesting new observations are inhomogeneous and too shallow for our science purposes. Figure 6.1(b) presents a one orbit GII observation of starburst galaxy NGC 5253 in which the high surface brightness areas of the starburst are evident. While sufficient for global measurements, the image is insufficient for spatially resolved measurements as very little structure is discernible.

6.4 Correlating Emission from Different Wavelengths

The starburst phenomenon is a global event that migrates around a galactic system (McQuinn et al. 2009) and is not constrained to one region of the galaxy or a single cluster of stars. We intend to study the spatial structure of the starburst by connecting *when* the burst is occurring in a galaxy with *where* a burst is occurring in the UV, MIR/Hα, and optical wavelengths. We present an example of the structure and connection between the resolved stars in the HST observations and the UV and MIR wavelengths in Figure 6.2. The top (bottom) panels compare where the stellar populations less than 10 Myr (200 Myr) old are predicted to be using the resolved SFH results with the *Spitzer* 24 μm image (GALEX NUV image). The distribution and structure of the star formation is highly correlated in the images. Linking the star formation events and spatial structure is a powerful tool for understanding this important mode of star formation. Interesting differences exist between the top and bottom panels indicative of the changing SFRs between the timescales measured at the UV and MIR wavelengths and reflecting the changing topography of a migrating starburst.

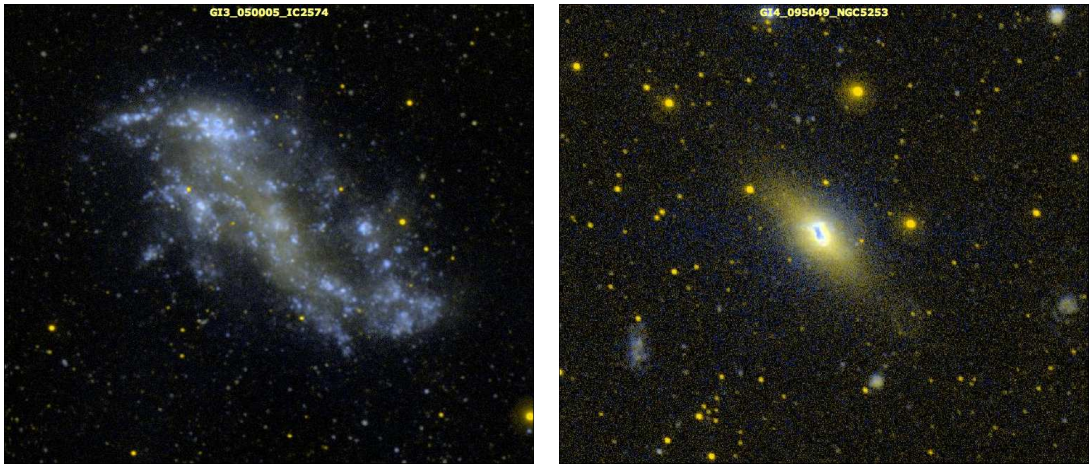

(a) Multi-orbit GALEX observations (b) One GALEX orbit observation

Figure 6.1 FUV (blue) and NUV (yellow) images of two starburst galaxies with similar magnitudes from the GALEX archive. The left hand image shows the detail and structure IC 2574 obtained with deep 12.9 ksec exposure times. This spectacular image shows what is possible with the resolution of the GALEX instruments and the integration times we propose. The quality of such observations for a set of starburst galaxies will leave a science legacy from the GALEX instruments that will be un-repeatable in the foreseeable future. The right hand image shows the high surface brightness regions of starburst galaxy NGC 5253 captured in one orbit of observation time. While sufficient for global measurements, the image is insufficient for spatially resolved measurements as very little structure is discernible.

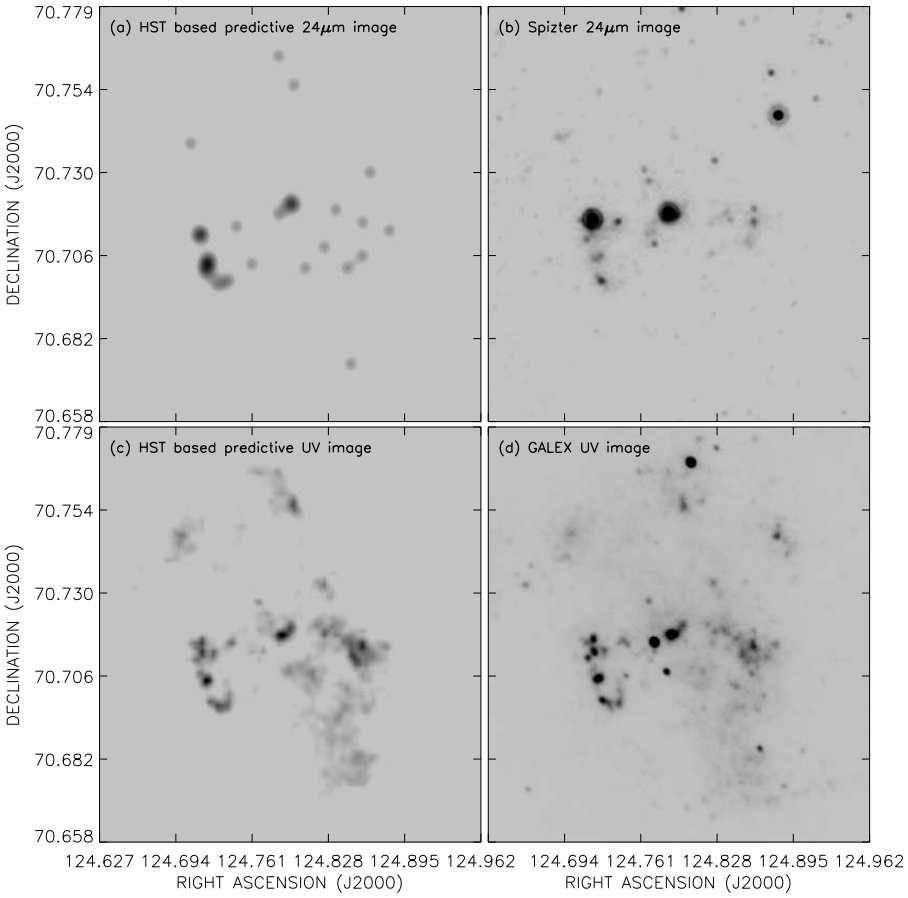

Figure 6.2 The top panels compare where emission from stars less than 10 Myr old is predicted to be based on the HST images and SFHs (a) to the actual *Spitzer* 24μm emission (b) for the starburst galaxy Holmberg II. The bottom panels show a similar comparison between predicted emission from stars less than 200 Myr old derived from the resolved stellar populations (c) and the actual GALEX NUV image (d). The similarities between the images are striking. Linking the spatial and temporal SF events from these multi-wavelength images will allow us to understand the true nature of starbursts in dwarf galaxies for the first time.

To rigorously explore this connection between the UV, MIR, and optical emission, we will predict the UV and IR luminosity using the time-resolved SFRs from our SFHs results and the Starburst99 synthetic modeling code (Leitherer et al. 1999; Vázquez & Leitherer 2005) which is designed to simulate the properties of evolving galaxies at multiple wavelengths. The energy distribution at the UV, IR, and optical wavelengths will serve as a baseline to compare against the observationally derived results. Combining the temporal variations, spatial structure, and multi-wavelength energy distribution of the starburst will help us understand how a SF phenomenon that lasts hundred of millions of years propagates through a galaxy and maintains its strength despite the feedback mechanisms of supernovae and stellar winds that were previously thought to disrupt the SF process.

6.5 Timescales of Emission

Building further on the temporal component of our analysis, we will rigorously define the time-scale of UV emission in starbursts using the GALEX observations and the expected energy distribution of the bursts. The UV emission time-scale is an essential input to the correct interpretation of the SF processes occurring locally and at high-redshift. The lifetime of the dominant UV emitting population is assumed to be $< 10^8$ (e.g., Kennicutt 1998), yet, to date, an accurate time-scale for UV emission has not been observationally derived. While starbursts may last a few hundred million years, the fluctuations in the SFR within a starburst vary on time-scales less than 10 Myr (McQuinn et al. 2009, 2010a,b) affecting the evolution of UV emission from a starburst galaxy and how the UV measurements are interpreted. Our time-resolved SFHs will be used to predict the UV luminosity using the synthetic modeling code Starburst99 (Leitherer et al. 1999; Vazquez & Leitherer 2005). Starburst99 is specifically designed to model the properties of an evolving galaxy including predicting the energy budget of star-forming galaxies. We will generate UV predictions using the Starburst99 model at different time-scales stepping from 10 Myr to 300 Myr. The predictions will be compared with the measured GALEX UV emission and derived FUV SFR (Kennicutt 1998) enabling a calibration of the UV emission time-scale and an assessment of the uncertainty in applying a simple formula to determine all UV SFRs. Interpreting the

integrated UV measurements produced by GALEX requires detailed calibration made possible only with resolved stars. Ultimately, we will be building results that will enable us to infer star formation patterns from integrated UV measurements.

An important aspect of our sample of galaxies is that it covers different phases of starbursts including systems that show starbursts that are just beginning, systems that have been bursting for prolonged periods of time (on the order of a few 100 Myr), and systems that are "post-burst". The UGC 6456 (VII Zw 403) galaxy is an example of a young burst whose UV emission may show different characteristics than a "mature" burst that may have lasted much longer such as the starburst galaxies ESO $154-023$ or UGC 4483. DDO 165 is an example of a "post" or "relic" burst system with low SFRs at the current epoch, corresponding low H_α emission, but large SFRs within the last 200 Myr; the time frame that is important for producing emission in the UV. By spanning a range of ages of starbursts we can study all phases of the starburst phenomenon.

6.6 Creating a Public Archive of Nearby Starburst Observations

Our galaxy sample of twenty-one nearby bursting dwarf galaxies is a unique and scientifically important group of objects. Individually, many of these galaxies have been cited hundreds of times in the literature. For example, NGC 5253 returns 620 separate citations, NGC 4449 registers 498, and NGC 4214 lists 424 when queried in the NASA/IPAC Extragalactic Database. These are widely studied systems because they offer an important opportunity to study star formation, galactic evolution, IGM enrichment, and feedback mechanisms in great detail. The research on resolved starburst galaxies has yielded important contributions to our understanding of galactic structure, chemical evolution, and the interplay between star formation, gravity, energy, and mass transfer within a system and its environs. While large statistical studies can be done on the population of galaxies at high redshift, detailed understanding of the star formation processes and their impact on galactic evolution can only be achieved by studying the local galaxy population. Nearby galaxies that show similar properties to their distant cousins can be used as proxies to gain detailed understanding of the star formation processes and their effects. These nearby objects are our only window into the details

of galactic starbursts which is why they have warranted such intense study.

The trend in recent years has been to create public archives for observational data and for the reduced data at individual wavelengths. However, these archives typically do not link multiple wavelength observations. We propose to create a public archive of multi-wavelength imaging for these nearby galaxies with all the observations re-binned or re-sampled to the same resolution, flux calibrated, and registered to the same coordinate system. Specifically, we propose to bin the HST images to the native pixel scales of the GALEX and *Spitzer* instruments, re-sample the GALEX data to the native pixel scales of HST and *Spitzer*, and bin/re-sample *Spitzer* to the two pixel scales of the other instruments. Having each set of observations on a galaxy binned or re-sampled to the three different native pixel scales will provide as much flexibility as possible for future users of the data. The observations will be re-gridded and registered to the same coordinate system. As much as these galaxies are cited in the literature, a dedicated archive accessible to anyone in the scientific community will facilitate further research on these galaxies *without* having to start from scratch and duplicate effort by homogenizing the data. This archive can be a repository for other galaxies and other wavelengths (e.g., Chandra X-Ray and EVLA radio continuum observations) in the future to allow access to multi-wavelength data pre-processed to the same pixel scale and primed for further research. We have already reduced the HST observations. Here we propose to process the UV and MIR data for our science goals stated above. It is a natural extension of the project to create a useful archive for the research community.

6.7 Project Impact

The proposed work will contribute an understanding of the true nature of starbursts in dwarf galaxies for the first time. No study to date has yet to comprehensively analyze how a starburst migrates around a galaxy and whether this mode of star formation is causally connected or is a more stochastic process based on the gas and dynamical conditions of the host galaxy. Our study will directly build our understanding of how galaxies change over time; one of NASA's strategic goals.

In addition, our program will contribute an important connection between SFRs derived at different wavelengths using not only UV, MIR, and Hα data but also the

longer baseline of SFRs derived from HST observations. This proposal is a direct successor to an HST archival grant and directly builds on the accomplishments and results on that project. There are a number of NASA telescope surveys being completed that measure the integrated light at the UV and IR wavelengths of both nearby and distant galaxies. One of the goals frequently cited is the calculation of the SFRs from these wavelengths applicable to a relevant timescale. Our results will provide a benchmark for the integrated light and detailed, resolved stellar populations SFHs using temporally and spatially resolved SFRs. Thus, our results can be used by future NASA programs to correlate these wavelengths and provide a perspective on which wavelengths can provide the most salient information on star formation in the local and early universe.

The proposed work will also provide a multi-wavelength public archive to the astronomy community of observations on our sample of galaxies from the different surveys re-binned/re-sampled to the native pixel scales of the HST instruments, *Spitzer*, and GALEX re-gridded and registered to the same world coordinate system. Our sample of galaxies are of great interest to the community reflected by the high number of citations on papers written about the individual galaxies. While there are some excellent archives dedicated to individual instruments, these repositories facilitate single telescope studies. Our proposed archive would link observations on nearby galaxies from three NASA space telescopes processed to identical pixel scales to eliminate repeating processing steps in future research. Providing such an archive can help facilitate future archival based studies at multiple wavelengths for these galaxies. This archive can be expanded in the future to include a larger sample of galaxies and data obtained at additional wavelengths such as future Chandra X-ray and EVLA radio continuum observations.

Chapter 7

Conclusion

For the first time, the duration of starbursts has been measured using SFHs reconstructed from optically resolved stellar populations in a sample of twenty nearby dwarf galaxies. Much longer than the $5-10$ Myr timescale often reported, the starbursts in this galaxy sample last at least 450 Myr and, in two cases, as long as 1.3 Gyr; comparable to or longer than the dynamical timescale of the host galaxies. The shorter durations often cited are measuring small pockets of enhanced SF or "flickering" that contribute to a burst event, but do not represent the extant of a burst. In fifteen galaxies, the duration measured is a lower limit as the burst is ongoing; in five galaxies, the bursts have ended creating a sample of "fossil" bursts. These longer duration times rule out the theory that these starbursts are "quenched" by the feedback processes of the massive stellar populations created. The bursts deposit $10^{53.9}-10^{57.2}$ erg of energy into the interstellar medium through stellar winds and supernovae and produce 3.2%−26% of the host galaxy's mass.

These results were obtained using optical data from the HST data archive to reconstruct the SFHs of a sample of nearby starburst dwarf galaxies. The SFHs show large variations from galaxy to galaxy, and, while the galaxies represent a class of objects undergoing significant recent star formation, there is no "idealized" SFR profile that characterizes the starburst phenomenon. Not only are the changes in the SFR during a burst varied, but the peak SFRs during the bursts span nearly three orders of magnitude in value indicative of the range in physical conditions present in each of the galaxies studied. The SFRs fall on a continuum between bursting and "regular" with

the distinction between the two dependent on the individualized history of each host system and the complicated feedback mechanisms created during the bursts. With this in mind, we examined three metrics for identifying starbursts with the following results and conclusions:

• The gas consumption timescale provides a coarse evaluation of whether a galaxy's SFR is sustainable over a cosmic timescale. For the sixteen galaxies with HI mass measurements, fifteen systems can be classified as starbursts based on their gas consumption timescales being significantly shorter than the Hubble time. The remaining galaxy (NGC 6822) has an upper limit of the gas consumption timescales of 26 Gyr calculated from SFRs derived from a limited field of view of the optical disk.

• The Hα emission from fourteen galaxies measured by Lee et al. (2009) correlates with the SFR in our most recent time bin of $4-10$ Myr. Four galaxies classified as starbursts in the most recent time bin show non-starburst levels of Hα emission indicating that while the bursts are long-lasting events, the SFR can change on timescales of only a few Myr. If the longer durations of a few hundred Myr for this sample of galaxies is typical of starbursts, this longer lived phenomenon is best studied at wavelengths correlating with comparable emission timescales; the short timescale of Hα emission will miss identifying bursting galaxies experiencing short-lived fluctuations / dips in the SFR.

• The ratio of recent SFRs to the average SFR over the past 6 Gyr (a modified birthrate parameter, $b_{recent} \equiv$ SFR $/<\text{SFR}>_{0-6\ \text{Gyr}}$) gives an indication of how significant the rate of recent SF has been in the context of a galaxy's evolutionary history, avoiding a comparison of absolute values of SFR biased towards larger systems. Nineteen of the galaxies showed $b_{recent} > 2$ in the past 500 Myr, not only confirming the bursting nature of these systems, but also providing a metric with which to measure the burst duration. The exception is NGC 625 which presents a unique SFH. The initial onset of SF occurred 3 Gyr in NGC 625 and proceeded in three bursts until the current epoch. This galaxy shows evidence of a starburst at other wavelengths although it does not fit our burst metric.

Preliminary results on the spatial structure of the bursts show that the bursts are global in nature covering a large areal fraction of the host galaxies as evident in the SFHs of both high and low surface brightness regions. For the initial systems studied,

the spatial paths the SF takes are different and may be a result of the initial distribution of the gas or the triggering mechanism for the burst or both. Ongoing research continues to focus on combining the spatial and temporal SFHs for the entire sample of galaxies. Future work will extend this study into the nature of starbursts with observations of the galaxy sample at the UV and IR wavelengths. These observations will enable both a measurement of the emission timescale at these wavelengths and a calibration of the SFRs derived from these wavelengths with the SFRs derived in the SFHs from optically resolved stellar populations.

Bibliography

Aloisi, A., van der Marel, R. P., Mack, J., Leitherer, C., Sirianni, M., & Tosi, M. 2005, ApJL, 631, L45

Angeretti, L., Tosi, M., Greggio, L., Sabbi, E., Aloisi, A., & Leitherer, C. 2005, AJ, 129, 2203

Annibali, F., Greggio, L., Tosi, M., Aloisi, A., & Leitherer, C. 2003, AJ, 126, 2752

Annibali, F., Aloisi, A., Mack, J., Tosi, M., van der Marel, R. P., Angeretti, L., Leitherer, C., & Sirianni, M. 2008, AJ, 135, 1900

Aparicio, A., & Hidalgo, S. L. 2009, AJ, 138, 558

Babul, A., & Ferguson, H. C. 1996, ApJ, 458, 100

Barnes, D. G., & de Blok, W. J. G. 2001, AJ, 122, 825

Barone, L. T., Heithausen, A., Hüttemeister, S., Fritz, T., & Klein, U. 2000, MNRAS, 317, 649

Bastian, N., Gieles, M., Ercolano, B., & Gutermuth, R. 2009, MNRAS, 392, 868

Begum, A., Chengalur, J. N., Karachentsev, I. D., Sharina, M. E., & Kaisin, S. S. 2008, MNRAS, 386, 1667

Bertelli, G., Bressan, A., Chiosi, C., Fagotto, F., & Nasi, E. 1994, A&AS, 106, 275

Bolatto, A. D., Leroy, A. K., Rosolowsky, E., Walter, F., & Blitz, L. 2008, ApJ, 686, 948

Bonnarel, F., et al. 2000, A&AS, 143, 33

Bottinelli, L., Gouguenheim, L., Fouque, P., & Paturel, G. 1990, A&AS, 82, 391

Brinchmann, J., Charlot, S., White, S. D. M., Tremonti, C., Kauffmann, G., Heckman, T., 2004, MNRAS, 351, 1151

Calzetti, D., Meurer, G. R., Bohlin, R. C., Garnett, D. R., Kinney, A. L., Leitherer, C., & Storchi-Bergmann, T. 1997, AJ, 114, 1834

Cannon, J. M., Dohm-Palmer, R. C., Skillman, E. D., Bomans, D. J., Côté, S., & Miller, B. W. 2003, AJ, 126, 2806

Cannon, J. M., & Skillman, E. D. 2004, ApJ, 610, 772

Cole, A. A., et al. 2007, ApJL, 659, L17

Colless, M., Schade, D., Broadhurst, T. J., & Ellis, R. S. 1994, MNRAS, 267, 1108

Comins, N. F. 1983, ApJ, 266, 543

Condon, J. J., Condon, M. A., Gisler, G., & Puschell, J. J. 1982, ApJ, 252, 102

Conti, P. S. 1991, ApJ, 377, 115

Cooper, J. L., Bicknell, G. V., Sutherland, R. S., & Bland-Hawthorn, J. 2008, ApJ, 674, 157

Dalcanton, J. J. 2007, ApJ, 658, 941

Davies, J. I. & Phillipps, S., 1988, MNRAS, 233, 553

de Blok, W. J. G., & Walter, F. 2000, ApJL, 537, L95

de Vaucouleurs, G., de Vaucouleurs, A., & Pence, W. 1974, ApJL, 194, L119

de Vaucouleurs, G., de Vaucouleurs, A., Corwin, H. G., Jr., Buta, R. J., Paturel, G., & Fouque, P., 1991, Volume 1-3, XII, Third Reference Catalogue of Bright Galaxies, Springer (Verlag Berlin Heidelberg New York)

Dekel, A., & Silk, J. 1986, ApJ, 303, 39

Dohm-Palmer, R. C., et al. 1997, AJ, 114, 2527

Dohm-Palmer, R. C., & Skillman, E. D. 2002, AJ, 123, 1433

Dolphin, A. E. 2000, PASP, 112, 1383

Dolphin, A. E., et al. 2001, MNRAS, 324, 249

Dolphin, A. E., 2002, MNRAS, 332, 91

Dolphin, A. E., et al. 2003, AJ, 126, 187

Dolphin, A. E., Weisz, D. R., Skillman, E. D., Holtzman, J. A. 2005, astro-ph

Drozdovsky, I. O., Schulte-Ladbeck, R. E., Hopp, U., Crone, M. M., & Greggio, L. 2001, ApJL, 551, L135

Drozdovsky, I. O., Schulte-Ladbeck, R. E., Hopp, U., Greggio, L., & Crone, M. M. 2002, AJ, 124, 811

Elmegreen, B. G. 2000, ApJ, 530, 277

Fanelli, M. N., O'Connell, R. W. & Thuan, T. X., 1988, ApJ, 334, 665

Ferguson, H. C. & Babul, A., 1998, MNRAS, 296, 585

Ferrara, A. & Tolstoy, E., 2000, MNRAS, 313, 291

Gallagher, J. S., III, & Hunter, D. A. 1986, AJ, 92, 557

Gallart, C., Aparicio, A., & Vilchez, J. M. 1996, AJ, 112, 1928

Gallart, C., Zoccali, M. & Aparicio, A., 2005, ARA&A, 43, 387G

Gerola, H., Seiden, P. E., & Schulman, L. S. 1980, ApJ, 242, 517

Gieren, W., Pietrzyński, G., Nalewajko, K., Soszyński, I., Bresolin, F., Kudritzki, R.-P., Minniti, D., & Romanowsky, A. 2006, ApJ, 647, 1056

Gil de Paz, A., Madore, B. F., Pevunova, O., 2003, ApJS, 147, 29

Gogarten, S. M., et al. 2009, ApJ, 691, 115

Grebel, E. K. 2001, Astrophysics and Space Science Supplement, 277, 231

Greggio, L., Tosi, M., Clampin, M., de Marchi, G., Leitherer, C., Nota, A. & Sirianni, M., 1998, ApJ, 504, 725

Grocholski, A. J., et al. 2008, ApJL, 686, L79

Harris, J., & Zaritsky, D. 2001, ApJS, 136, 25

Harris, J., Calzetti, D., Gallagher, J. S., Smith, D. A. & Conselice, C. J., 2004, ApJ, 603, 503

Heckman, T., 1998, ASP Conf. Ser. Volume 148, Origins, ed. Woodward, C. E., Shull, J. M., & Thronson Jr., H. A. (San Francisco: ASP), 127

Heckman, T., 2005, ASSL Volume 329, Starbursts from 30 Doradus to Lyman Break Galaxies, eds., De Gris, R. & González Delgado, R. M., Springer (the Netherlands), 3

Heydari-Malayeri, M., Melnick, J., & Martin, J.-M. 1990, A&A, 234, 99

Hodge, P. W. 1980, ApJ, 241, 125

Hogg, D. W. & Phinney, E. S., 1997, ApJL, 488, L95

Holmberg, E. 1958, Meddelanden fran Lunds Astronomiska Observatorium Serie II, 136, 1

Holtzman, J. A., et al. 1999, AJ, 118, 2262

Holtzman, J. A., Afonso, C., & Dolphin, A. 2006, ApJS, 166, 534

Huchra, J. P., Geller, M. J., Gallagher, J., Hunter, D., Hartmann, L., Fabbiano, G., & Aaronson, M. 1983, ApJ, 274, 125

Huchtmeier, W. K., Seiradakis, J. H., & Materne, J. 1981, A&A, 102, 134

Huchtmeier, W. K., Gopal, K., & Petrosian, A. 2005, VizieR Online Data Catalog, 343,

40887

Hunter, D. A., Gallagher, J. S., & Rautenkranz, D. 1982, ApJS, 49, 53

Hunter, D. A., O'Connell, R. W., Gallagher, J. S. & Smecker-Hane, T. A., 2000, AJ, 120, 2383

Hunter, D. A., & Elmegreen, B. G. 2004, AJ, 128, 2170

Israel, F. P., Tacconi, L. J., & Baas, F. 1995, A&A, 295, 599

Israel, F. P. 1997, A&A, 328, 471

Kaisin, S. S., Kasparova, A. V., Knyazev, A. Y., & Karachentsev, I. D. 2007, Astronomy Letters, 33, 283

Karachentsev, I. D., et al. 2002, A&A, 383, 125

Karachentsev, I. D., et al. 2003, A&A, 398, 467

Karachentsev, I. D., Dolphin, A., Tully, R. B., Sharina, M., Makarova, L., Makarov, D., Karachentseva, V., Sakai, S. & Shaya, E., J., 2006, AJ, 131, 1361

Kauffmann, G., Guiderdoni, B., & White, S. D. M. 1994, MNRAS, 267, 981

Kaviraj, S., Kirkby, L. A., Silk, J., & Sarzi, M. 2007, MNRAS, 382, 960

Kennicutt, R. C., Jr., Roettiger, K. A., Keel, W. C., van der Hulst, J. M., & Hummel, E., 1987, AJ, 93, 1011

Kennicutt, R. C., Jr., Tamblyn, P., & Congdon, C. E. 1994, ApJ, 435, 22

Kennicutt, R. C., Jr., 1998, ARA&A, 36, 189

Kennicutt, R. C., Jr., & Skillman, E. D. 2001, AJ, 121, 1461

Kennicutt, R. C., Jr., Lee, J. C., Funes, J. G., Sakai, S., & Akiyama, S., 2005, ASSL Volume 329, Starbursts from 30 Doradus to Lyman Break Galaxies, eds., De Gris, R. & González Delgado, R. M., Springer (the Netherlands), 187

Kobulnicky, H. A., & Skillman, E. D. 1997, ApJ, 489, 636

Krueger, H., 1995, A&A, 303, 41

Larsen, S. S., Origlia, L., Brodie, J., & Gallagher, J. S. 2008, MNRAS, 383, 263

Lee, H., Skillman, E. D., Cannon, J. M., Jackson, D. C., Gehrz, R. D., Polomski, E. F., & Woodward, C. E. 2006, ApJ, 647, 970

Lee, J., 2006, PhD Thesis, University of Arizona

Lee, J. C., et al. 2008, Astronomical Society of the Pacific Conference Series, 396, 151

Lee, J. C., Kennicutt, R. C., José G. Funes, S. J., Sakai, S., & Akiyama, S. 2009, ApJ, 692, 1305

Leitherer, C., et al. 1999, ApJS, 123, 3

Leroy, A., Bolatto, A. D., Simon, J. D., & Blitz, L. 2005, ApJ, 625, 763

Loose, H.-H. & Thuan, T. X., 1986, ApJ, 309, 59

López-Sánchez, Á. R., Koribalski, B., Esteban, C., Popping, A., van Eymeren J., & Hibbard, J. in press, Star Forming Galaxies Workshop Proceedings

Mac Low, M. M. & Ferrara, A., 1999, ApJ, 513, 142

Marigo, P., & Girardi, L. 2007, A&A, 469, 239

Marigo, P., Girardi, L., Bressan, A., Groenewegen, M. A. T., Silva, L., & Granato, G. L. 2008, A&A, 482, 883

Marlowe, A. T., Meurer, G. R., Heckman, T. M., & Schommer, R. 1997, ApJS, 112, 285

Marlowe, A. T., Meurer, G. R., & Heckman, T. M. 1999, ApJ, 522, 183

Martin, C. L., Kobulnicky, H. A., & Heckman, T. M. 2002, ApJ, 574, 663

Martin, C. L. 2007, IAU Symposium 235, Galaxy Evolution Across the Hubble Time, ed. F. Combes & J. Palous, Cambridge University Press (Cambridge), 280

Mas-Hesse, J. M. & Kunth, D., 1999, A&A, 349, 765

Mas-Hesse, J. M., Kunth, D., & Cerviño, M. 2000, New Astronomy Review, 44, 229

Mateo, M. L. 1998, ARA&A, 36, 435

Mayer, L., Governato, F., Colpi, M., Moore, B., Quinn, T., Wadsley, J., Stadel, J., & Lake, G. 2001, ApJL, 547, L123

Mayer, L., Governato, F., Colpi, M., Moore, B., Quinn, T., Wadsley, J., Stadel, J., & Lake, G. 2001, ApJ, 559, 754

Mayer, L., Mastropietro, C., Wadsley, J., Stadel, J., & Moore, B. 2006, MNRAS, 369, 1021

McQuinn, K. B. W., Skillman, E. D., Cannon, J. M., Dalcanton, J. J., Dolphin, A., Stark, D., & Weisz, D. 2009, ApJ, 695, 561

McQuinn, K. B. W., et al., 2010, ApJ, submitted, Paper I

McQuinn, K. B. W., et al., 2010, ApJ, submitted, Paper II

Meurer, G. R., Heckman, T. M., Leitherer, C., Kinney, A., Robert, C., Garnett & D. R., 1995, AJ, 110, 2665

Meurer, G. R., Heckman, T. M., Lehnert, M. D., Leitherer, C., & Lowenthal, J. 1997, AJ, 114, 54

Meurer, G. R., 2000, ASP Conf. Ser. Volume 211, Massive Stellar Clusters, ed. A.

Lançon, & C. Boily (San Francisco: ASP), 81

Méndez, B., Davis, M., Moustakas, J., Newman, J., Madore, B. F., & Freedman, W. L. 2002, AJ, 124, 213

Nishi, R., & Tashiro, M. 2000, ApJ, 537, 50

O'Connell, R. W., 2005, ASSL Volume 329, Starbursts from 30 Doradus to Lyman Break Galaxies, eds. De Grijs, R. & González Delgado, R. M., Springer (The Netherlands), 333

Oey, M. S., et al. 2007, ApJ, 661, 801

Omukai, K., & Nishi, R. 1999, ApJ, 518, 64

Östlin, G., Zackrisson, E., Bergvall, N. & Rönnback, J., 2003, A&A, 408, 887

Pasetto, S., Chiosi, C., & Carraro, G. 2003, A&A, 405, 931

Paturel, G., Theureau, G., Bottinelli, L., Gouguenheim, L., Coudreau-Durand, N., Hallet, N., & Petit, C. 2003, A&A, 412, 57

Pelupessy, F. I., van der Werf, P. P., & Icke, V. 2004, A&A, 422, 55

Recchi, S., Hensler, G., Angeretti, L., & Matteucci, F. 2006, A&A, 445, 875

Reynolds, R. J. 1984, ApJ, 282, 191

Roberts, M. S. 1963, ARA&A, 1, 149

Romano, D., Tosi, M. & Matteucci, F., 2006, MNRAS, 365, 759

Sakai, S., Ferrarese, L., Kennicutt, R. C., Jr., & Saha, A. 2004, ApJ, 608, 42

Salpeter, E. E. 1955, ApJ,

Salzer, J. J., Rosenberg, J. L., Weisstein, E. W., Mazzarella, J. M., & Bothun, G. D. 2002, AJ, 124, 191

Scalo, J. M. 1986, Fundamentals of Cosmic Physics, Volume 11, 1

Schaerer, D., Contini, T., & Kunth, D., 1999, A&A, 341, 399

Schlegel, D. J., Finkbeiner, D. P., & Davis, M. 1998, ApJ, 500, 525

Schulte-Ladbeck, R. E., Hopp, U., Greggio, L., Crone, M. M., & Drozdovsky, I. O. 2001, AJ, 121, 3007

Searle, L., & Sargent, W. L. W. 1972, ApJ, 173, 25

Searle, L., Sargent, W. L. W., & Bagnuolo, W. G. 1973, ApJ, 179, 427

Sharina, M. E., et al. 2008, MNRAS, 384, 1544

Silk, J., Wyse, R. F. G., & Shields, G. A., 1987, ApJ, 322, L59

Skillman, E. D., Terlevich, R., Teuben, P. J., & van Woerden, H. 1988, A&A, 198, 33

Skillman, E. D., Kennicutt, R. C., & Hodge, P. W. 1989, ApJ, 347, 875

Skillman, E. D. 1996, The Minnesota Lectures on Extragalactic Neutral Hydrogen, 106, 208

Skillman, E. D. 1997, Revista Mexicana de Astronomia y Astrofisica Conference Series, 6, 36

Skillman, E. D., & Gallart, C. 2002, Observed HR Diagrams and Stellar Evolution, 274, 535

Skillman, E. D., Tolstoy, E., Cole, A. A., Dolphin, A. E., Saha, A., Gallagher, J. S., Dohm-Palmer, R. C., & Mateo, M. 2003, ApJ, 596, 253

Skillman, E. D. 2005, New Astronomy Review, 49, 453

Smith, L. J., & Gallagher, J. S., III, 2000, ASP Conf. Ser. Volume 211, Massive Stellar Clusters, ed. A. Lançon, & C. Boily (San Francisco: ASP), 90

Spaans, M. & Norman, C. A., 1997, ApJ, 483, 87

Stinson, G. S., Dalcanton, J. J., Quinn, T., Kaufmann, T., & Wadsley, J. 2007, ApJ, 667, 170

Strickland, D. K., & Stevens, I. R. 2000, MNRAS, 314, 511

Strickland, D. K., Heckman, T. M., Colbert, E. J. M., Hoopes, C. G., & Weaver, K. A. 2004, ApJS, 151, 193

Swaters, R. A., & Balcells, M. 2002, A&A, 390, 863

Taylor, C. L., Kobulnicky, H. A., & Skillman, E. D. 1998, AJ, 116, 2746

Telesco, C. M., Wolstencroft, R. D., & Done, C. 1988, ApJ, 329, 174

Telles, E. 2009, arXiv:0908.2966, To appear in ASP Series; Galaxy Wars

Thompson, R. I., 2005, ASSL Volume 329, Starbursts from 30 Doradus to Lyman Break Galaxies, eds., De Gris, R. & González Delgado, R. M., Springer (the Netherlands), 289

Thornley, M. D., Schreiber, N. M. F., Lutz, D., Genzel, R., Spoon, H. W. W. & Kunze, D., 2000, ApJ, 539, 641

Thuan, T. X., & Seitzer, P. O. 1979, ApJ, 231, 327

Thuan, T. X., & Martin, G. E. 1981, ApJ, 247, 823

Tolstoy, E., & Saha, A. 1996, ApJ, 462, 672

Tolstoy, E., et al. 1998, AJ, 116, 1244

Tolstoy, E., Hill, V., & Tosi, M. 2009, ARA&A, 47, 371

Tosi, M., Greggio, L., & Focardi, P. 1989, Ap&SS, 156, 295

Tremonti, C. A., Calzetti, D., Leitherer, C. & Heckman, T. M., 2001, ApJ, 555, 322

Tully, R. B., et al. 2006, AJ, 132, 729

van Eymeren, J., Marcelin, M., Koribalski, B., Dettmar, R.-J., Bomans, D. J., Gach, J.-L., & Balard, P. 2009, A&A, 493, 511

van Zee, L. 2001, AJ, 121, 2003

van Zee, L., Salzer, J. J. & Skillman, E. D., 2001, AJ, 122, 121

van Zee, L., Skillman, E. D., & Haynes, M. P. 2004, AJ, 128, 121

Vázquez, G. A., & Leitherer, C. 2005, ApJ, 621, 695

Walter, F., Taylor, C. L., Hüttemeister, S., Scoville, N., & McIntyre, V. 2001, AJ, 121, 727

Walter, F., Brinks, E., de Blok, W. J. G., Bigiel, F., Kennicutt, R. C., Thornley, M. D., & Leroy, A. 2008, AJ, 136, 2563

Weisz, D. R., Skillman, E. D., Cannon, J., Dolphin, A., Kennicutt, R., Lee, J., & Walter, F. 2008, ApJ, 689, 160

Weisz, D. R., Skillman, E. D., Cannon, J. M., Dolphin, A. E., Kennicutt, R. C., Lee, J., & Walter, F. 2009, ApJ, 704, 1538

Weldrake, D. T. F., de Blok, W. J. G., & Walter, F. 2003, MNRAS, 340, 12

Whiting, A. B., Irwin, M. J., & Hau, G. K. T. 1997, AJ, 114, 996

Williams, B. F., et al. 2009, arXiv:0911.4121

Wilson, C. D. 1995, ApJL, 448, L97

Yin, Q. F., Huang, J. H., & Zheng, W. 2003, ApJ, 597, 274

Appendix A

Press Release from the Hubble News Center

Hubble Space Telescope News Center Press Release, April 30, 2009
News Release Number: STScI-2009-19
by Donna Weaver / Ray Villard
Space Telescope Science Institute

Starbursts in Dwarf Galaxies are a Global Affair

Bursts of star making in a galaxy have been compared to a Fourth of July fireworks display: They occur at a fast and furious pace, lighting up a region for a short time before winking out.

But these fleeting starbursts are only pieces of the story, astronomers say. An analysis of archival images of small, or dwarf, galaxies taken by NASA's Hubble Space Telescope suggests that starbursts, intense regions of star formation, sweep across the whole galaxy and last 100 times longer than astronomers thought. The longer duration may affect how dwarf galaxies change over time, and therefore may shed light on galaxy evolution.

"Our analysis shows that starburst activity in a dwarf galaxy happens on a global scale," explains Kristen McQuinn of the University of Minnesota in Minneapolis and

leader of the study. "There are pockets of intense star formation that propagate throughout the galaxy, like a string of firecrackers going off." According to McQuinn, the duration of all the starburst events in a single dwarf galaxy would total 200 million to 400 million years.

These longer timescales are vastly more than the 5 million to 10 million years proposed by astronomers who have studied star formation in dwarf galaxies. "They were only looking at individual clusters and not the whole galaxy, so they assumed starbursts in galaxies lasted for a short time," McQuinn says.

Dwarf galaxies are considered by many astronomers to be the building blocks of the large galaxies seen today, so the length of starbursts is important for understanding how galaxies evolve.

"Astronomers are really interested to find out the steps of galaxy evolution," McQuinn says. "Exploring these smaller galaxies is important because, according to popular theory, large galaxies are created from the merger of smaller, dwarf galaxies. So understanding these smaller pieces is an important part of filling in that scenario."

McQuinn's team analyzed archival Advanced Camera for Surveys data of three dwarf galaxies, NGC 4163, NGC 4068, and IC 4662. Their distances range from 8 million to 14 million light-years away. The trio is part of a survey of starbursts in 18 nearby dwarf galaxies.

Hubble's superb resolution allowed McQuinn's team to pick out individual stars in the galaxies and measure their brightness and color, two important characteristics astronomers use to determine stellar ages. By determining the ages of the stars, the astronomers could reconstruct the starburst history in each galaxy.

Two of the galaxies, NGC 4068 and IC 4662, show active, brilliant starburst regions in the Hubble images. The most recent starburst in the third galaxy, NGC 4163, occurred 200 million years ago and has faded from view.

The team looked at regions of high and low densities of stars, piecing together a picture of the starbursts. The galaxies were making a few stars, when something, perhaps an encounter with another galaxy, pushed them into high star-making mode. Instead of forming eight stars every thousand years, the galaxies started making 40 stars every thousand years, which is a lot for a small galaxy, McQuinn says. The typical dwarf is 10,000 to 30,000 light-years wide. By comparison, a normal-sized galaxy such

as our Milky Way is about 100,000 light-years wide.

About 300 million to 400 million years ago star formation occurred in the outer areas of the galaxies. Then it began migrating inward as explosions of massive stars triggered new star formation in adjoining regions. Starbursts are still occurring in the inner parts of NGC 4068 and IC 4662.

The total duration of starburst activity depends on many factors, including the amount of gas in a galaxy, the distribution and density of the gas, and the event that triggered the starburst. A merger or an interaction with a large galaxy, for example, could create a longer starburst event than an interaction with a smaller system.

McQuinn plans to expand her study to a larger sample of more than 20 galaxies. "Studying nearby dwarf galaxies, where we can see the stars in great detail, will help us interpret observations of galaxies in the distant universe, where starbursts were much more common because galaxies had more gas with which to make stars," McQuinn explains.

McQuinn's results appeared in the April 10 issue of The Astrophysical Journal.

Appendix B

Acronyms

Care has been taken in this thesis to minimize the use acronyms, but this cannot always be achieved. This appendix contains a table of acronyms and their meaning.

Table B.1: Acronyms and their meanings

Acronym	Meaning
b_{recent}	Ratio of current to 6 Gyr average rate of star formation
BHeB star	Blue Helium Burning star
CMD	Color-Magnitude Diagram
Gyr	Billion years (10^9 yr)
HST	Hubble Space Telescope
MS star	Main Sequence star
Myr	Million years (10^6 yr)
RHeB star	Red Helium Burning star
SF	Star Formation
SFR	Star Formation Rate
SFH	Star Formation History